SIMULATING THE CHARACTERISTICS OF WEST AFRICAN MONSOON USING THE MPAS MODEL

BY

LAOUALI, IBRAHIM TANIMOUNE

M.Sc (MET/19/3752)

A Thesis of the Doctoral Research Programme of the West Africa Climate Systems, under the West Africa Science Service Centre on Climate Change and Adapted Land Use, in the Department of Meteorology and Climate Science submitted to the School of Postgraduate Studies in partial fulfilment of the requirements for the award of the degree of Doctor of Philosophy in Meteorology and Climate Science of the Federal University of Technology, Akure, Nigeria.

June, 2023.

DECLARATION

I hereby declare that this Thesis was written by me and is a correct record of my own research work. It has not been presented in any previous application for any degree of this or any University. All citations and sources of information are clearly acknowledged by means of references.

Candidate's Name: LAOUALI, IBRAHIM TANIMOUNE

Signature: Date……/……/2023

CERTIFICATION

We certify that this Dissertation entitled "Simulating the Characteristics of West African Monsoon using the MPAS model" is the outcome of the research carried out by Laouali, Ibrahim Tanimoune under the WASCAL DRP-WACS in the Department of Meteorology and Climate Science of the Federal University of Technology, Akure.

Prof. Harald Kunstmann …….

(Major Surpervisor) Signature Date
Institute of Geography, University of Augsburg.
Germany.

Prof. Babatunde J. Abiodun …….

(Co-Supervisor) Signature Date
University of Cape Town, South Africa

Dr. Ajayi O. Vincent …….

(Co-Supervisor) Signature Date
Department of Meteorology and Climate Science,
Federal University of Technology,
Akure, Nigeria.

Prof. Zachariah Debo Adeyewa …….

(Director) Signature Date
Doctoral Research Program – West African Climate Systems
West African Science Service Center on Climate Change and
Adapted Land Use (DRP-WACS, WASCAL),
Federal University of Technology,
Akure, Nigeria.

ABSTRACT

This research evaluates the Model for Prediction Across Scale (MPAS) to simulate the West African monsoon. The research aims to investigate how well the MPAS model simulates the characteristics of the West African monsoon. The specific objectives are to examine the performance of the MPAS model in reproducing observed spatial pattern and seasonality of the West African Monsoon (WAM) rainfall, examine the capability of MPAS to reproduce the rainfall producing system of the West African Monsoon and to investigate the capability of MPAS to simulate temperature and precipitation based extreme events over West Africa.The West African monsoon (WAM) plays a crucial role in the West African climate system. It is the primary process for transporting moisture from the Atlantic Ocean to land masses during the boreal summer. The ability of the Model for Prediction Across Scales-Atmosphere (MPAS-A) with a mesh with a quasi-uniform resolution of 60 km to reproduce the WAM rainfall-producing system was evaluated. The model is run from 1981 to 2010 using the "mesoscale reference" physics parametrization. The model results are compared with satellite-derived datasets (Climate Hazards Group InfraRed Precipitation with Stations, CHIRPS), gridded observation datasets (Climate Research Unit, CRU), and reanalysis datasets (Climate Forecast System Reanalysis, CFSR; the National Oceanic and Atmospheric Administration, NOAA; and the European Centre for Medium-Range Weather Forecasts version 5, ERA5). MPAS reproduces the rainfall pattern over West Africa and the different phases of the monsoon dynamics, including the position of the Inter-tropical Discontinuity (ITD). However, MPAS shows weaknesses in reproducing the orographic rainfall, maximum over the Guinea Coast, Jos Plateau, and Mount Cameroon; likewise, the magnitudes of the vertical

velocity and zonal wind are underestimated. In addition, MPAS shows a cold bias in the temperature gradient. Also, a large ensemble of 51 simulations with the MPAS has been applied to assess its ability to reproduce extreme temperatures and heat waves in the area of West Africa and the Eastern Sahel. With its global approach, the model avoids transition errors influencing the performance of limited area climate models. The MPAS simulations were driven with SST and sea ice extent as the only boundary condition. The results reveal moderate cold biases in the range from -0.6° to -0.9° C for the daily mean temperature and -1.4°to -2.0° C for the area mean of the daily maximum temperature. The bias in the number of tropical nights ranges from +3 to -10 days. An underestimation by up to 50% is also present regarding the number of summer days. The heat wave duration index is underestimated regionally by 10% to 60%. Compared to the reanalyzes, the biases revealed by the MPAS simulations are generally smaller than with measured observational reference. The results from long-term runs and from short-term runs with selected SST years are similar. The shortcomings in the reproduction of the temperatures and precipitation found in the present investigation with the MPAS approach are similar to that of regional climate models.

DEDICATION

To my late Parents, Ibrahim Tanimoune, Fatima Nari

ACKNOWLEDGEMENTS

Firstly, I would like to express my sincere gratitude to the Almighty ALLAH for giving me the health, energy, and inspiration to successfully write each letter, word, sentence, paragraph, chapter of this thesis. Thank for all, ALLAH.

The German Federal Ministry of Education and Research (BMBF) primarily funded this research through the West African Science Service Center on Climate Change and Adapted Land-Use Doctorate Research Programme in West African Climate Systems (WASCAL DRP-WACS) host in the Federal University of Technology Akure, Nigeria. I am grateful to my Major Supervisor, Prof. Harald Kunstmann, Co-Supervisors, Prof. Babatunde Joseph. Abiodun and Dr. Vincent O. Ajayi, for their encouragement, constructive criticism, insightful suggestions and comments throughout the conduct of this research.

I sincerely thank the executive Director and the staff of WASCAL Head office, Accra, Ghana, I am also grateful to the Director, Prof. Z. D. Adeyewa, the Deputy Director, Prof. I. A. Balogun, the Scientific Coordinator, Prof. A. Oluleye and staff of WASCAL GRP-WACS, FUTA, Nigeria for their strong support and encouragement throughout the period of the study. I am grateful to Dr. A. Akinbobola, the Head of Department of Meteorology and Climate Science, FUTA and the members of staff, for their cooperation.

The initial model configuration was done on The Centre for High Performance Computing (CHPC, South Africa). I would like to thank the University of Cape Town for providing supercomputing facilities.

Many thanks to the Institute of Meteorology and Climate Research (IMK-IFU), Karlsruhe Institute of Technology, for giving me the opportunity for the scientific visit and providing

high-performance computing to achieve some of the objectives of this study. Also, many thanks to Dr. Gerhard Smiatek.

I would like to also express my gratitude to the Centre Regional de Formation et d'Application en Agrométéorologie et Hydrologie Opérationnelle (AGRHYMET), Niamey, Niger Republic for providing space and facilities to conduct my research during the field work, many thanks to my advisor Dr. Ibrah Seidou Sanda for technical support.

Special thanks go to my amazing brothers, Mahaman Sani, Mahaman Salissou, Hassane, Housseina, Mahaman Rabiou, my siblings, and colleagues. Also, I sincerely thank and appreciate my dear wife, Mrs. Laouali Fati Hamadou, for her moral support and understanding. I will not forget my lovely kids, Ahmad, Aliya, and Soffia, God bless you.

TABLE OF CONTENTS

LIST OF FIGURES

LIST OF TABLES

LIST OF EQUATIONS

LIST OF ABREVIATIONS

AEJ	African Easterly Jet
AEWs	African Easterly Waves
AGCM	Atmospheric General Circulation Models
AWJ	African Westerly Jet
C	Celsius
CCN	Cloud Condensation Nuclei
CFSR	Climate Forecast System Reanalysis
CHIRPS	Climate Hazards Group InfraRed Precipitation with Stations
CMIP	Coupled Model Intercomparison Project Phase
CORDEX	Coordinated Regional Climate Downscaling
CPC	Climate Prediction Center
CPU	Central Processing Unit
CRU	Climate Research Units
DJF	December, January, February
ECMWF	European Center for Medium-range Weather Forecast
ENSO	El Nino Southern Oscillation
ERA5	European Center for Medium-Range Weather Forecasts version 5

ESGF	Earth System Grid Federation
ETCCDI	Expert Team on Climate Change Detection, Monitoring and Indices
F	Coriolis force parameter
FAO	Food and Agriculture Organization
GCMs	Global Circulation Models
GG	Gulf of Guinea
GMTED	Global Multi-Resolution Terrain Elevation
GPCC	Global Precipitation Climatology Center
GUI_C	Guinea Coast
IPCC	Inter-governmental Panel on Climate Change
ITCZ	Inter-Tropical Convergence Zone
ITD	Inter-Tropical Discontinuity
JJA	June, July, August
JRA-55	Japanese 55-year Reanalysis
K	Kelvin
LW	Long Wave
MAM	March, April, May
MB	Mean Bias
MCM	Mesoscale Climate Model

MCS	Mesoscale Convective System
MERRA-2	Modern-Era Retrospective Analysis for Research and Application, v2
MPAS	Model for Prediction Across Scales
NCEP2	National Centers for Environmental Prediction v2
Noah-LSM	Community Noah Land- Surface Model
nTDK	New Tiedtke
PBL	Planetary Boundary Layer
R	Correlation Coefficient
R	Perfect gas constant
RCM	Regional Climate Model
RMSE	Root Mean Square Error
RRTMG	Rapid Radiative Transfer Model
SAH_E	Sahel East
SAH_W	Sahel West
SG	Stretch Grid
SHL	Saharan Heat Low
SON	September, October, November
SST	Sea Surface Temperature
SW	Short Wave
TEJ	Tropical Easterly Jet
U	Zonal components of wind

UN	United Nations
USAID	United States Agency for International Development
U_t	Zonal component of thermal wind wind
V	Meridional components of wind
V_t	Meridional component of thermal wind
WA	West Africa
WAM	West African Monsoon
WAWJ	West African Westerly Jet
WDM6	WRF Double-Moment 6-Class Micro-physics
WRF	Weather Research and Forecast Model
YSU	Yonsei University

CHAPTER ONE

1.0 INTRODUCTION

1.1 Background of the study

The West African monsoon (WAM) plays a crucial role in the climate of West Africa (WA). It modulates the wind system over WA and controls the spatial distribution of temperature and precipitation over the region. Two seasonal winds characterize the WAM (Figure 1.1): the northeasterly wind, which blows dry cold air to the region in winter; and the southwesterly wind, which brings moist warm air over the region in summer (Krishnamurthy *et al*., 2010). The southwesterly flow transports moisture from the Atlantic Ocean to WA and causes seasonal rainfall over the subcontinent. Seasonal rainfall is essential for millions of West African people, whose cultures and lifestyles depend on the behaviour of the monsoon rains and the associated growing season (Sivakumar *et al*., 2014). In addition, given that rainfed agriculture is the mainstay of the economies of most West African countries, variations in WAM rainfall often devastate socio-economic activities and food security in WA (Omotosho & Abiodun, 2007).

The WAM system includes a multitude of atmospheric features (Figure 1.2) that interact in a complex way to generate rainfall over WA. These atmospheric features include the heat low, African easterly jet (AEJ), African easterly waves (AEWs), and mesoscale convective systems (MCSs). For example, during summer, the heat low induces maximum heating over the continent, resulting in a temperature gradient between the West African subcontinent and the Atlantic Ocean. The temperature gradient drives the southwest monsoon flow from the ocean to the continent (Caniaux *et al*., 2011; Sultan *et al*.,

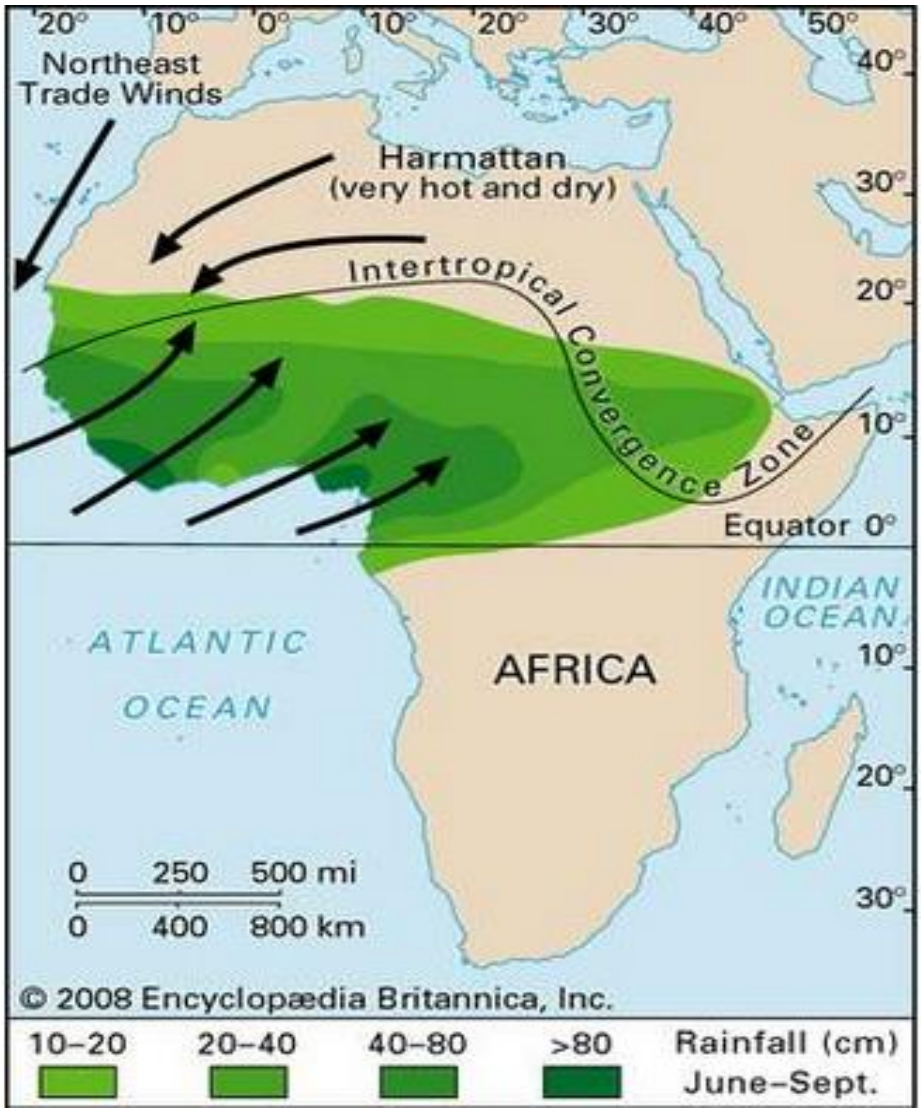

Figure 1.1: Illustration of monsoon flow, shaded in green, source: Encyclopedia Britannica, 2008.

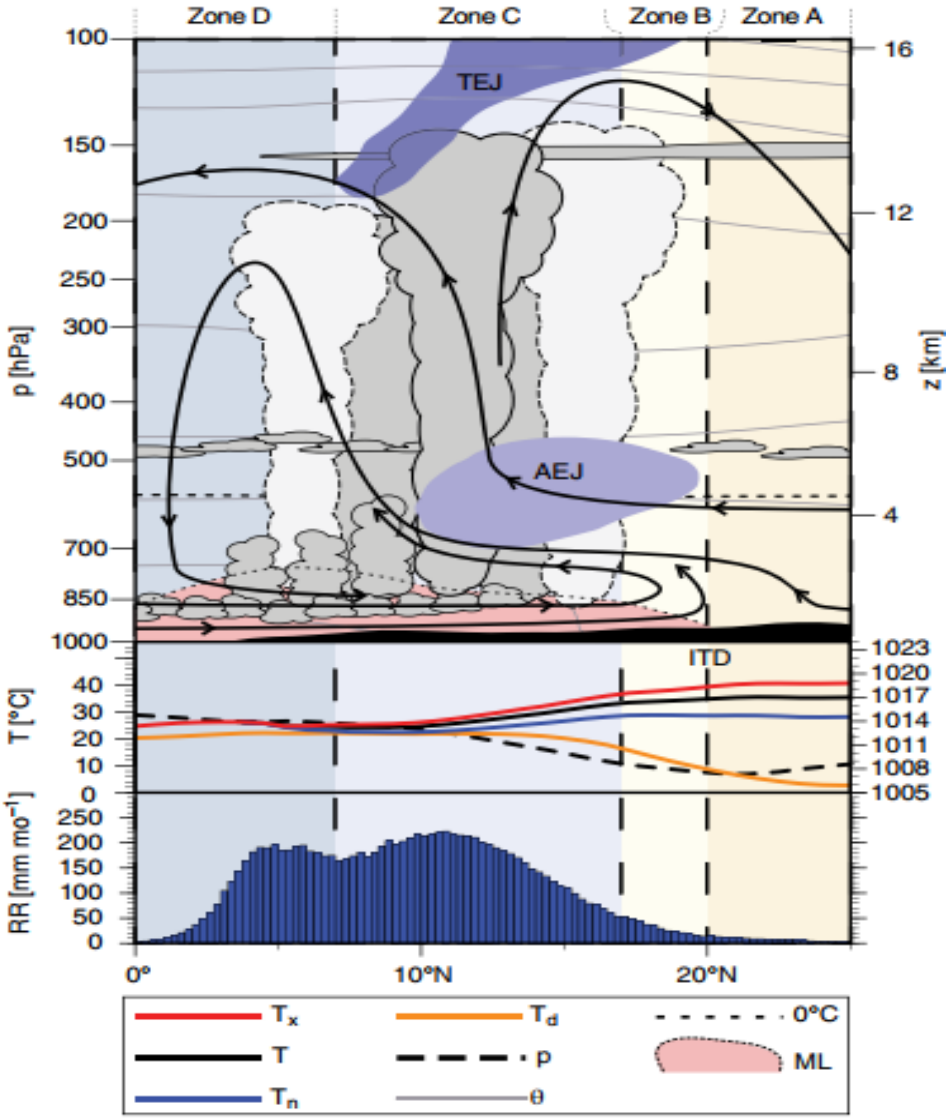

Figure 1.2: Interaction between the differentrainfall producing system. (John Wiley & Sons Ltd ,2017).

2003) and produces the AEJ due to the thermal wind effect, and when the AEJ becomes unstable, it generates AEWs (Grist & Nicholson, 2001). The low-level convergence associated with AEWs lift the warm moist southwest monsoon flow to the level of free convection, thereby initiating thunderstorms and mesoscale convective systems that produce heavy rainfall and account for more than 75% of the rainfall over WA (Hagos & Cook, 2007). Therefore, for a model to correctly simulate rainfall characteristics over WA, it must reproduce all these atmospheric systems and their complex interactions.

West African rainfall depends on the northward displacement of the rain belt, which is associated with the Inter-Tropical Discontinuity (ITD) position. This displacement of the rain belt over West Africa monitors the rainfall over the different climatic zones (Guinea Coast, Savannah, and Sahel) to high interannual and interdecadal variability. Over the past decennaries, the variability has produced a negative trend in the rainfall amount experienced during the wet season (Biasutti & Giannini, 2006; Dai *et al*., 2004; L'Hôte *et al*., 2002; Nicholson *et al*., 2000), thereby causing droughts, which may lead to famine in the Sahel. To grasp the cause of this variability, several factors have been studied by previous works. Among the elements, the Sea Surface Temperature (SST) anomalies are highlighted (Eltahir & Gong, 1995; Fontaine *et al*., 1998; Giannini *et al*., 2003; Hagos & Cook, 2008; Hoerling *et al*., 2006; Nicholson & Webster, 2007), inland surface conditions (Charney *et al*., 1977; Semazzi & Sun, 1997; Wang & Eltahir, 2000), atmospheric composition (Jenkins *et al*., 2005; Nicholson & Grist, 2001; Nicholson, 2008), and potential impact of global climate change (Held & Soden, 2006; Paeth & Hense, 2004). Moreover, studies also found that the monsoon wind system, such as the

low-level monsoon flow, the mid-tropospheric AEJ, and the upper-level TEJ, have adjusting effect on the precipitation and variability between seasons and between years (Nicholson *et al*., 2000).

West Africa (WA) and the Eastern Sahel are characterized by high temperatures and large variability in rainfall and have been historically affected by extreme weather anomalies (Nicholson & Webster, 2007; Sultan *et al*., 2013; Poan *et al*., 2016). A long-standing example are the droughts of 1974–1975 over the Sahel. They caused severe increase in mortality in the population and livestock, and despite the recent occurrence of a regreening, the Sahel region is still suffering from these droughts (Janicot *et al*., 1996; Cook, 2008).

Numerous modeling studies on WAM have been conducted. However, there are still fundamental gaps in the knowledge on how atmospheric climate models capture its features and the cause of the errors in the outputs. This has pushed atmospheric climate models to become a valuable tool for studying and understanding the WAM and associated features. The Global Circulation Models (GCMs) are tool used to study the dynamics of WAM, however, these models are inadequate in simulating main features of the WAM climate and its spatio-temporal rainfall distribution (Hourdin *et al*., 2010; Sylla *et al*., 2010; Vizy & Cook, 2002; Xue *et al*., 2010). This is due to several reasons such as, their coarse horizontal resolution (Druyan *et al*., 2009; IPCC, 2007), model type, and the initialization of their land surface/soil moisture (Xue *et al*., 2010; Yamada *et al*., 2012). These issues may cause the GCMs to fail to reproduce the local, regional topographical forcing and the mesoscale system.

An option to resolve issues on coarse resolution of GCMs is the use of Regional Climate Models (RCMs). The RCMs can be used at higher resolution, which allows them to simulate regional and mesoscale features. The RCMs are also efficient for dynamical downscaling of the GCMs simulation or reanalysis, and they allow skillful performance of climate and weather simulation at higher horizontal grid resolution (Giorgi & Mearns, 1999; Klein *et al*., 2015). However, the RCMs have limitation to correctly simulate rainfall over WA due to boundary conditions, which leads to underestimate or overestimate rainfall over the region (Fox-Rabinovitz *et al*., 2006; Fox-Rabinovitz *et al*., 2008; Harris *et al*., 2016; Abiodun *et al*., 2011).

So far, the Model for Prediction Across Scales (MPAS) is a potential toll for simulating atmospheric processes over the subregion. A limited number of studies have utilized MPAS throughout Africa. MPAS-atmosphere is a global, fully compressible non-hydrostatic model (Klemp, 2011, Skamarock *et al*., 2012). The model also has different physics options similar to the WRF model. For example, the mesoscale-reference suite is the recommended physics suit for any MPAS applications where the mesoscale resolution is higher than 10 km. MPAS also uses Voronoi tessellations to create irregular multigonal around grid points and a global irregular grid (Skamarock *et al*., 2002). The irregular grid structure permits a simple transition from coarse to fine resolution, in contrast to the nesting techniques of classical regional models (Kramer *et al*., 2018). Also, MPAS does not require the standard grid transformation in the polar regions, which depend on good computational performance for a global simulation compared to classical methods (Skamarock *et al*., 2012).

Furthermore, MPAS has shown to be skillful on supercomputers. As supercomputers are potential tools to use likely more cores per node in the upcoming years, this technical aspect will probably increase (Heinzeller *et al*., 2016). The skill of supercomputers makes MPAS a feasible option for operational use on a high-performance computing cluster. MPAS is also known for its quasi-equity distance between grids, the problem of the limited timestep to respond to the computational fluid dynamic's state for small grids in the polar regions (Kramer *et al*. 2020). In addition, MPAS offers a suitable environment for weather modeling. Due to this good technical aspect, MPAS is rising attention in the field of atmospheric modeling. For instance, the MPAS model has been mostly improved and primarily tested for tropical cyclones (Davis *et al*., 2016; Lui *et al*., 2021; Michaelis *et al*., 2019; Donkin and Abiodun. 2022). MPAS is also used to simulate atmospheric processes such as the Intertropical Convergence Zones, the Madden-Julian Oscillation, and the West African Monsoon dynamics (Landu *et al*., 2014; Heinzeller *et al*., 2016; Pilon *et al*., 2016); these studies conclude that MPAS was able to simulate those atmospheric features accurately. However, MPAS has never been tested to simulate the characteristics of the West African Monsoon. Possible causes of the biases in the MPAS simulation will also be investigated.

1.2 Statement of problem

Climate and weather models are crucial for studying and understanding regional atmospheric features. However, these models still give a significant error. These errors could be fatal to the precision of the model results, and this will constitute a barrier to using the findings to implement necessary socio-economic plans and policies. So far, most studies link the error in the models to the parameterization of physical atmospheric

processes within the model. Sometimes, the sources of errors are implicit in the input data used for the initialization, reproduction of the land use land cover of the model domain, and somehow touch the computational resources. All those factors mentioned above restrict the precision of reproducing the atmospheric preprocesses of interest and, thus, obstruct the generation of reliable climate information fundamental for the achievement of the sustainable development goals in different contributors of the economy, such as agriculture, water resource management, energy, etc. Moreover, several studies have provided important information and attempted to evaluate the performance of models in simulating the WAM, its related features, and climate extremes during summer by climate models.

1.3 Aim and objectives

1.3.1 Aim

The study aims to investigate how well MPAS simulates the West African monsoon-related atmospheric features and temperature indices.

1.3.2 Objectives

The specific objectives of the research are to:

(i) examine the performance of MPAS in reproducing observed spatial pattern and seasonality of the West African Monsoon rainfall,

(ii) examine the capability of MPAS to reproduce the rainfall producing system of the West African Monsoon and,

(iii) investigate the capability of MPAS to simulate temperature and precipitations-based extremes over West Africa.

1.4 Justification of the study

The main idea behind this research is to evaluate the MPAS model to see the possibility of using the model by the different National Meteorological Agencies over WA, because the meteorological services provide useful climate information that will guide policy preparation and decision-making in sectors of the economy related to climate at the national and regional level. Model assessment, application, and improvement are the essential fields that have been investigated in the last decade and nowadays research, especially in Africa where there is a low density of observed data. It is thus essential to continuously look at the performance of new models undergoing modification and periodic updates. Even though much literature exists on the performance of climate model to simulate the WAM, more research is needed because of the importance monsoon has on the life of millions of people living in WA (Janicot *et al*., 2008; Mounier *et al*., 2008; Redelsperger *et al*., 2006). Another barrier to understanding the large-scale monsoon system and its associated rainfall-producing systems is the lack of an essential observational data network over the continent. However, previous studies have given solid background on modeling the WAM, such as model development and the sensitivity of WAM to Physics and configuration.

Nevertheless, most of the results contain critical uncertainties leading to implicit systematic biases. Hence, there is a need to conduct more modeling studies on the dynamic meteorology of West Africa. For example, to study the capability of MPAS to reproduce the WAM system. The study of MPAS model performance in simulating the WAM and related features, temperature, and precipitation indices are crucial to deciding if the model

can be proposed as a tool for hindcasting in WA. Hence, understanding how contemporary climate models link West African precipitation with these atmospheric features is essential for improving the seasonal prediction over the sub-continent. The research will also consolidate previous works by contributing to the state-of-the-art of model's performance in simulating the WAM.

1.5 Contribution of the research to knowledge

The outcome of this thesis will benefit the model improvement community in identifying the part of the model structure that needs to be modified for better model results. It will deepen the understanding on how atmospheric models capture the WAM features and rainfall. In addition, if the performance of MPAS is good enough in simulating extreme temperature and heat waves, the model can be used as hindcasting tool by meteorological services over West Africa to inform, population, farmers, and other end-users. Besides, the study will open ways to new research areas for future studies.

CHAPTER TWO

2.0 LITERATURE REVIEW

2.1 The West African Monsoon

Monsoon represents a seasonal reversal of the low-level wind direction with variation in precipitation. The West African summer monsoon is an atmospheric feature that controls the rainfall from May to September, carrying the necessary quantity of rainfall to the region (Hagos & Cook, 2007; Janicot *et al*., 2008; Sylla *et al*., 2013). Monsoon rainfall is mainly formed due to the advective warm-moist airmass from the Gulf of Guinea in the low atmosphere (Sultan & Janicot, 2000). Some studies have discussed the factors that control monsoon variability. Most of these studies linked the variability to the ocean sea surface temperature (Fontaine *et al*., 1998; Giannini *et al*., 2003; Tamoffo *et al*., 2022), land surface conditions over the continent (Charney *et al*., 1977; Wang & Eltahir, 2000) and atmospheric circulation (Jenkins *et al*., 2005; Nicholson & Grist, 2001; Nicholson & Grist, 2002).

In the field of dynamic meteorology, the WAM is a global circulation system accommodating different rainfall-producing systems such as the Inter-Tropical Convergence Zone (ITCZ), Inter-Tropical Discontinuity (ITD), African Easterly Jet (AEJ), Tropical Easterly Jet (TEJ), Warm Saharan Air (above the Saharan heat low (SHL)), and Dry Air (Figure 2.1). Previous studies have demonstrated that the interannual variability of the WAM rainfall, generally in the Sahel, is related to the atypical latitudinal movement of the ITCZ (Bryson, 1973; Kraus, 1977; Lele *et al*., 2010), although others defended that the relation between ITCZ location and the Sahel rainfall was feeble (Miles & Follard,

1974; Nicholson, 1981). Nevertheless, the link between the ITCZ determined by the rainfall magnitude is clear. After these misunderstandings on the ITCZ relationship, Nicholson (2013) showed that the interannual variability is linked to the fluctuation in the upper-level circulation features. Furthermore, two additional low-level westerly jets are included in the rainfall-producing system, the African Westerly Jet (AWJ) over the continent and the West African Westerly Jet (WAWJ). These features also contribute to the interannual variability of the WAM system climatology.

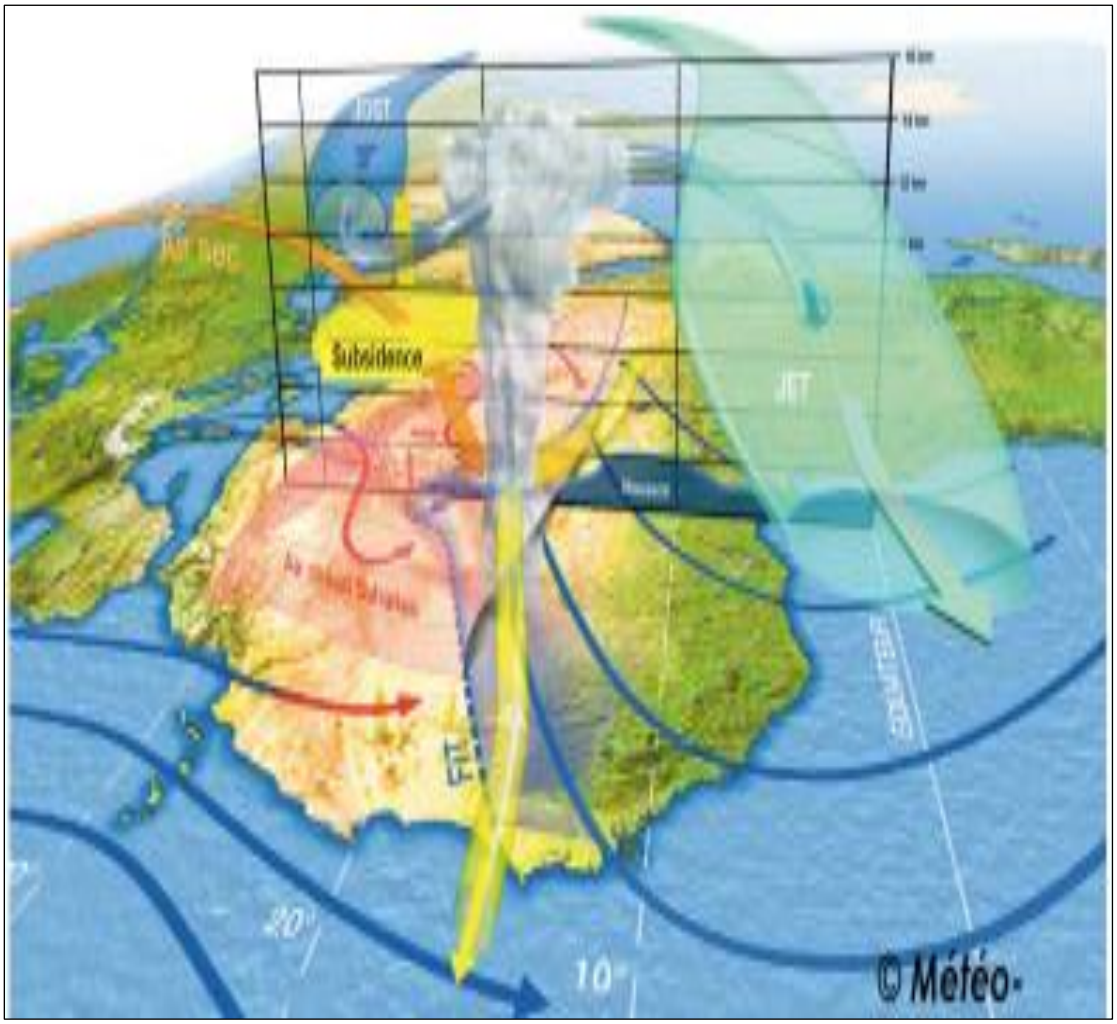

Figure 2.1: Conceptual design of the West African monsoon showing the inter connec tion between different rainfall producing features.

NOTE: FIT represents ITD, "Air Chaud Saharien" represents "Warm Saharian Air", JEA repre sent AEJ, JET represents TEJ and "Air sec" represents "Dry Air" (Source: Lafore et al., 2010).

2.1.1 African Easterly Jet

The African Easterly Jet (AEJ) is one of the essential features with strong zonal components of wind characterized by a core up to 10ms^{-1}, generally found between 600–700 hPa, moving from East to Western Africa (Lafore *et al*., 2010; Sylla *et al*., 2013; Cook, 1999). The jet extends between 30° W et 30° E during the summer period (Figure 2.2) and is recognized to have two central cores such as the western and eastern cores, which periodically fuse (Hall *et al*., 2006). Nicholson & Grist (2003) reported that the mean feature of the AEJ is more pronounced between May to June, whereas the mean core speed of the western (10° W to 10° E) and eastern (10° E to 30° E) part is in the range of 12ms^{-1} and 10ms-1, respectively. They also argued that the core of this jet could reach 16ms^{-1} and may lessen during the monsoon period in the Sahel. The western part is more important and relatively stable, with a latitudinal location around 6° N. At the same time, for the eastern core, the jet responses on average around 13° E during the boreal summer but could fluctuate between 20° N to 10° N during some wet and dry years, respectively.

The AEJ is mainly considered a result of thermal wind from the lower tropospheric meridional temperature gradient (baroclinicity; Cook, 1999). Strongly linked to the thermal wind balance, the baroclinicity decreases to zero between the surface and the level of the AEJ. Thorncroft and Blackburn (1999) indicated that the decrease in baroclinicity with height is harmonious with the meridional variations in convection, with most convection prevalent equatorward of the AEJ and dry convection prevalent poleward of the AEJ. It is also important to note that the convection activities are linked to the meridional gradient of temperature, which is strongly controlled by the gradients of surface proper-

ties, for instance, soil humidity gradient (Cook, 1999); albedo, vegetation, and evapotranspiration (Wu *et al*., 2009). Therefore, the AEJ is mainly maintained by deep and shallow meridional features connected with the monsoon. These conditions are driven by local Hadley circulations and the Saharan Heat Low (SHL), respectively (Cook, 1999; Thorncroft &Blackburn, 1999).

2.1.2 African Easterly Waves

The African Easterly Waves (AEWs) grow and expand on the AEJ over tropical North West Africa during summer in the northern hemisphere. The AEWs are the main driver of convection and rainfall (Diedhiou *et al*., 1998; Nicholson & Grist, 2003) over West Africa. Their presence was discovered during the first half of the twentieth century from African observational data, which indicated different cycles up to 3-day intervals (Piersig, 1944). In the field of forecasting, it was noted that the same perturbation that conveyed this cyclicity was displacing westward into the Atlantic Ocean, growing into a tropical cyclone (Simpson *et al*., 1968). Besides, studies have discovered that AEWs are the predominant synoptic scale atmospheric feature incorporated in the WAM system and tropical Atlantic during the northern hemisphere summer (Burpee, 1974; Karyampudi & Carlson, 1988).

The AEWs are generally detected at the level of the AEJ around 650hPa. Carlson (1969) carried on synoptic analyses of different AEWs during the summer of 1967 and found a wave-like disturbance to the wind field around 700hPa, together with two cyclonic vortices around 925hPa. Most AEWs are generated between 15°E and 30°E over eastern Africa and spread westward alongside the WAM and in the tropical Atlantic,

where they are a general pioneer of cyclones in the tropics (e.g., Avila and Pasch, 1992; Mekonnen *et al*., 2006). In some examples, AEWs have been detected to expand consistently in the west, reaching the eastern Pacific Ocean (e.g., Avila and Pasch, 1992). Furthermore, several studies attempted to give more information on the characteristics of the AEWs; for instance, Carlson (1969) mentioned that the AEWs have wavelengths ranging between 2000 to 4000 km with a speed of propagation up to 8 ms^{-1} and a period in the range of 3 to 5 days. Burpee (1972) compared the AEWs to a tilt from the perturbation in the south between the surface and the level of AEJ and in the west at the upper side. Reed *et al*. (1977) established the first typical structure ("composite") of the eastern waves. Diedhiou *et al*. (1999) have generalized this analysis to many years (put a figure, Rodrigue), distinguishing the lower waves with a period in the range of 6 to 9 days (Cadet & Houston, 1984; Viltard *et al*., 1997). Therefore, a model needs to reproduce this low-level feature over WA in order to perform well.

2.1.3 Tropical Easterly Jet

The Tropical Easterly Jet (TEJ) is a zonal jet at the upper troposphere, generally located between 5°N et 10°N around 200hPa (Figure 2.2) and grows due to a strong north-south temperature gradient between the Himalayan plateau and the Indian Ocean. It extends from the South China Sea to the west coast of Africa and reaches a speed of up to 25 ms^{-1} over West Africa (Krishnamurti, 1971). The jet is conserved by both the zonal symmetrical part of the thermal meridional gradient between the Tibetan Plateau and the upper troposphere over the Indian Ocean (Flohn, 1964; Murakami *et al*., 1970) and by the zonal thermal asymmetry due to the land-sea contrast (Kanamitsi *et al*., 1970). Therefore, the TEJ originates from divergent tropical circulation associated with the

north-south Hadley and the east-west Walker circulation. The jet develops over Africa due to the divergent and anticyclonic circulation generated in altitude by the deep convection.

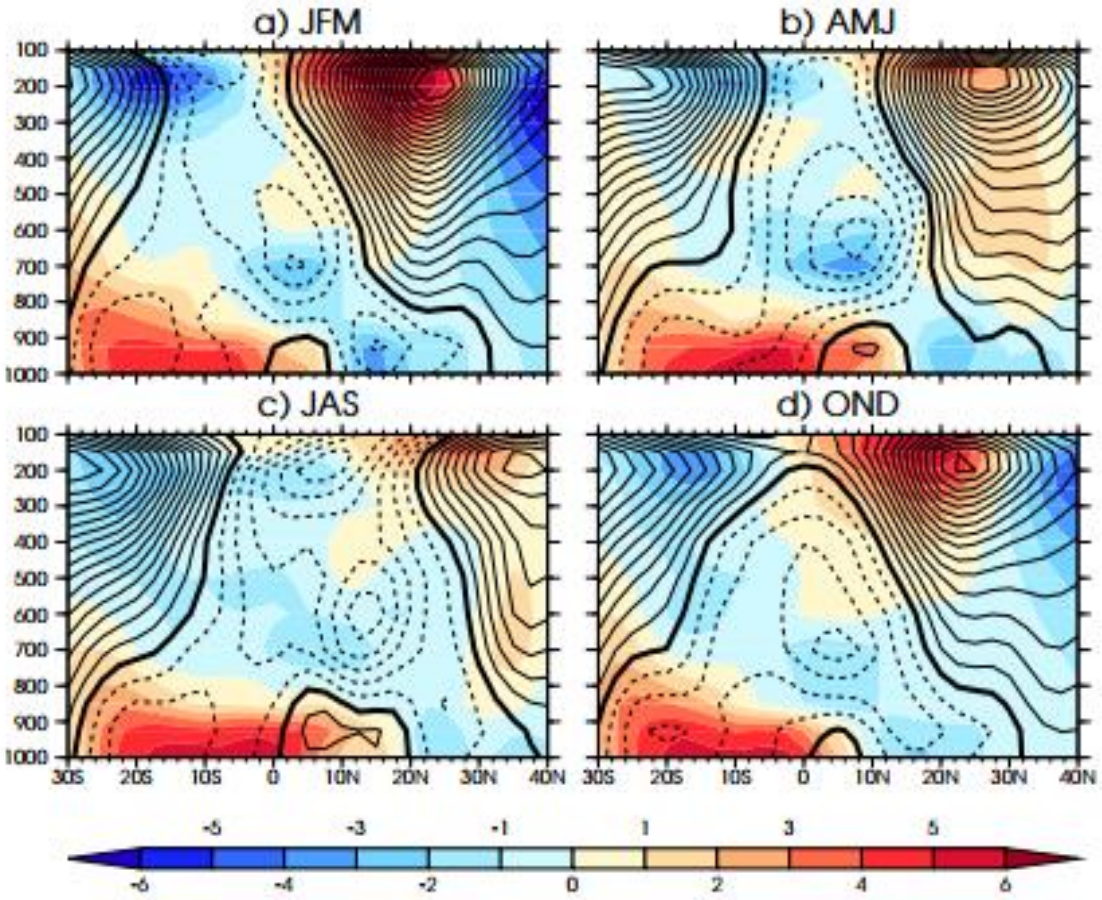

Figure 2.2: Climatology of meridional (shaded - m.s-1) components (a) and zonal (contour 2m.s-1) components (b) of wind, the zero contour in bold lines, the positive values in continue lines and negative in discontinue, averaged between 10◦O–10◦E (Roehrid, 2010*).*

The strength of the TEJ is associated with the soil conditions (wetness, dryness) over Sahel, Ethiopia, and India (Grist & Nicholson, 2001; Hulme & Tosdevin, 1989; Nicholson, 2008; Pattanaik & Satyan, 2000) as well as reduce (increase) in cyclone events in the Bay of Bengal (Rao *et al*., 2004). Its function on rainfall in equatorial Africa is crucial in both northern latitude's spring and autumn, which responds by impacting the mean climate of West Africa (Besler, 1984; Flohn, 1964; Webster & Fasullo, 2003). The jet was found over the east-west expanse of Africa with a mean speed of about $30ms^{-1}$ during August of some wet years over the Sahel (Nicholson, 2013). A decrease in the speed and extent of the TEJ led to dryer conditions in the Sahel between the 1950s and 1990s (Nicholson & Grist, 2001; Rao *et al*., 2004). In addition, TEJ is found to be associated with the cooler upper-troposphere tropical temperature gradients (Nicholson, 2008). Furthermore, Nicholson & Grist (2003) have shown clearly the relationship between the TEJ and rainfall closer to the upper-level divergence linked with the origin of the jet. This divergence derives from the essential meridional branches linked to the TEJ over Africa.

2.1.4 African Westerly Jet

Grist & Nicholson (2001) argued that the African Westerly Jet (AWJ) only appears through some years. It develops from month to month during the wet years in the Sahel. When this jet appears during the boreal summer (July to September), its mean speed is about $10ms^{-1}$ and can expand smoothly into the mid-troposphere. However, this jet disappears during dry years in the monthly mean, and the wind moves easterly beyond the 850 hPa level (Nicholson & Grist, 2003). Moreover, the AWJ westerly speeds range between 2 to $4ms^{-1}$, and its maximum activity is found at the low-level monsoon flow,

about 925 hPa. Nicholson & Grist (2003) demonstrated that the AWJ differs from the result of the southwest monsoon flow; they argued that its core is located above the monsoon layer. During the peak of the rainy season over the Sahel, the core of the AWJ correlates well with the surface pressure gradient in the area located between the latitude of 20° S and 20° N (Nicholson & Grist, 2003). Nevertheless, the jet does provide geostrophic feedback to this gradient over this location, and the region is tight to the equator for a geostrophic balance. The jet develops in a narrow belt where the cross-equatorial pressure gradient is lowest. Its source is associated with the inertial instability that increases in response to this pressure gradient, which increases both the jet and the rainfall (Nicholson & Webster, 2007; Tomas & Webster, 1997).

2.1.5 West African Westerly Jet

The West African Westerly Jet (WAWJ) is a low-level westerly jet over the Atlantic Ocean. It is described to appear as a near-surface wind maximum over the equatorial Atlantic and is identified from May to September (Grodsky *et al*., 2003). This jet is necessary around 10°N and confined in the region where the trade winds converge. The jet differs from the AWJ because it appears at the surface in response to the mid-troposphere westerly wind maximum with speed ranging between 10-15ms^{-1} (Grist & Nicholson, 2002). The WAWJ plays a crucial role in transporting moisture from the Atlantic to the continent in the area located between 8°N to 11°N. Though this jet does not exist over this location, it has been demonstrated that a strong correlation exists between the speed of the WAWJ and the western Sahel moisture transportation (Tomas & Webster, 1997). This moisture transport has much more significant decadal-scale variability in the rainfall than that associated with the southwest monsoon. Therefore, it may carry

much moisture in years when the monsoon weakens (Flaouna *et al*., 2012). The WAWJ is also crucial to stabilize the regional vorticity balance by introducing strong relative vorticity gradients (Nicholson, 2013).

2.1.6 Mesoscale Convective system

Convection is essential for forming rainfall over the tropics because it contributes to forming essential clouds, such as cumulonimbus clouds, which deliver the majority of seasonal rainfall over West Africa. Although the MCSs are favored by local, near-surface conditions of necessarily sensible heat flux, high humidity, and dry lapse rate, the installation of this local system is favored by mesoscale rising (Couvreux *et al*., 2012; Nicholson, 2012). These systems generate convective rainfall generally during the afternoon, with most convective activities lasting 3 hours or less over land (Ricciardulli & Sardeshmukh, 2002; Nicholson, 2012).

The main problem with convection in Sahelian West Africa is its generation and relationship with AEWs (Nicholson, 2012). Convective events tend to rise in the lee of elevated terrain, compatible with thermal forcing from upper-level heat sources (Laing *et al*., 2008). The spread of the MSCs is mainly linked with moderate low to mid-tropospheric shear, which fluctuates with a change in the latitude of the AEJ displacement and with the phase of the WAM (Nicholson, 2012). MCSs are most of the cases associated with AEWs. Nevertheless, the position within the wave relies on factors such as the longitude, latitude, and period of the wave. This aspect was evaluated by (Mohr & Thorncroft, 2006). They independently considered feeble and convective solid systems over the Sahel as the lowest and highest scores in the intensity distribution. The highest position of the robust systems

moved during the rainy season, following the seasonal displacement of the AEJ, and the weak systems are placed around 10°N. In addition, other factors that boost the increase of the MCSs include intense potential temperature strong wind shear near the AEJ (Nicholson, 2012).

2.2 Modeling of the West African Monsoon

Numerical models are valuable tools for understanding the complex interaction between multiscale processes (Sylla *et al*., 2013). Therefore, these models can be used for a better understanding of the West African monsoon. However, even though simulations have been performed using Global Climate Models (GCMs), the model's horizontal resolution is still challenging due to the coarse resolution (100km) and, therefore, causes uncertainties in the measurement that limits the precision of capturing the characteristics of the WAM (Hourdin *et al*., 2010; Sylla *et al*., 2010; Xue *et al*., 2010). This limitation in GCMs pushes people to use Regional Climate Models (RCMs). The high resolution of RCMs has improved the representation of the fine-scale forcing and land surface proprieties, including topography, vegetation change, and land surface heterogeneity which represent the physical feedback to general and regional climate signals (Rummukainen, 2010; Sylla *et al*., 2013; Tomaffo., 2022). However, studies reported that the RCMs have issues to correctly simulate the WAM rainfall due to boundary conditions (Pal *et al*., 2007; Klutse and Sylla., 2012; Odoulami *et al*., 2019). Therefore, new models must be tested over the region to see their ability to capture the WAM rainfall systems. For that, the stretched grid models are being used in atmospheric science. These models do not need boundary conditions and can be used at high resolution (e.g., Fox-Rabinovitz

et al., 2006; Fox-Rabinovitz *et al*., 2008; Harris *et al*., 2016; Abiodun *et al*., 2011; Martini *et al*., 2015; Smith *et al*., 2013).

2.2.1 Modeling the WAM using Global and Regional Climate Models

Several studies have discussed the strengths and weaknesses of global climate models (GCMs) when it comes to simulating atmospheric systems and rainfall over WA (Ajibola *et al*., 2020; Akinsanola *et al*., 2018; Chagnaud *et al*., 2020; Cook and Vizy, 2006; Hourdin *et al*., 2010; Matte *et al*., 2017; Sylla *et al*., 2012, 2013; Xue *et al*., 2010). For instance, by applying the 5th generation European Centre Hamburg General Circulation Model (ECHAM5) over WA, Sylla *et al*. (2012) showed that the model captures the characteristics of rainfall events over the entire Guinea Coast. After evaluating CMIP6 GCMs, Ajibola *et al*. (2020) found that these models can reproduce wet and dry conditions over WA. However, the GCMs typically have issues in reproducing the main WAM features, probably due to the coarse grid spacing that is usually used (Chagnaud *et al*., 2020; Hourdin *et al*., 2010; Sylla *et al*., 2010, 2013; Vizy & Cook, 2006; Xue *et al*., 2010). For example, Cook and Vizy (2006), after evaluating several GCMs, found that most models fail to properly represent the precipitation over WA. Xue *et al*. (2010) evaluated how well several GCMs simulate the characteristics of the WAM and found that most models struggle to reproduce the intensities of the AEJ and the tropical easterly jet (TEJ).

Arguing that using regional climate models (RCMs) with a higher resolution than GCMs may be a solution to the resolution problem, some studies have employed and evaluated RCMs over WA (Abiodun *et al*., 2010; Afiesimama *et al*., 2006; Diallo *et al*.,

2012; Klutse *et al*., 2016; Odoulami *et al*., 2019; Pal *et al*., 2007; Sylla *et al*., 2010, 2012; Tamoffo *et al*., 2022). Sylla *et al*. (2010) found that RegCM3 realistically simulates the precipitation over the region, but other studies noted some uncertainties in the simulation (Browne & Sylla., 2012; Odoulami *et al*., 2019; Pal *et al*., 2007). Pal *et al*. (2007) found that RegCM3 produces excess precipitation over WA. Odoulami *et al*. (2019) found that the models generally overestimate the magnitudes of the rainfall indices over the Guinea Coast. Browne & Sylla (2012) attributed the precipitation biases in RCMs to boundary condition problems. Hence, the attempt to address the low-resolution problem of GCMs and the boundary conditions problem of RCMs has prompted several studies to utilize stretched-grid GCMs (SG-GCMs) (e.g., Abiodun *et al*., 2011; Fox-Rabinovitz *et al*., 2006, 2008; Harris *et al*., 2016; Martini *et al*., 2015; Smith *et al*., 2013).

2.2.2 Modeling using Stretched Grid Models

The idea of SG-GCMs was initially proposed by Schmidt (1977) for spectral models and Staniforth and Mitchell (1978) for grid-point models. Fox-Rabinovitz *et al*. (2008) showed that SGMIP-2 (Stretched-Grid Model Intercomparison Project, phase 2) models provide a good simulation of the monsoon core in the United States. Smith *et al*. (2013) applied the Conformal Cubic Atmospheric Model (CCAM) over the New Guinea region and showed that the pattern of the simulated precipitation variance replicates the observed pattern. Harris *et al*. (2016) found that the Geophysical Fluid Dynamics Laboratory (GFDL) with a stretched grid improves the representation of the finer-scale simulation, and Fox-Rabinovitz *et al*. (2006) argued that the SG-GCMs simulate atmospheric features well with a high resolution. Abiodun *et al*. (2011) demonstrated how the Non-

Hydrostatic Atmospheric Climate Model with Grid Stretching (CAM-EULAG) improves the simulation of WAM features and rainfall over West Africa. Several studies have demonstrated the reliability of MPAS in the simulation of atmospheric features (Heinzeller *et al*., 2016; Kramer *et al*., 2020; Maoyi & Abiodun, 2021; Martini *et al*., 2015; Park *et al*., 2014; Zhao *et al*., 2019). Lui *et al*. (2021) found that MPAS performs better than Weather Research and Forecasting (WRF) model in reproducing the western North Pacific tropical cyclone. Heinzeller *et al*. (2016) found that MPAS performs well in reproducing the rainfall pattern over WA. However, only Abiodun *et al*. (2011) and Heinzeller *et al*. (2016) have used the SG-GCM approach over WA. Both studies had a limited simulation period. These studies did not investigate the sources of the model biases. Thus, despite the potential of MPAS for hindcasting over WA, there is no information on how well the model captures the characteristics of the WAM system. Therefore, before using MPAS with a stretched grid (variable resolution), it is essential to look at how the model performs when it is used with a regular grid (uniform resolution).

2.3 Selected SST effect in simulating the WAM

It has been demonstrated by several studies how SST affects Sub-Saharan summer rainfall. For instance, the recognized dipole between Sahelian and Gulf of Guinea (GG) precipitation (Janicot, 1992; Rowell *et al*., 1995; Ward, 1998) has been related to Tropical Atlantic variability. Several studies (Janicot *et al*., 1998: Vizy and Cook, 2002; Paeth & Friederichs, 2004) have shown how normal SST in the GG is linked to positive precipitation anomalies in the coastal area and negative precipitation anomalies over the Sahel. Some of these findings found the southward shift of the tropical rain belt as the cause of the dipolar response of the precipitation (Janicot *et al*., 1998), while others

(Shinoda & Kawamura, 1994; Vizy & Cook, 2002) argued that other aspects related to the dynamic, which is crucial to this precipitation response. Furthermore, Vizy and Cook (2002) have simulated the dipolar response to SST anomalies in the Tropical Atlantic Ocean using a Mesoscale Climate Model (MCM). Nevertheless, some simulations performed with Atmospheric General Circulation Models (AGCM) fail to produce the same feedback (Vizy & Cook, 2001; Giannini *et al*., 2005). (Nicholson, 2009; Nicholson & Webster, 2007) shown that the dipole precipitation anomalous depends on the conditions of conditional inertial instability criteria West Africa. These conditions are filled in years where Monsoon is vigorous; this particularity of the Monsoon coincides with wet Sahelian years, which are also characterized by a firm surface westerly jet that increases the horizontal and vertical wind shear, conducting to a northward shift of the AEJ. The progression of the westerly jet is directly related to the cross-equatorial pressure gradient and, thus, indirectly to the SST pattern (Nicholson and Webster, 2007, Losada *et al*., 20010). Janicot *et al*. (2001) argued that the relation between the Sub-Saharan summer rainfall and SST includes different oceanic basins at different periods thus, the first issue discovered in the above-referenced studies is the utilization of observations involving the dry and wet Sahelian episodes in the same analysis and so different oceanic impacts synchronous with the Equatorial mode.

2.4 Temperature extreme and heatwaves simulation over West Africa

Several studies have provided evidence for considerable warming in West Africa and the Sahel in the recent past. New *et al*. (2006) showed that most stations in West Africa reveal positive trends in the minimum and maximum temperature over the period 1961–2000. That study also found increases in both the number of hot days and of cold days.

Evaluating reanalyses and CORDEX models, Adeniyi and Oyekola (2017) found that the magnitude of the frequencies of heat waves in West Africa has increased. Oueslati *et al*. (2017) found that heat waves are spatially increasing with high intensity. Similar findings are reported concerning increases in temperatures and the frequencies of heat waves, particularly in the Sahel (Ringard *et al*., 2016; Russo *et al*., 2016; Dosio, 2017). Further increases are projected for the future. From results based on CMIP5 model simulations, Ringard *et al*. (2016) reported significant increases in heat waves for the Sahel in all applied scenarios.

An increase in the severity and frequency of droughts and heat wave events can lead to the loss of human lives and the destruction of crops which negatively impact the agriculture yields then leading to famine. Extreme temperatures and heat waves strongly affect the socio-economic conditions in various sectors, such as agriculture, infrastructure, and energy (Lobell *et al*., 2011; Coumou & Rahmstorf, 2012; Perkins *et al*., 2015). A weak economy, inefficient policy, and a limited resilience increase the vulnerability. Drought, excessive rains, or heatwaves during the growing season can potentially diminish crop yield, especially in the Sahel, where water is a particularly determining element for the growth of the crops (Ahmed *et al*., 2015). Hence, modeling tools capable of simulating extreme present and expected future climate conditions have gained increasing importance for the support of policymakers.

2.5 Research needs

West Africa is one of the regions where people are challenged with the multiform level of risk related to climate change and variability. Therefore, investing in quality

scientific research through how the contemporary climate model simulates the West African Monsoon is crucial for the region. This will allow us to understand and discover the weaknesses of the climate model in simulating the WAM, the most critical rainfall-producing system for Sub-Saharan countries. Long-term Observations and measurements of weather parameters during the WAM period (such as temperature, rainfall, relative humidity, wind speed, and direction) can be used to look at any change in the monsoon system. However, the networks of the observed data in West Africa could be better, and the deficiency of data makes it very complicated to understand the region's climate.

A classical use of global and regional models has been for elementary research on atmospheric processes (Tomkins, 2011). The model can accomplish a historical or future evaluation of atmospheric processes. However, the current climate models are imperfect due to broad uncertainties initiated through initial data, parametrization of subgrid scale processes, model domain, spin-up, and model dynamics. These uncertainties may not be ended definitively but can be weakened to make the model's results closer to reality (Gbode *et al*., 2015). Thus, perpetual model development is needed as new procedures and technology arise. So, the uncertainties in the climate model are a significant threat within atmospheric science as researchers have tried to resolve the issues. Research is still in progress to reduce model biases which limit the consideration of the model's information in supporting the policymakers' decision.

The role of research on climate models is to evaluate the model on how it reproduces atmospheric processes and recommend ways for their development. Several Climate

models have been identified, and their outputs have been used to guide policy formulation and decision-making in climate-related sectors of the economy. Therefore, research on climate model development, evaluation, and application is crucial for human life in the contemporary world. Also, the availability of computational resources is increasing exponentially the number of models used in the scientific community. Nonetheless, these aspects of research are yet to be fully mature, especially in a data-sparse region like Africa. Therefore, it is crucial to continuously evaluate the available model to see their degree of performance in simulating atmospheric processes and propose ways to model development. Also, there is still a gap in fulfilling the increasing demand for accurate simulation of the monsoon system because of its impact on the ecosystem which in turn influences the life of the nation over the World and West Africa in particular (Janicot *et al*., 2008; Mounier *et al*., 2008; Redelsperger *et al*., 2006). This concern is strengthened by the scarcity of observational data networks, which limits our understanding of the most critical atmospheric circulation, denoted monsoon system, which provides most of the rainfall.

Nevertheless, previous studies were merely descriptive about simulating the WAM. Thus, the added value of this study is to test the contemporary model (MPAS) and propose a way to improve the simulation of critical atmospheric processes. Also, none studies investigate the model ability reproduces the monsoon rainfall-producing system and temperature and precipitation based extreme events. Hence, there is a need to consolidate previous works by testing new modeling tools in simulating extreme, present, and future climate conditions, which significantly support policymakers.

CHAPTER THREE

3.0 METHODOLOGY

3.1. Description of the study areas

The study is conducted in WA (Figure 3.1). Due to climatic differences, the region is sub-divided into three zones: the Guinea Coast zone (4–8°N), the Savanna zone (8–11°N), and the Sahel zone (11–16°N). These areas have been considered in previous studies (Abiodun et a., 2011; Ajibola *et al*., 2020; Gbode *et al*., 2019; Sylla *et al*., 2010). The Guinea Coast zone is humid, with an annual rainfall ranging from 1575 to 2533 mm (Gbode *et al*., 2019; Oguntunde *et al*., 2011), and the Savanna zone is a semi-arid area, with an average annual rainfall in the range of about 897–1535 mm. The decrease in rainfall over the Savanna zone is due to the monsoon jump, which is the observed abrupt latitudinal displacement of maximum precipitation from the Guinea Coast to the Sahel zone around June (Hagos & Cook, 2007b; Le Barbé *et al*., 2002; Lebel *et al*., 2003; Sultan & Janicot, 2000). The northward displacement of the rainfall belt thus initiates the recognized "little dry season" between July and August along the Guinea Coast (Gbode *et al*., 2019). The Sahel zone is characterized by a single peak season from July to September, with a maximum in August that coincides with the northernmost location of the Intertropical Discontinuity (ITD) from 21–22° N (e.g., Nicholson, 2013). This area is arid compared to the two zones mentioned above, and the Sahel zone has an average annual rainfall between 434 and 969 mm (Gbode *et al*., 2019; Oguntunde *et al*., 2011). The focus on the June-July-August (JJA) season is because it provides the most significant precipitation amounts over WA, especially over the Sahel zone (Nicholson, 2013).

Nevertheless, the results of the performed simulations are analyzed in two areas in the Sahel region, SAH_W and SAH_E, and one area at the coast of Guinea, GUI_C, as well as for the entire region (Figure 3.2). There are no standard evaluation areas available so far for West Africa and the Sahel. However, the areas SAH_W and SAH_E have been used by several studies and thus allow putting the results in the context of previous investigations (Dosio *et al*., 2021a, 2021b; Smiatek & Kunstmann, 2023). The model meshes used in the simulation are shown in Figure 3.3. The Quasi-uniform meshes of 60-km mesh have 163842 horizontal cells.

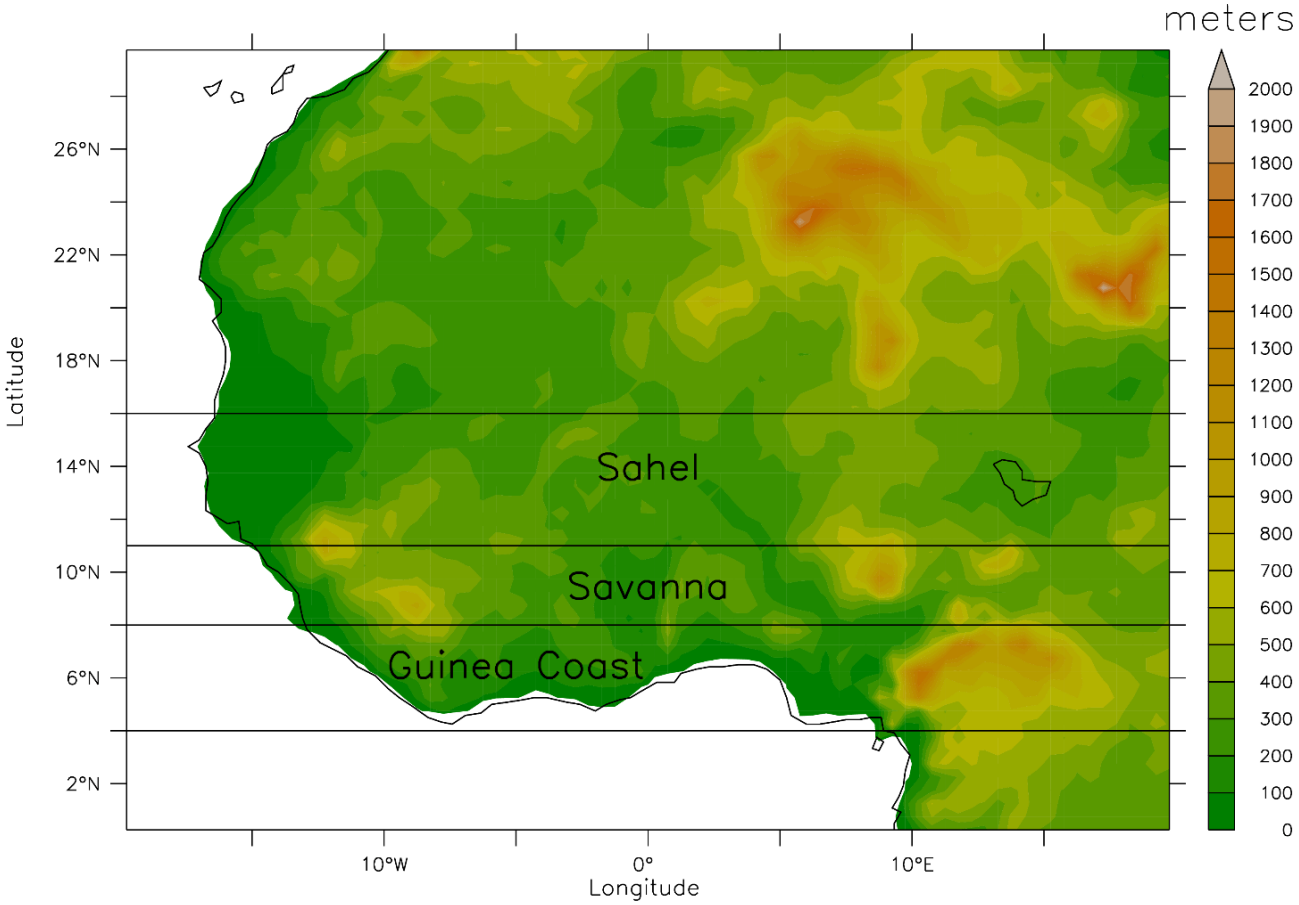

Figure 3.1: Map of West Africa showing the topography of the investigated area narrowed in three sub-regions: Sahel, Savana, and Guinea Coast (Adapted from Omotosho and Abioudun, 2010)

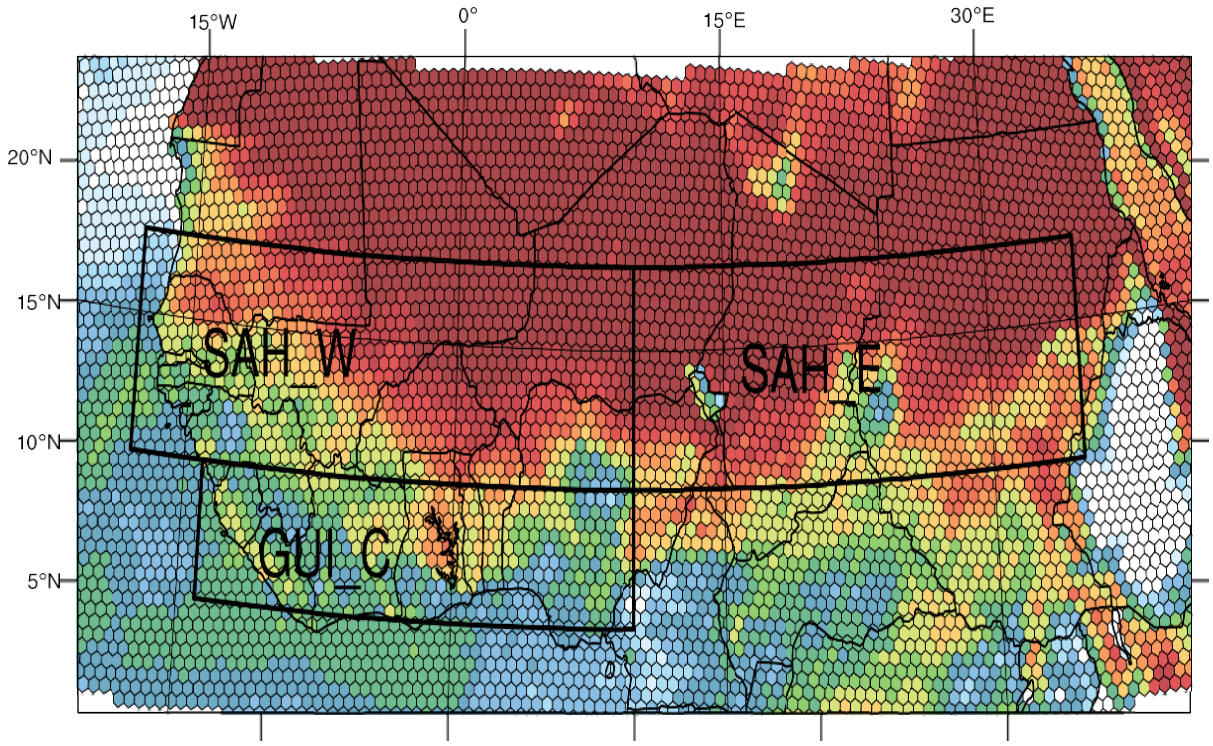

Figure 3.2: MPAS 60 km mesh and investigated areas SAH_W, SAH_E and GUI_C for the second run. Simulated 2m temperature 01.07.2010:12:00 UTC, Dosio et al., 20121)

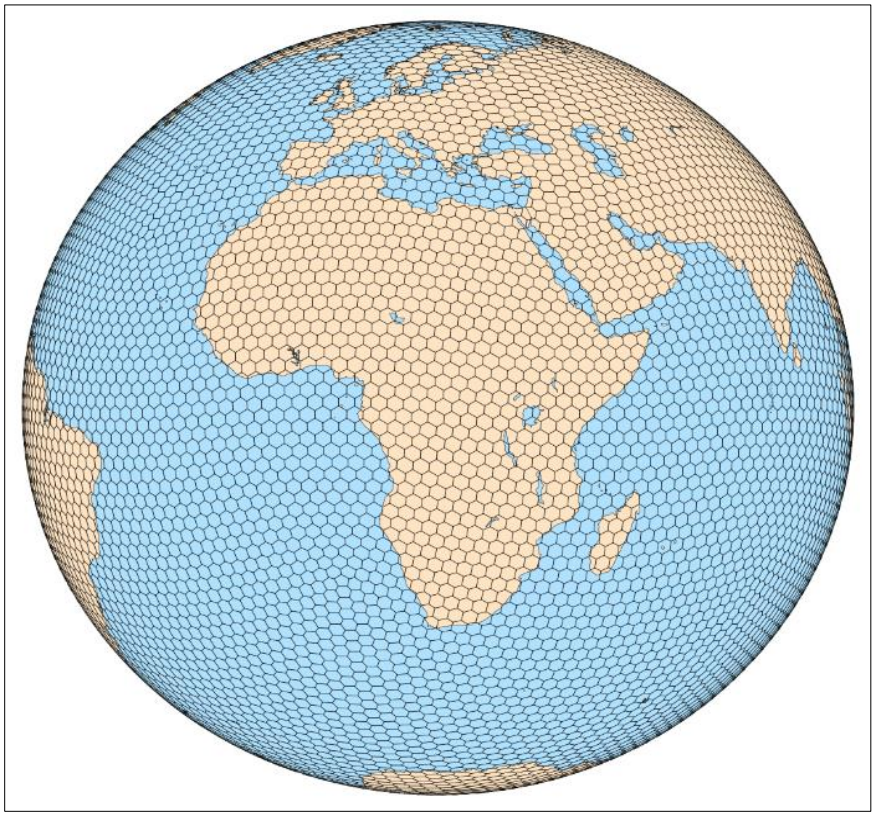

Figure 3.3: The quasi-uniform mesh at 60 km resolution used for MPAS simulation.

3.2 Data

3.2.1 Observations, Reanalysis, and modeled data

Different observations, reanalyses, and model simulation datasets are analyzed for this study. The observed datasets provide only precipitation and temperature data. They are either gauge-based, satellite-derived, or rain-gauge (Table 3.1), including the Climate Hazards Group InfraRed Precipitation with Stations (CHIRPS), the Climate Hazards Group InfraRed Temperature with Stations (CHIRTS), the Climate Research Units (CRU), and the Climate Prediction Center (CPC). Variables such as zonal and meridional winds component (u, v), vertical wind velocity, pressure, and geopotential height (z) were obtained from reanalyses (Table 3.1). These reanalyzes include the European Center for Medium-Range Weather Forecasts (ECMWF) reanalysis v5 (ERA5), Japanese 55-year Reanalysis (JRA-55), Climate Forecast System Reanalysis (CFSR), the Modern-Era Retrospective Analysis for Research and Application, version 2 (MERRA-2), and National Centers for Environmental Prediction v2 (NCEP-2). To put MPAS model in the context of GCMs, four Coupled Model Intercomparison Project Phase 6 (CMIP6, Table 3.2) are also compared. These data are archived on the Earth System Grid Federation (ESGF) website under CMIP6 HighResMIP (https://esgf-node.llnl.gov/search/cmip6/) (Ajibola *et al.*, 2020). All the datasets were interpolated at 0.5 ° x 0.5 ° resolution using the first-order conservative remapping method (Jones, 1999).

Table 3.1. Observed and Reanalysis data applied in the present study (period used are 1981-2010 and 1990-2019)

`Dataset	Name	Horizontal resolution	References
CHIRPS	Climate Hazards Infrared Precipitation with Stations	0.05°	Funk *et al*. (2015)
CHIRTS	Climate Hazard Group Infrared Temperature with Station Data	0.05°	Funk *et al*. (2019)
CPC	Climate Prediction Center	0.5°	Xie *et al*. (2007)
CRU	Climate Research Unit	0.5°	Harris *et al*. (2020)
GPCC	Global Precipitation Climatology Center	0.5°	Schneider *et al*. (2022)
ERA5	European Center for Medium-Range Weather Forecast (ECMWF)	0.25°	Hersbach *et al*. (2020)
CFSR	Climate Forecast System Reanalysis	0.5°	Saha *et al*. (2014)
JRA-55	Japanese 55-year Reanalysis	0.5625°	Kobayashi and Iwasaki (2016)
MERRA-2	Modern-Era Retrospective Analysis for Research and Application, version 2	0.5x0.625°	Gelaro *et al*. (2017)
NCEP-2	National Centers for Environmental Prediction v2	1.875°	Kanamitsu *et al*. (2002)

Table 3.2. Details of CMPI6 data used in this study (period is from 1981-2010)

Acronyms	Institution	Horizontal resolution	Country
CNRM-CM6-1	Centre National de Recherches Météorologiques	0.5°	France
MOHC-HadGEM3-GC31-HM	Met Office Hadley Centre	0.35°×0.2°	United Kingdom
MPI-M-MIP-ESMI.2-XR	Max Planck Institute for Meteorology	0.935°	Germany
EC-EARTH-Consortium	European EC-Earth consortium	0.35°	United Kingdom

3.3 Model setup for the long-term runs simulation

3.3.1 MPAS model configuration

The applied meteorological model is the Model for Prediction Across Scales (MPAS), which is based on unstructured Voronoi meshes and C-grid discretization (Thuburn *et al*., 2009; Ringler *et al*., 2010). MPAS-atmosphere (Skamarock *et al*., 2012), used in the present study, is a global, fully compressible non-hydrostatic model (Klemp, 2011). The model is run at an approximately 60-km resolution mesh with a total of 163,842 cells, applying the mesoscale reference physics suite, 55 vertical levels up to a height of 30 km, and 4 soil levels. The land–surface physics component is the Community Noah Land Surface Model (Noah-LSM) (Chen *et al*., 1996).

The first run is a continuous simulation, initialized with the NCEP CFSR data available from https://rda.ucar.edu/datasets/ds093.1/. MPAS was set to periodically update with 6 hours of CFSR sea surface temperature (SST) and sea-ice data. The model simulation started from 1st December 1980 to 1st January 2011. Therefore, the months of December 1980 and January 2011 are considered spin-up; only data from January 1981 to December 2010 was used for the study.

3.3.2 Model physics

Table 3.3 shows the associated parameterization schemes of the standard model configuration. For instance, the new Tiedtke (nTDK; Tiedtke, 1989; Zhang *et al*., 2011) is a mass flux scheme with updrafts and downdrafts. The WDM6 is a six-class scheme that allows the investigation of the aerosol effects on cloud properties and precipitation

processes with the prognostic variables of cloud condensation nuclei (CCN), cloud water, and rain number concentration (Hong *et al*., 2010). The WRF/Noah LSM Coupled system consists of an actual number of comprehensive terrestrial data sets, their processing onto the WRF grid through WRF/SI and Real routines, and the Unified Noah LSM as part of the WRF physics package. YSU Planetary Boundary Layer is a non-local closure scheme with a parameter that permits the augmentation of vertical mixing and removal of air from the bottom of the PBL, this is applicable in an impartial boundary layer where the vertical gradient of potential temperature is null (Hong *et al*., 2006). The Monin–Obukhov combines near-surface observations such as turbulent kinetic energy production, surface roughness, and surface fluxes (Monin & Obukhov, 1954). The Radiation (long-wave, short-wave) scheme uses a constant value for carbon dioxide, representing the year's situation around 2004. The static input data are from the MODIS 20-class land cover, which depends on the global land cover climatology collected in 2001–2010 at 500 m resolution (Broxton *et al*., 2014) and Global Multi-Resolution Terrain Elevation Data) GMTED2010) (Danielson & Gesch, 2011) topography. The albedo and vegetation indices are updated with the monthly climatology of MODIS satellite images.

Table 3.3. Parametrization schemes used

Parametrization	Scheme
Convection	New Tiedtke
Microphysics	WSM6
Land surface	Noah-LSM
Boundary layer	YSU
Surface layer	Monin–Obukhov
Radiation, LW	RRTMG
Radiation, SW	RRTMG
Cloud fraction for radiation	Xu–Randall
Gravity wave drag by orography	YSU

3.3.3 Model evaluation methods

Several statistical methods can be used to evaluate model performance. Nevertheless, more than one method is required to resolve all needs in model evaluation. For that, it is crucial to consider various performance statistics and grasp the information they might give. In this study, some statistics on the model results to investigate the degree of correlation on systematic error, and accuracy of the model compared to observations are used, as detailed below.

Among the statistics used, one of the most prominent methods is the spatial correlation coefficient (r), which assesses the strength of the relationship between the model and observations.

$$r = \frac{1}{(n-1)} \sum_{i=1}^{n} \left(\frac{M_i - M}{\sigma M} \left(\frac{O_i - \bar{O}}{\sigma O} \right) \right) \quad 3.1$$

Where *O* represents Observation or Reanalysis, M model output, σ standard deviation, and n number of data points in the series.

Another statistic is the Mean Bias which determines the mean error between model and observation regardless of whether it is over or underestimation. It also conserves the units of the variables being quantified.

$$MB = \frac{1}{n} \sum_{i=1}^{n} (M_i - O_i) \quad 3.2$$

The last statistic used is the Root Mean Square Error (RMSE) which measures the error magnitude but gives greater weight to the larger error.

$$RMSE = \sqrt{\frac{1}{n} \sum_{i=1}^{n} x_i - y_i} \quad 3.3$$

Where x_i indicates the estimated value of rainfall at point i while y_i is the observed value at the same point, and N represents the total number of points.

The performance of MPAS to simulate the seasonal rainfall will therefore be investigated through the WAM features; for instance, the monsoon flow, the AEJ, the TEJ, and the upward motion at the pressure level at the jets that are supposed to be formed. The cause the of biases in MPAS are diagnosed (temperature gradient, thermal wind, geostrophic wind) in comparison with ERA5. To diagnose the thermal activities during summer, the temperature gradient, the thermal wind and the geostrophic wind are calculated using respectively the following formulars:

Temperature gradient.

$$\nabla T = (\partial T_m/\partial x) + (\partial T_m/\partial y) \quad 3.4$$

Where Tm is the mean temperature in Kelvin (K)

Thermal wind, zonal and meridional, respectively

$$U_t = -(R/f)(\partial T_m/\partial y)(\ln P_{925}/P_{700}) \quad 3.5$$

$$V_t = (R/f)(\partial T_m/\partial x)(\ln P_{925}/P_{700}) \quad 3.6$$

Geostrophic wind, zonal and meridional, respectively

$$U_g = -(1/\rho f)(\partial p/\partial y) \quad 3.7$$

$$V_g = (1/\rho f)(\partial p/\partial x) \quad 3.8$$

Where f is the Coriolis force parameter, f = 7.29x10-5 s^{-1}; ρ is the air density, ρ 1.2kgm-3

g is the gravity, g = 9.8ms-^{1}

3.4 Model setup for short term runs with selected SST

3.4.1 MPAS model configuration

An MPAS simulation with SST and sea ice extent as the only boundary condition does not reproduce the weather of a specific year, but it creates weather patterns that fit these conditions. Thus, in order to reproduce the observed climatology, multiple runs

with different initialization dates are required. Here, 51 MPAS simulations are used. They form three experiments, denoted by MPAS_A, MPAS_B and MPAS. Experiment MPAS_A applies the initialization data, SST and sea ice extent from the ERA-Interim reanalysis (Dee *et al*., 2011) and follows the procedure applied by Smiatek and Kunstmann (2023). Six years have been selected according to the SST anomaly in the Gulf of Guinea during the summer season (Figure 3.4). The Gulf of Guinea has a central influence on the precipitation in West Africa (Son & Seo, 2020). The considered period covers 30 years around 2004, from 1990 to 2019. Specific years are 1992 and 1997, revealing a positive anomaly, 1998 and 2010 with a negative anomaly, and 2003 and 2016 are neutral. These anomalies basically correspond to positive and negative ENSO states. Within each SST–year, five simulations initialized from May 15 through May 19 and run until September 1 have been performed.

Experiment MPAS_B is a continuous MPAS simulation initialized in December 1980, from which the results for the period 1990–2010 are applied in the present investigation. For the initialization, the SST and sea ice extent data from the Climate Forecast System Reanalysis (CFSR) (Saha *et al*., 2014) are used. CFSR data is available until 2010. The chosen period covers the largest SST anomalies in the Gulf of Guinea (Figure 3.2).

MPAS experiment consists of MPAS_A and MPAS_B simulations lumped into a single ensemble. The investigated period is the summer season (JJA). Potential heat waves and extreme temperatures in this season can devastate the region's socioeconomic activities and food security (Omotosho & Abiodun, 2007). Moreover, during this period, the Sahel region receives most of its rainfall, leading to a concentration of agricultural activities (Sivakumar *et al*., 2014).

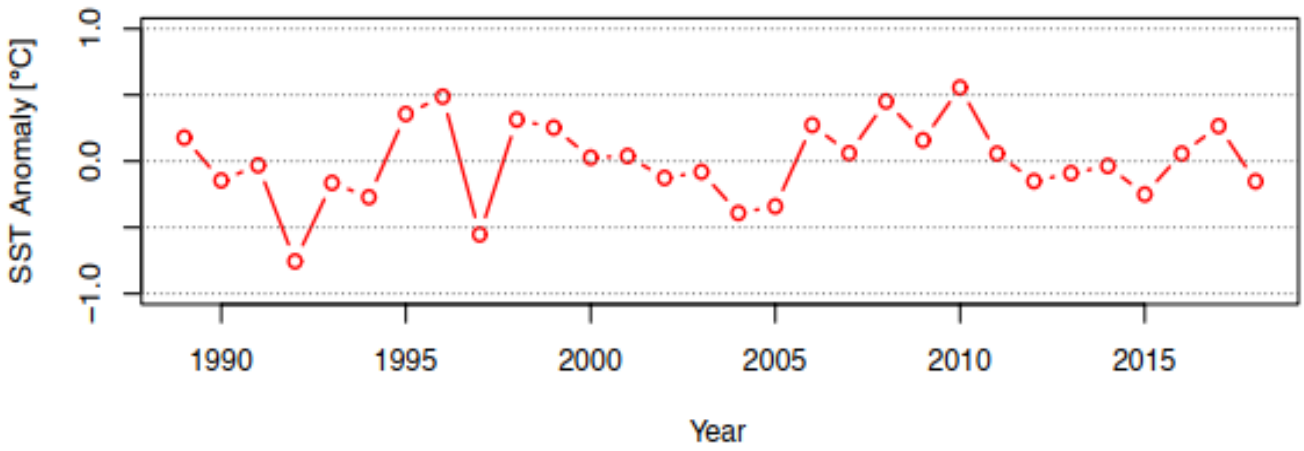

Figure 3.4: SST anomaly over the Gulf of Guinea as in ERA-Interim 1989–2018

3.4.2 Investigated indices

The investigated temperature related indices were selected from the perspective of the socio-economic activities in the investigated region and comprise indices used by similar investigations (Engdaw *et al*., 2022), mostly defined by the Expert Team on Climate Change Detection, Monitoring and Indices (ETCCDI) (Karl *et al*., 1999) with adjusted thresholds. They are the daily mean (TG), minimum (TN) and maximum (TX) temperature, the number of tropical nights (TR) with TN > 24°, the percentage of warm nights (TN90p) with TN > 90th percentile, the number of summer days (SU) with TX > 35°, the percentage of warm days (TX90p) with TX > the 90th percentile, and the heat wave duration index (HWDI) with TX > TXnorm +3°over at least three days. TXnorm is calculated as the mean of the maximum temperatures of a five-day window over all simulations and with the reference data from the entire investigated period.

The indices related to precipitation are the daily mean precipitation (RR), the number of wet days (RR1), and the maximal daily rainfall (RX1day). These indices allow a comparison with the investigation of the observed and simulated precipitation characteristics provided by Dosio *et al*. (2021a) and Dosio *et al*. (2021b). Table 3.3 shows the indices, their definitions, and their units. All indices are calculated for land points only and were derived from instantaneous 3-hourly MPAS output.

Table 3.4. List of indices analyzed in this study. The indices are calculated on seasonal (JJA) base

Index	Definition	Unit
TG	Daily mean temperature	°C
TN	Seasonal mean of daily minimum temperature	°C
TX	Seasonal mean of daily maximum temperature	°C
TXx	Seasonal maximum of TX	°C
TR	Tropical nights with TN > 24°	d
TN90p	Percentage of days when TN > 90th percentile	%
SU	Number of summer days with TX > 35	d
TX90p	Percentage of days when TX > 90th percentile	%
HWDI	Heat wave duration index. TX > TXnorm +3°over at least 3 days	d
RR	Daily mean precipitation	mm/d
RR1	Number of wet days when RR >= 1 mm	d
RX1day	Maximal daily RR	mm/d

Table 3.5. CPU demand for MPAS 7.0

Resolution	Repetitions	Processors	1 day hours}	4 Months [hours]	Repetitions [hours]	Repetitions [days]	CPU [hours}
60 km	**10**	**768**	**0.04**	**5.13**	**51.25**	**2.14**	**39360.0**
60 -10 km	10	768	0.73	90.20	902.00	37.58	692736.0
60 - 3 km	10	3072	0.77	94.30	943.00	39.29	2896896.0
							3628992.0
						plus 10 %	362899.2
							3991891.2
						Mill. CPU hours	4.0

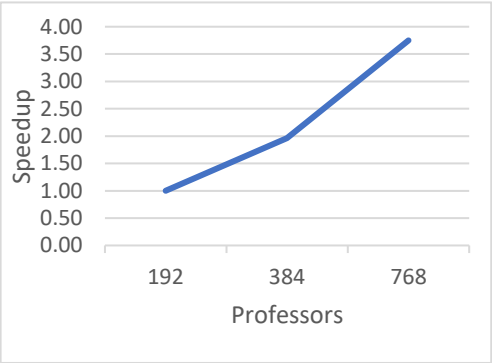

Outputs	Size
History	2.8Gb/6h
Diagnostic	138Mb/6h
Restarts	5.8Gb/24h

CHAPTER FOUR

5.0 Results and discussion

4.1 Simulating the characteristics of the WAM with MPAS

In this section, the ability of MPAS to simulate the seasonal rainfall and spatial pattern of the WAM over WA is discussed. Two observational datasets (CHIRPS and CRU) to evaluate MPAS are used. In addition, two reanalyses (ERA5 and CFSR) are used as the intermediate data between the observed data and model output. CHIRPS is used as a reference because of its high horizontal grid spacing (0.25°). The resolution of CHIPRS reduces errors during interpolation (Tamoffo *et al*., 2022).

4.1.1 Seasonal cycle of West African Monsoon

All the observational datasets show that WA rainfall exhibits three main phases (the onset, the peak, and the retreat), consistent with previous studies (Abiodun *et al*., 2011; Sylla *et al*., 2009). MPAS realistically reproduces the three phases (Figure 4.1). For instance, as in the observed datasets, the simulated onset is from March to June in MPAS, and it is characterized by the northward extension of the rain belt from the coast (6°N). The simulated peak is characterized by a northward (10° N to 14° N) jump of the rain belt and the end of the rainfall south of 6°N; this peak occurs from June to September in MPAS, as in the observations. In addition, MPAS shows good performance in simulating the bimodality of rainfall over Guinea (Figure 4.1j) and the unimodality of rainfall over the Savanna (Figure 4.1k) and Sahel zones (Figure 4.1l), as depicted in the observations. However, there are substantial dry biases in the MPAS simulation of the monsoon peak over the Guinea Coast and Savanna zone. The error confirms these bi-

ases, for instance, it ranges from -1 to -5 mm/day which is out of the range of the differences between the observed data (-1 mm/day). MPAS performs better than CNRM (Centre National de Recherches Météorologiques) models (MPAS: r = 0.88, RMSE = 1.71 mm/day; CNRM: r = 0.85; RMSE = 1.79 mm/day, relative to CHIRPS). Nevertheless, most CMIP6 models are better than MPAS at simulating the WAM seasonal cycle. This can be linked to the finer resolution of CMIP6 models. The dry bias of the monsoon rainfall is a common problem found in many GCMs and RCMs (Abatan, 2011; Abiodun *et al*., 2010; Ajibola *et al*., 2020; Sylla *et al*., 2010). For instance, Sylla *et al*. (2010) found that RegCM3 underestimates the rain rate during the onset period. Abiodun *et al*. (2010) found that finite volume dynamics (CFV) GCMs fails to capture the maximum monsoon peak. Ajibola *et al*. (2020) found that most CMIP6 models underestimate the rainfall over WA. The dry biases in GCMs have been attributed to the coarse grid spacing and boundary layer of the models (Diallo *et al*., 2012; Sylla *et al*., 2013).

MPAS captures the annual cycle of zonal wind at 700 hPa well (Figure 4.2). For instance, the pattern of the monsoon flow, the peak in August, and the southward retreat are simulated well in all the investigation areas. However, MPAS reproduces north-easterly winds from January to March and from October to December over the Sahel zone with higher magnitudes; the bias (Figure 4.2g, contours) is up to 5 m/s relative to ERA5. MPAS also fails to simulate the strength of the monsoon flow (-8 m/s) during the peak period of August over the Sahel and Savanna zones compared to ERA5 (-12 m/s). Additionally, MPAS weakly simulates the annual cycle of the zonal wind magnitude compared to all the CMIP6 models according to ERA5. The underestimation of the monsoon flow and the overestimation of the north-easterly wind may contribute to

MPAS's shortcomings in representing the peak of the monsoon rainfall over WA. Overall, monsoon dynamics have been the subject of several modelling studies in WA (Grist & Nicholson, 2001; Nicholson & Grist, 2003; Tamoffo *et al*., 2022). For instance, Grist and Nicholson (2001) argued that the low-level monsoon flow contributes enormously to the rainfall activities over the Sahel zone. Tamoffo *et al*. (2022) found that the dry biases over the Gulf of Guinea are strongly related to the underestimation of the mid-level tropospheric flux.

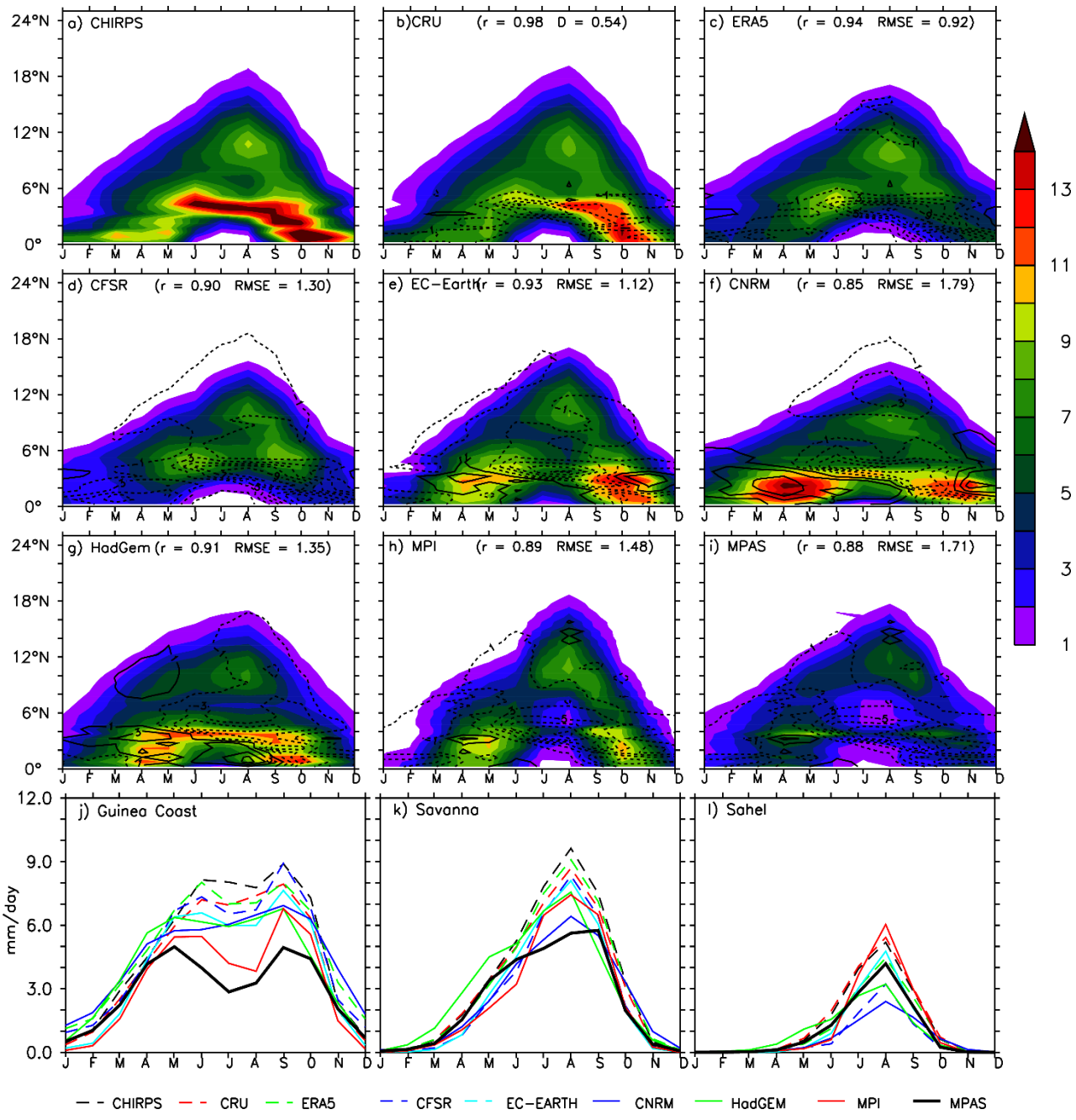

Figure 4.1: Time latitude diagrams of monthly mean precipitation (mm/day) averaged over 10°W-10°E for the period 1981-2010.

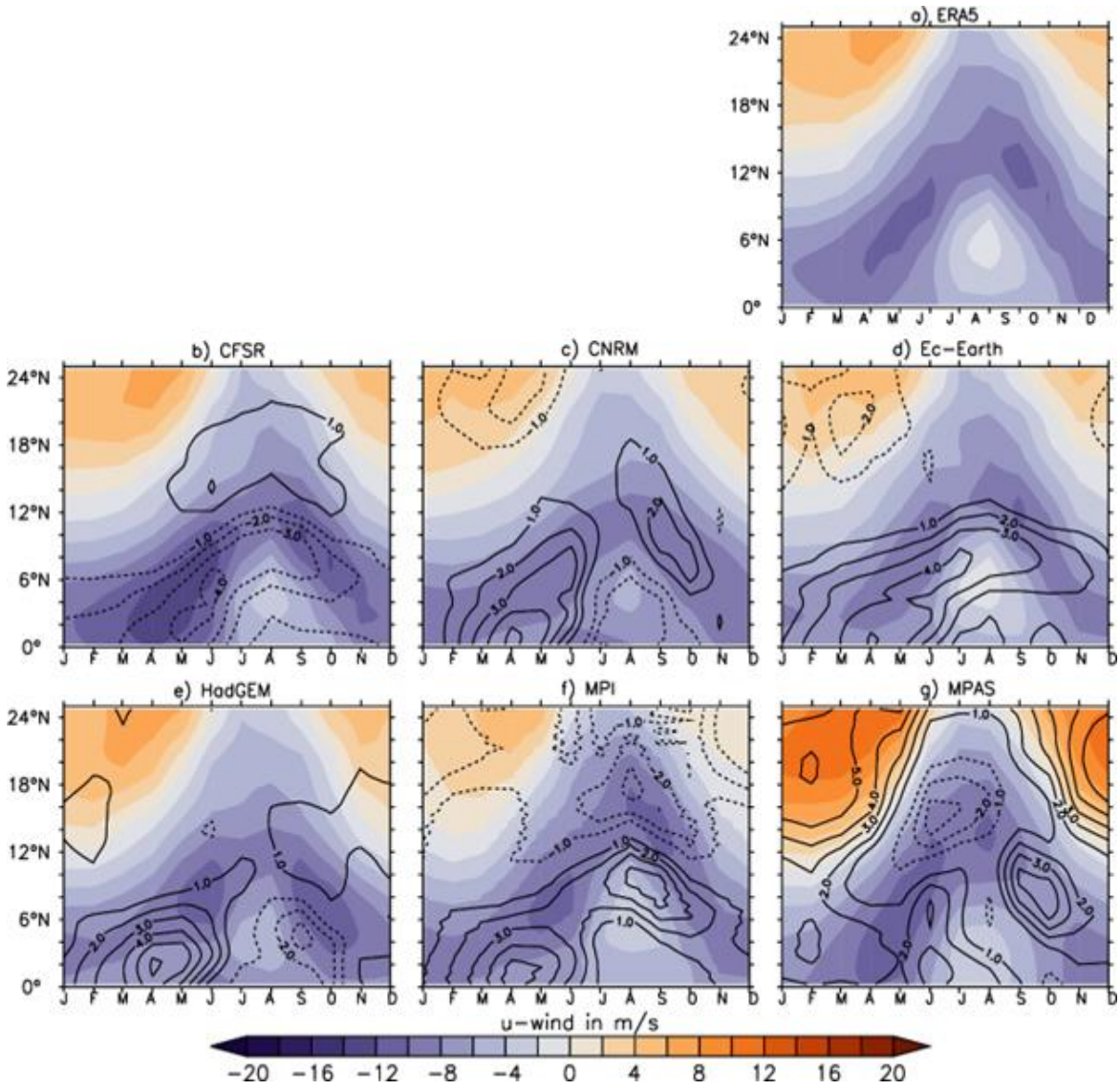

Figure 4.2: Time-Latitude diagrams of monthly mean zonal wind (ms-1; shaded) at 700 hPa, averaged over 10°W-10°E for the period 1981 to 2010.

4.1.2 Spatial distribution of WAM rainfall

Figure 4.3-6 shows the JJA precipitation climatology from CHIRPS, CRU, ERA5, CSFR, the CMIP6 models, and MPAS from 1981–2010. MPAS provides a realistic representation of the WAM rainfall pattern, which follows the displacement of the ITCZ. The zonal gradients of the rainfall on both sides of the ITCZ are captured well, and areas with little or no precipitation are correctly located. Most notably, MPAS reasonably places the ITZC position between 6 and 14°N and shows that the rainfall decreases northward up to 18°N (see the vectors), which is in good agreement with ERA5. MPAS reproduces the rainfall amounts around 12–16°N, 9–20°E that are given by the observed data. Furthermore, MPAS performs better than all the CMIP6 datasets during DJF and MAM seasons, as depicted respectively in Figure 4.5 and Figure 4.6. However, MPAS struggles to capture the maxima (5 mm/day) of the orographic rainfall (Guinea Highlands, Mount Cameroon, Jos Plateau) compared to the observed (9 mm/day) data and the reanalysis (8 mm/day). For instance, the bias in MPAS is in the range from -1 to -3 mm/day, which is out of the range of the uncertainties between the observed data. The monsoon rain belt is more sharply defined in the CMIP6 models than in MPAS (r = 0.8 relative to CHIRPS), which performs worse when it comes to simulating the spatial pattern of the seasonal rainfall than the CMIP6 models (r is in the range from 0.9–0.94 for CMIP6, relative to CHIRPS). MPAS also shows a larger bias than the CMIP6 models (RMSE = 2.81 for MPAS, and RMSE = 1.66–2.80 for CMIP6). The better performance of the CMIP6 models may be related to their higher resolution. The issue with simulating the spatial variability of the WAM rainfall is a common problem within GCMs, which struggle to reproduce mesoscale and local processes due to their coarse grid resolutions. Our results align

with those of previous studies (Klutse *et al*., 2021; Sylla *et al*., 2013; Vizy & Cook, 2002). For instance, Sylla *et al*. (2021) found that CMIP models miss the maxima over Mount Cameroon due to their low spatial resolution, and Klutse *et al*. (2021) found that GCMs have difficulty simulating mountainous rainfall over West Africa.

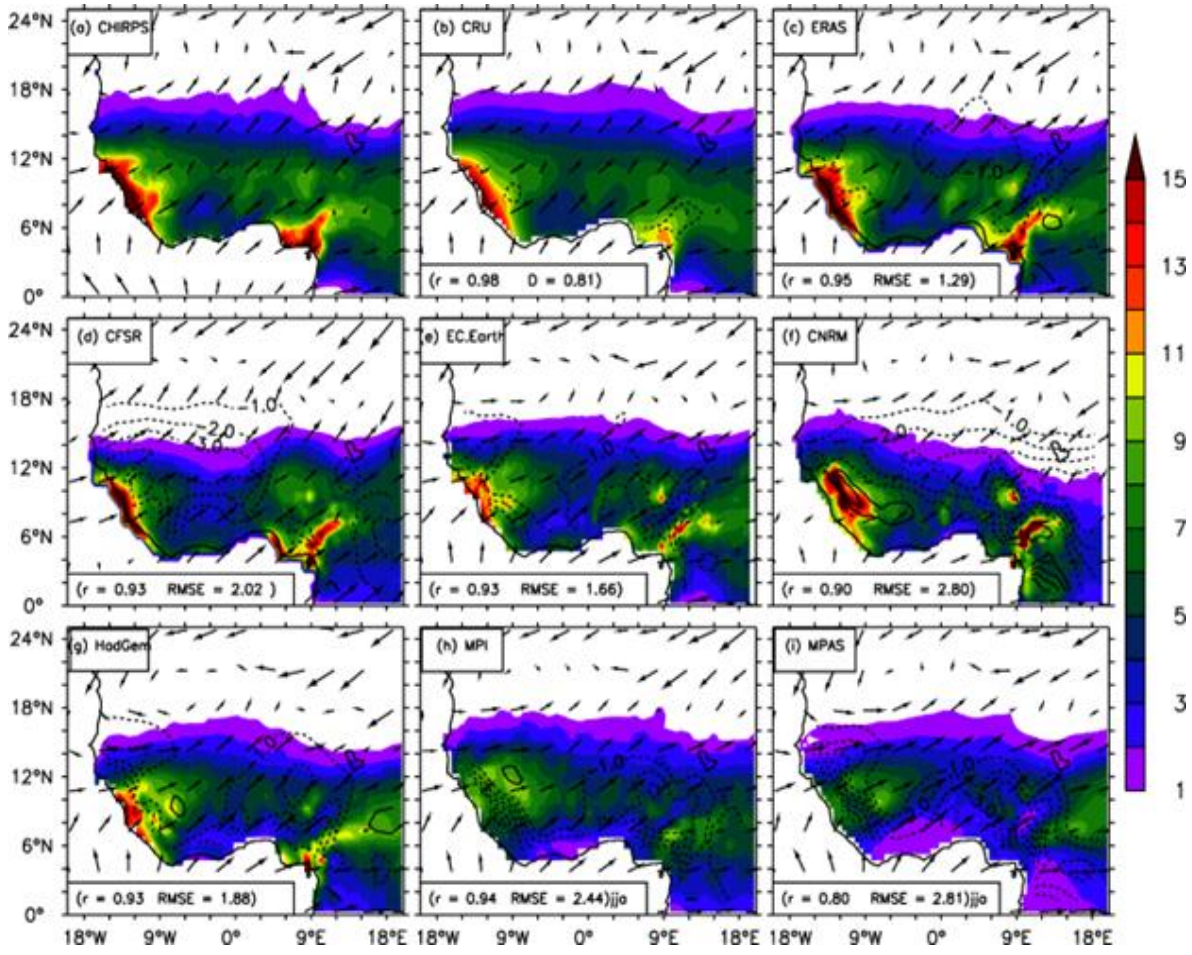

Figure 4.3: Averaged JJA precipitation (mm/day) for the period 1981-2010.

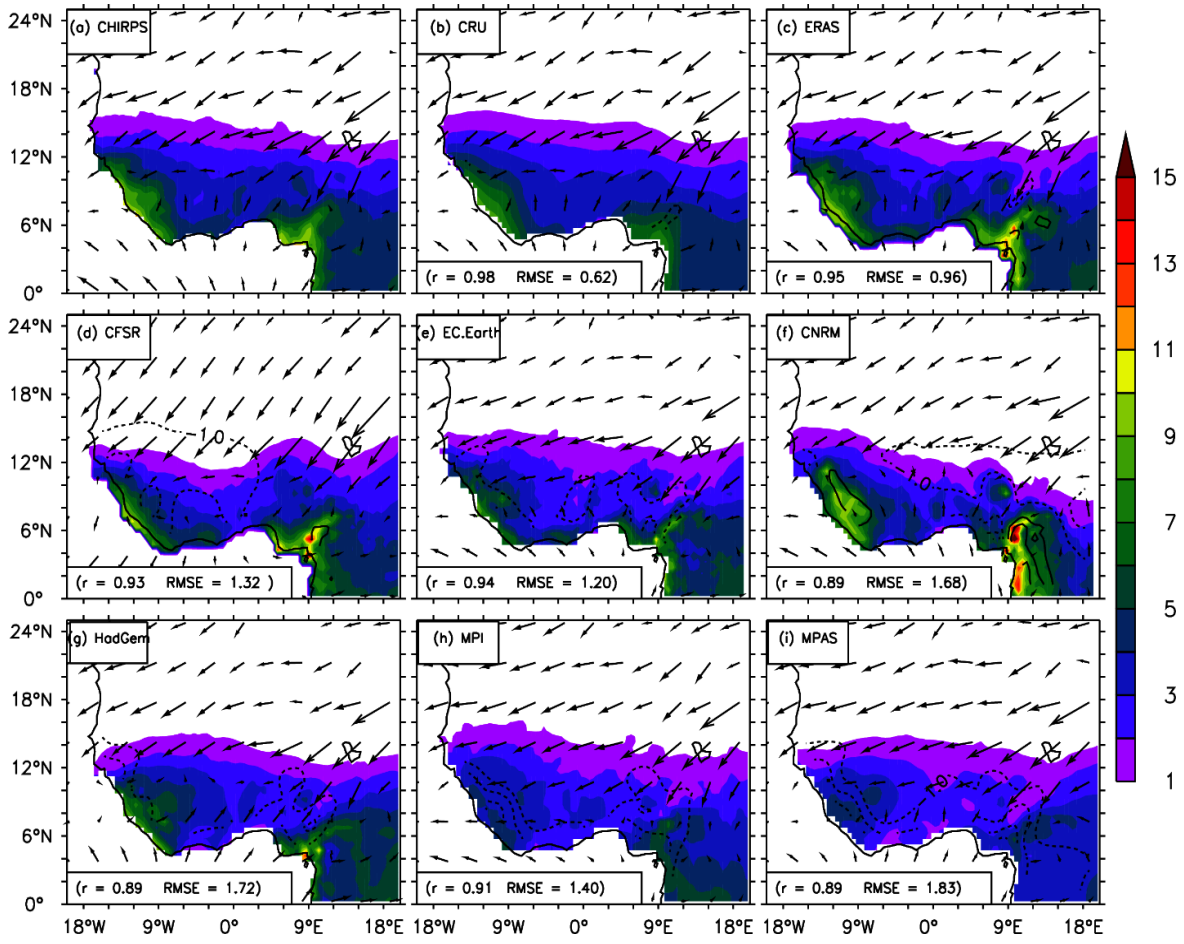

Figure 4.4: Averaged SON precipitation (mm/day) for the period 1981-2010.

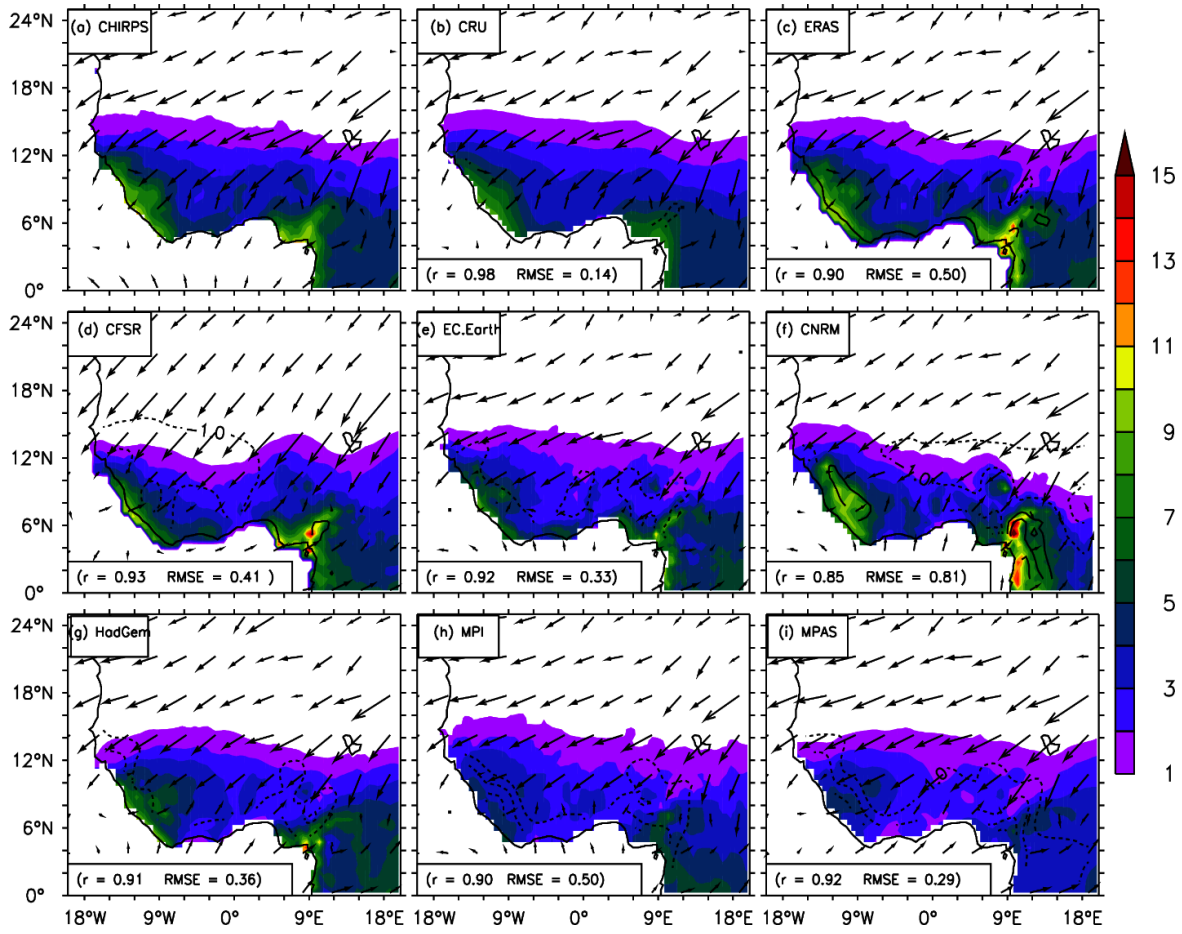

Figure 4.5: Averaged DJF precipitation (mm/day) for the period 1981-2010.

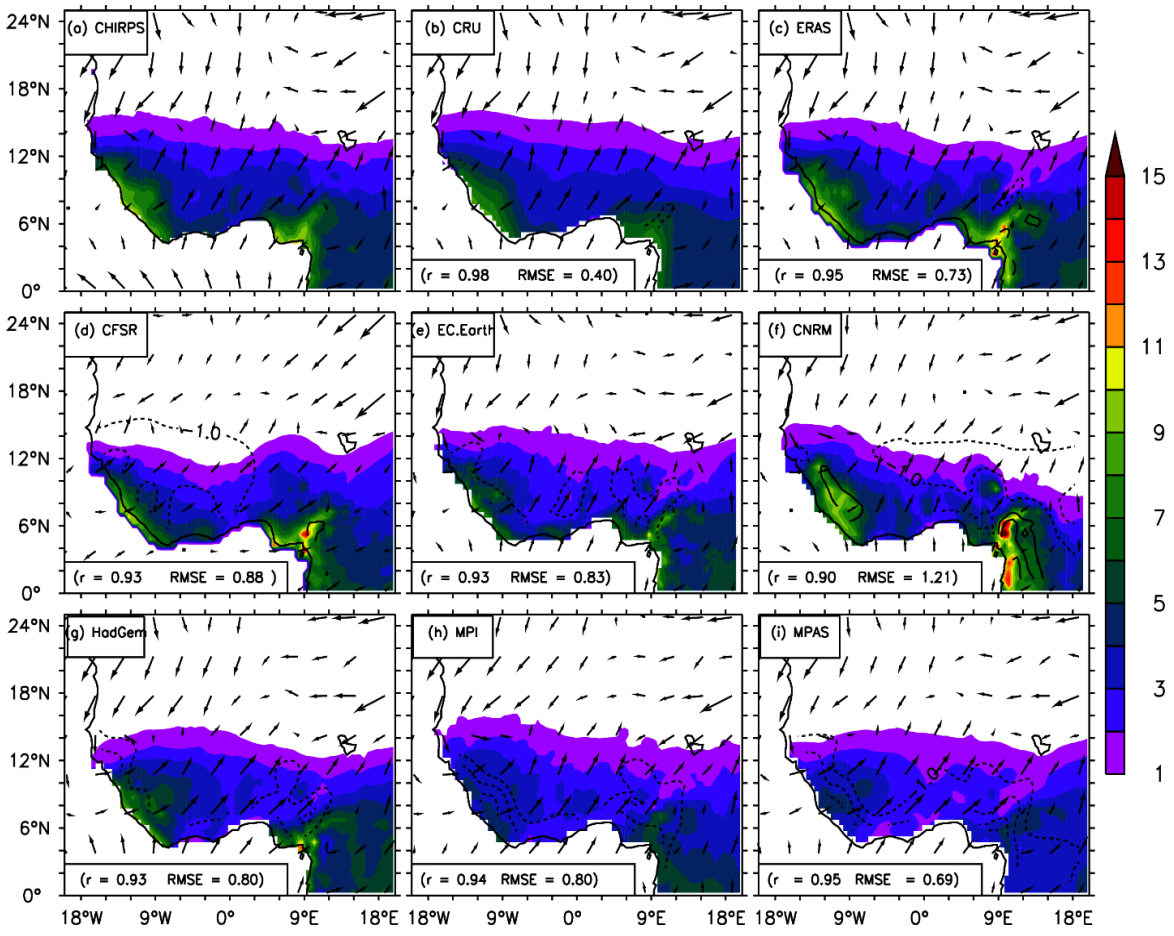

Figure 4.6: Averaged MAM precipitation (mm/day) for the period 1981-2010.

4.1.3 The West African Monsoon Wind system

In this subsection, it is evaluated how well MPAS captures the climatology of the wind system over WA. It is investigated why MPAS has shortcomings when it comes to reproducing rainfall climatology over the study zones. Therefore, the dynamics of upper and mid-tropospheric easterly jets (TEJ, AEJ) and the low levels of the monsoon flow (Akinsanola *et al*., 2017; Cook, 1999; Nicholson & Grist, 2003) are analysed using ERA5 as a reference.

The AEJ is a mid-tropospheric circulation which appears over WA during the boreal summer; it is caused by the strong meridional surface moisture and the temperature gradient at the surface (Cook, 1999). The core of the AEJ is located at around 15°N and 600 hPa in the reanalysis and all the CMIP6 models. The absence of MPAS output at the 600 hPa pressure level weakens the analysis of the AEJ in the model. Another circulation feature of the summer monsoon is the TEJ, which is connected to the upper-level outflow from the Asian monsoon. MPAS (Figure 4.7(j)) simulates quite well the strength of the TEJ (200 hPa) according to ERA5. However, MPAS overestimates (2 m/s) the low-level monsoon flow at around 12°N and fails to locate the TEJ found in ERA5 (4 to 11°N). These jets play a crucial role in the climate of WA, and simulating their strengths and locations is important for reproducing the climate conditions in this region (Sylla *et al*., 2009). The reason for this is that precipitation over WA is associated mainly with MCSs, which depend on the activities of the AEJ (Gaye *et al*., 2005). Furthermore, in WA, the MCSs are favored by a weaker TEJ during the summer. The MCSs (squall lines, mesoscale convective complexes) cross the region (Janicot, 1997) during summer and

overestimating of the MCSs and misrepresenting of the TEJ location in MPAS may contribute to the dry bias in the rainfall (Figure 4.1(j)–(l); Figure 4.1(n)) during the peak period over the Savanna and Sahel regions.

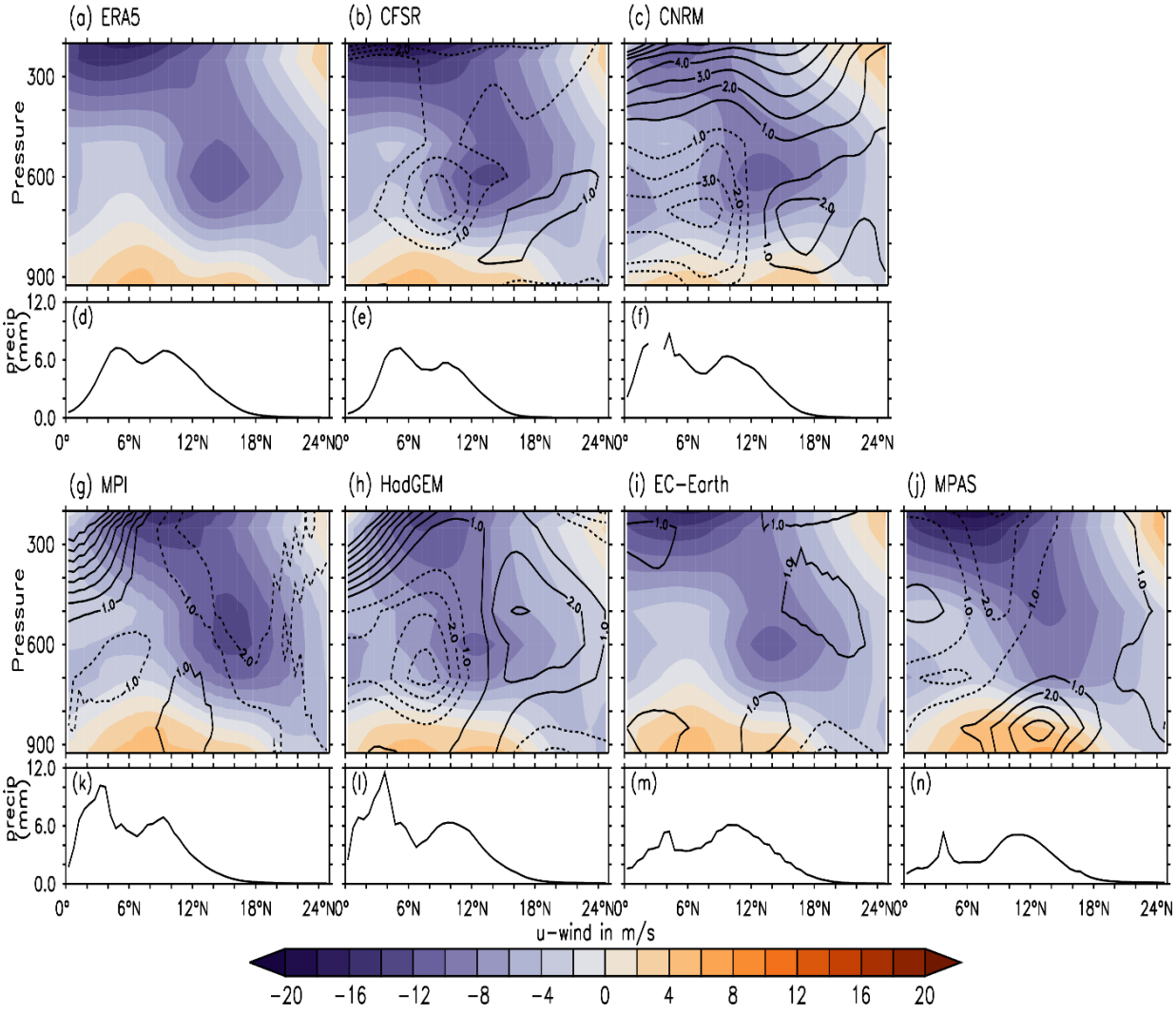

Figure 4.7: Latitude-height cross section of Zonal wind (m/s) in August average between 10°W-10°E(shaded) and seasonal precipitation (JJA) (mm/day, bottom rectangles) for the period 1981-2010.

The vertical cross-section of the vertical velocity (Pas^{-1}) as a function of latitude is shown in Figure 4.8 (a)–(c), (g)–(j) for August for the period from 1981–2010. Three regions of ascent are depicted in all the figures. MPAS shows the first ascent representing convection in the northern West Africa between 900 and 700 hPa as in ERA5, this corresponds to the ITCZ, defining dry convection during the Saharan heat low (Abiodun *et al*., 2011; Sylla *et al*., 2010). Next, MPAS locates the second column of air ascending from the surface to the mid-troposphere at around below 800 hPa around 18°N is in agreement with ERA5. Finally, the third ascent which is more pronounced than the others two ascent, MPAS places it between 950 hPa and 300 hPa as in ERA5; it is the result of deep convection over the Sahel zone (12°N). However, MPAS underestimates (by up to 2 Pas^{-1}) the vertical velocities of all three shallower zones compared to ERA5.All the CMIP6 models overestimate the vertical motion (see the contours). Hence, the convection activities are less substantial in MPAS compared to ERA5. Overall, the dry biases in MPAS may be related to the weak simulation of the convective activities over the investigated areas.

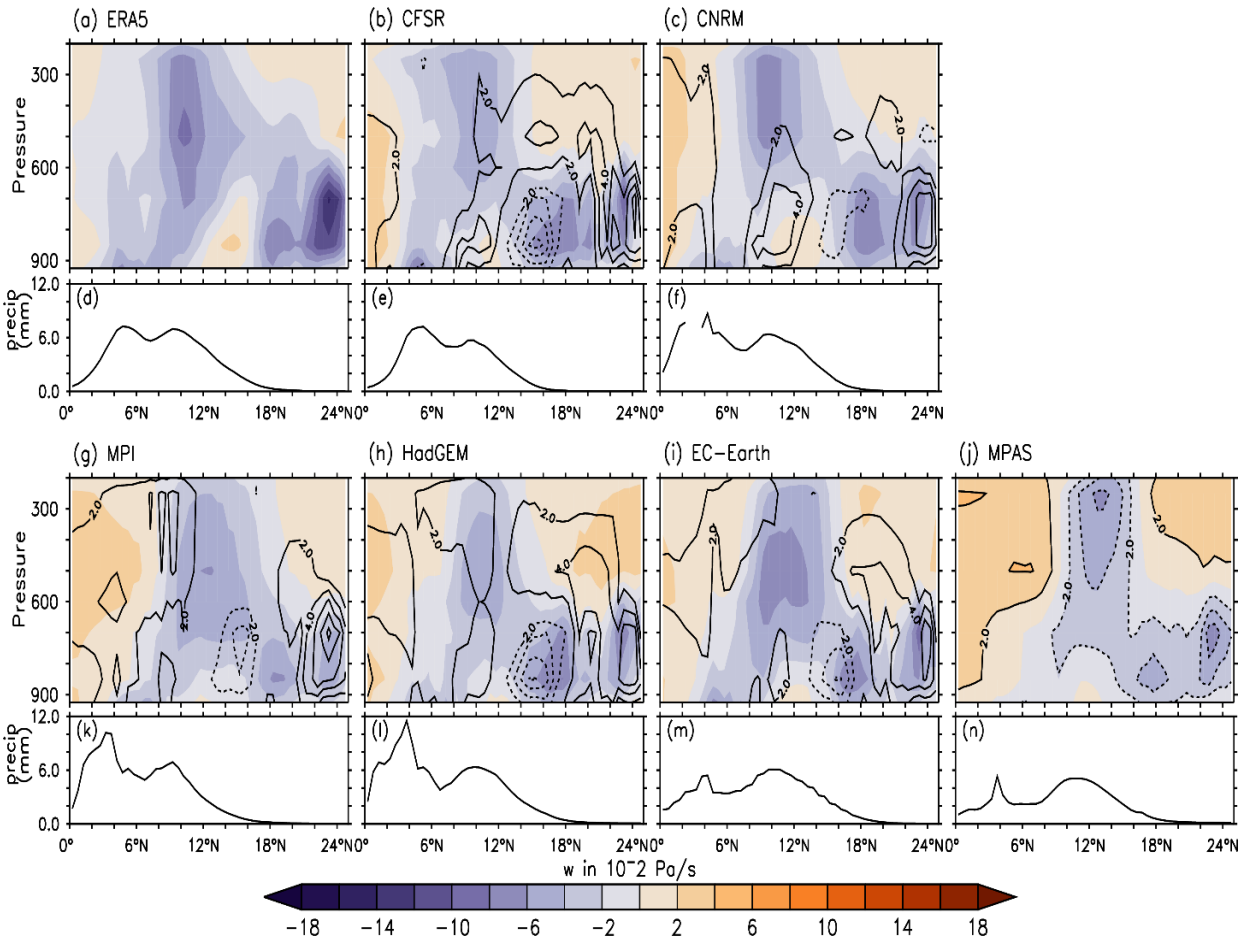

Figure 4.8: Latitude-height of vertical velocity (w in Pas-1, shaded) in August averaged between 10°W-10°E(shaded) and monthly precipitation (mm/day, bottom rectangles) for the period 1981-2010.

4.2 Diagnostics of the WAM thermal activities during summer

In this subsection, it is looked at how MPAS simulates the thermal activities in summer to determine if the issues (rainfall biases, absence of jets, strong winds) detected in the previous analysis occur because MPAS struggles to represent some of the processes that contribute to the dynamics of the WAM. For instance, how MPAS simulates the zonal wind over WA is looked, the temperature gradient, and the thermal wind.

4.2.1 Zonal wind spatial patterns

Figure 4.9 shows the zonal wind at 700 hPa for August (1981–2010) from (a) ERA5 and (b) MPAS. MPAS performs well (r = 0.98) in simulating the spatial pattern of the zonal wind over WA (it is in agreement with ERA5), but MPAS fails to reproduce the core of the jet (AEJ) located at around 15°N in ERA5. MPAS also places the boundary separating the westward and eastward flows of zonal wind farther north (between 20°E to 30°E) than ERA5 does. In addition, MPAS did not place the jets in the north at around 26°N (Egyptian desert) as ERA5 did. This issue in capturing the jet in northern WA may lead to a weaker AEJ in MPAS. A weaker jet might transport less moisture, resulting in less rainfall in the model (Tamoffo *et al*., 2022), which might cause dry biases in MPAS over the Sahel zone. Tamoffo *et al*. (2022) mentioned that dry biases over the Sahel zone are affected by the poleward or equatorward movement of the AEJ and the jet strength. Overall, the underestimation of the jet strength in MPAS may impact the number of mesoscale convective systems (MCSs) and then reduce the amount of rainfall over the Sahel zone, where the MCSs contribute enormously to the development of the rainy season (Nicholson & Webster, 2007; Tamoffo *et al*., 2022). Our results are consistent with

the results of Tamoffo *et al*. (2022), who found that the dry bias in RCMs is associated with weaker AEJ activities in the models.

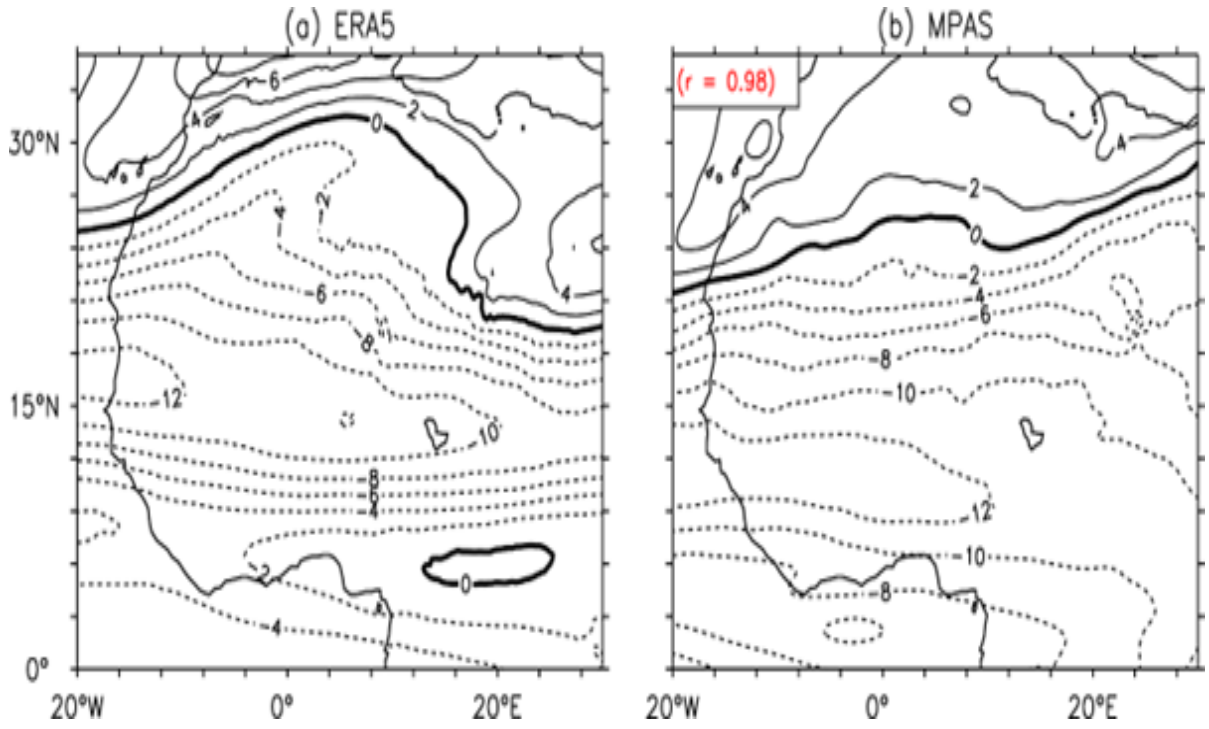

Figure 4.9: Zonal wind field (m/s) at 700 hPa in August from ERA5 and MPAS.

4.2.2 Temperature gradient during summer

Figure 4.10 depicts the mean temperature gradient at 850 hPa, averaged from 10°W to 10°E. MPAS performs well (r = 0.83) when it comes to simulating the temperature gradient's annual cycle, in agreement with ERA5. MPAS shows the minimum (2 K/[1000 km]) temperature gradient in January and December, as in ERA5, but MPAS seems colder than ERA5; for instance, it underestimates the maximum temperature gradient (8 K/[1000 km]) in June compared to ERA5 (10 K/[1000 km]). This result is in line with the work of Nicholson and Grist (2003), who found the same result in their analysis of the temperature gradient in the NCEP-NCAR reanalysis. The temperature gradient during the summer months is also explored; Figure 4.11 shows the temperature gradient from June to August at 850 hPa. MPAS performs well in simulating the spatial pattern of the monthly temperature gradient, but MPAS fails to locate the temperature gradient farther north that is shown by ERA5. In contrast to ERA5, MPAS simulates the temperature gradient at almost the same location in the north for all months. The misplacement of the temperature gradient in MPAS can influence the atmospheric circulation in the Sahelian zone because this gradient is responsible for the formation of the jet (Nicholson & Grist, 2003) and is among the factors that contribute to triggering the moisture advection from the Atlantic Ocean to the continent (Nicholson, 2009). Thorncroft and Blackburn (1999) argue that the origin of the AEJ in the Northern Hemisphere is essentially the temperature gradient caused by the difference between the Sahara and the humid Guinea Coast to the south. Thus, a weaker temperature gradient may lead to a weaker jet, which may transport less moisture and contribute to the dry biases in MPAS.

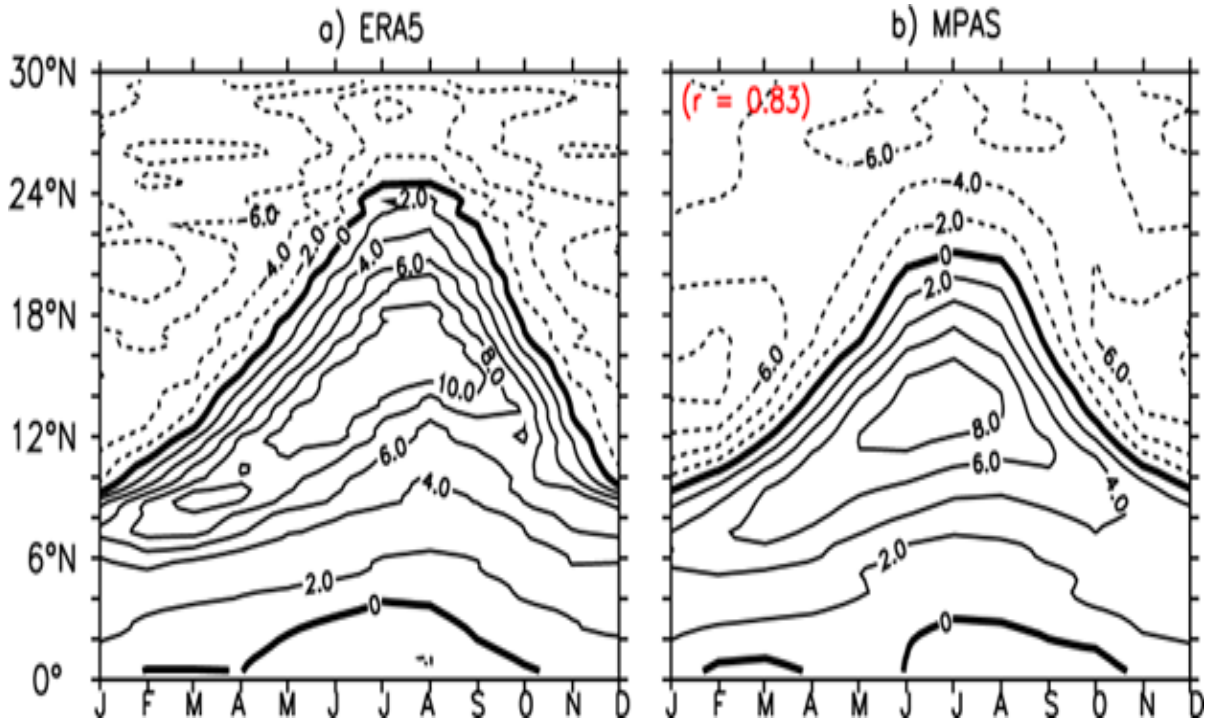

Figure 4.10: Time latitude of temperature gradient K [1000 km]$^{-1}$ at 850 hPa averaged between 10W–10E from ERA5 and MPAS.

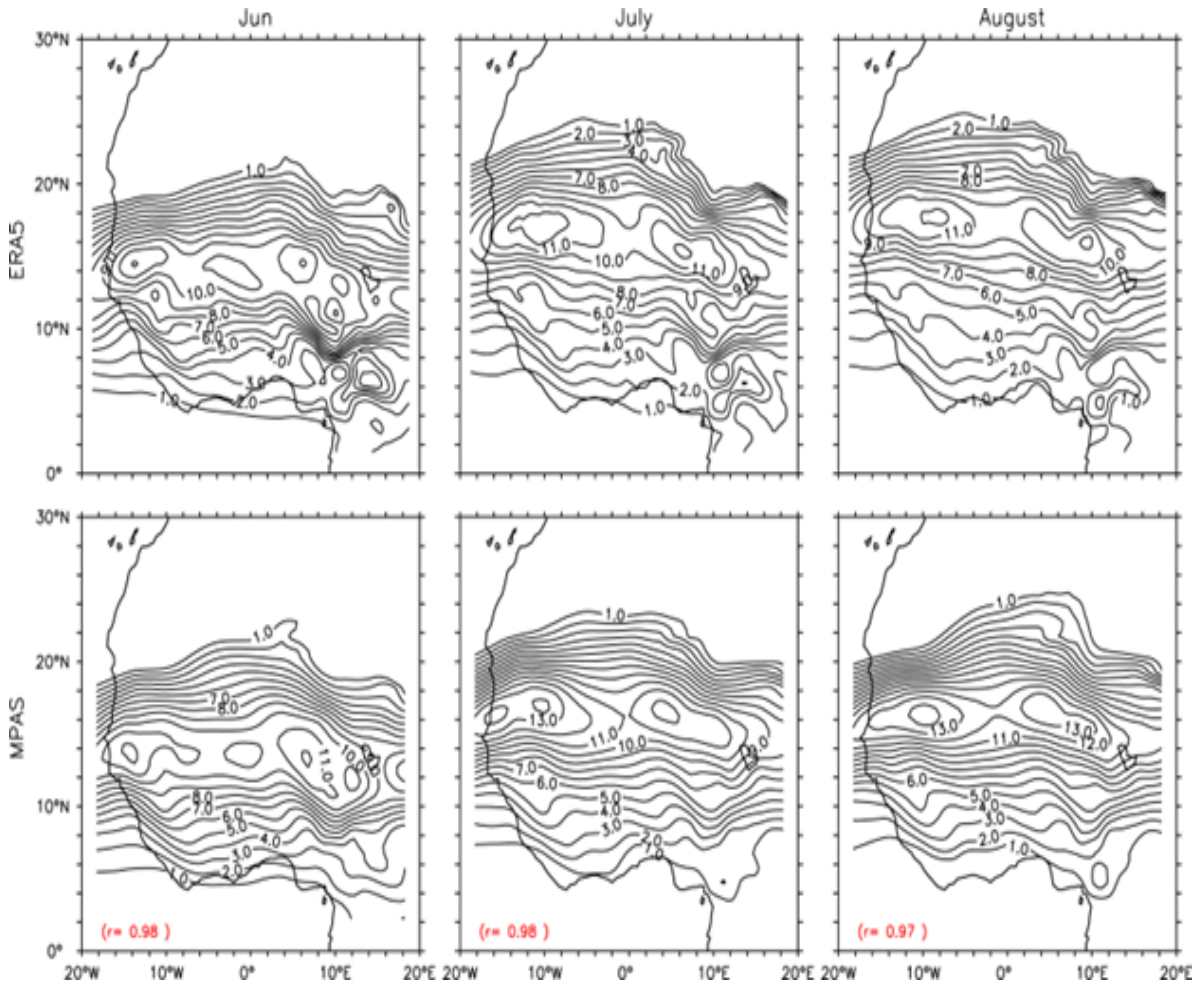

Figure 4.11: Month to month (June, July, August) spatial distribution of temperature gradient K $[1000km]^{-1}$, first raw is ERA5 and the second raw is MPAS.

4.2.3 Thermal wind during summer

Figure 12 shows the thermal wind between two pressure levels, 500 and 925 hPa, and 700 and 925 hPa. For the thermal wind between 500 and 925 hPa, MPAS simulates the magnitude given by ERA5 (>25 m/s), but the thermal wind does not extend as far eastward and northward as it does in ERA5. However, the thermal wind simulated by MPAS between 700 and 925 hPa is the opposite of the thermal wind between 500 and 925 hPa; simulating a small area of the thermal wind between these levels may influence the formation of the wind shear and hence the easterly jets, and it may cause MPAS to simulate a weaker AEJ that may contribute to the dryness in MPAS over the investigated area. This is highlighted in previous studies. For instance, Zhang *et al*. (2021) found that the WAM results from the thermal conditions over the African continent and the neighbouring ocean; therefore, the rainfall variability in a climate model would be actively compatible with the temperature variability.

.

.

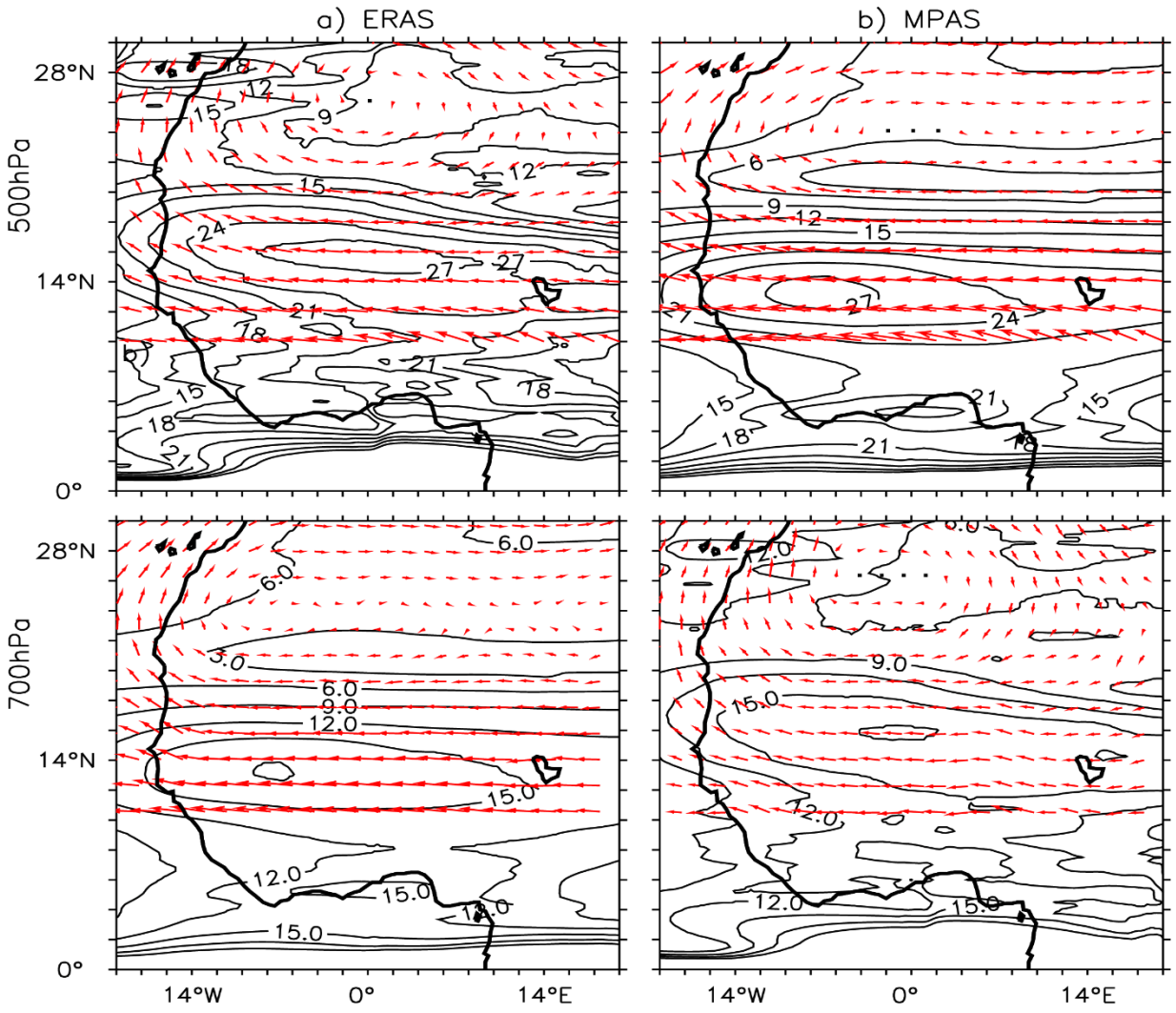

Figure 4.12: Thermal wind magnitude (contours) and vectors (arrow) for ERA5 and MPAS at 500 hPa and 700 hPa in July.

Summarizing, in this section, firstly, the model performance to simulate the seasonal cycle of the WAM is evaluated. It is found that MPAS performs well in representing the seasonality of WAM compared to observed datasets. However, MPAS shows shortcomings in reproducing the WAM peak. For example, it underestimates the peak of the WAM rainfall over Savanna and Guinea Coast, and the MPAS underestimates the zonal wind during August in most of the investigated areas. MPAS also performs well in simulating the spatial pattern of the WAM rainfall but struggles to capture the orographic rainfall over the Guinea Highland, Cameroon Mountains, and Jos Plateau. After looking at how MPAS represents the dynamics of the WAM, it is found that the model simulates the TEJ as ERA5 but is not as well located as in ERA5 and most of the CMIP6. The absence of the 600 hPa level limited us from analyzing the AEJ compared to other datasets. The study of the vertical velocity has allowed to analyze the convective activities over the investigated areas. It revealed that MPA performs well in reproducing the different MSCs but with a slight difference in the localization of those systems compared to the ERA5 and most of the CMIP6 models. Finally, the thermal activities within MPAS are diagnosed, and found difference in the representation of the thermal wind regarding ERA5. It can be concluded that biases in MPAS might be strongly linked to the shortcomings in simulating the wind system, the thermal wind, the convective system, and the resolution used, which plays a crucial role for the WAM in bringing rainfall over West Africa.

4.3 Simulating the temperature extreme, heat waves, and precipitation indices

4.3.1 Temperature extreme and heat waves

Figure 4.13 shows the distributions of the area mean summer (JJA) mean temperature TG in the investigated areas SAH_W, SAH_E, and GUI_C for both the reference data and the MPAS simulations. It reveals that the results obtained from MPAS are well within the range, and there are only small differences between the different simulation approaches of MPAS_A and MPAS_B.

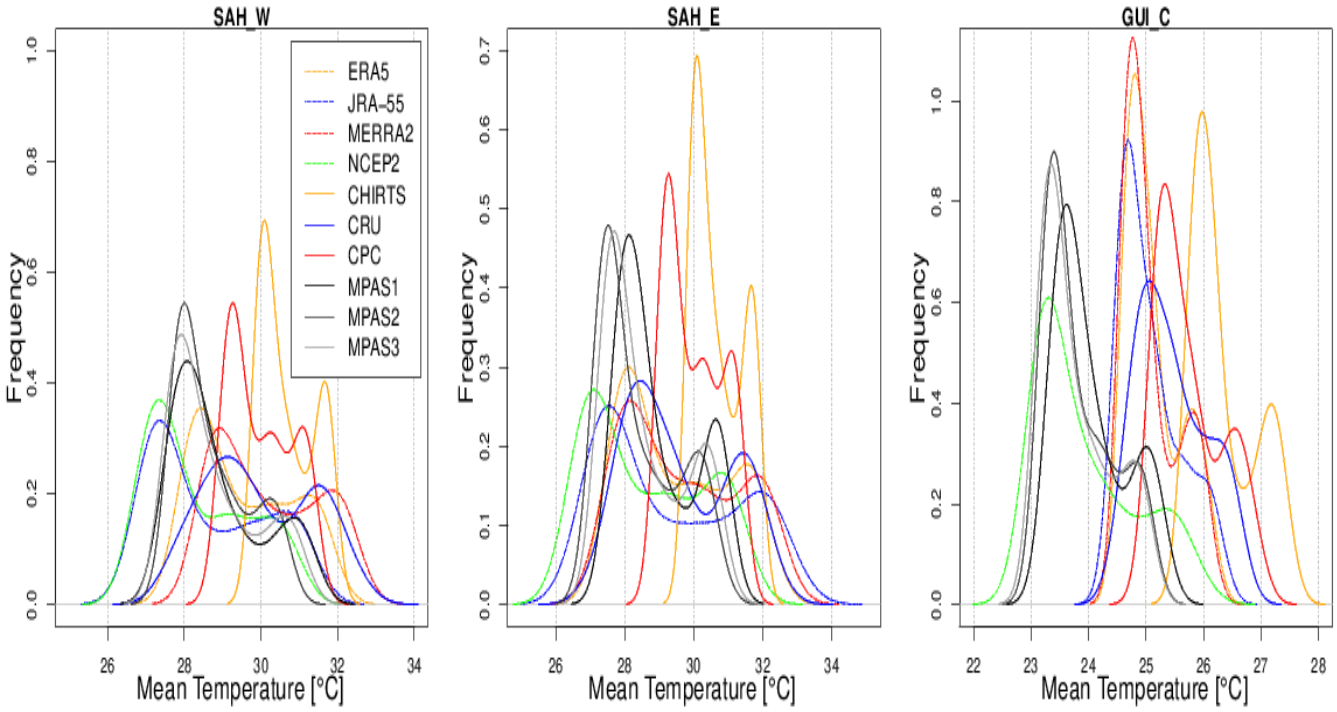

Figure 4.13: Distribution of the area mean summer (JJA) mean temperature TG in the investigated area, SAH_W, SAH_E and GUI_C.

4.3.1.2 Area mean values of temperature indices

Concerning the ranges and the area mean value, there are substantial differences in the reference data (Table 4.1). In the SAH_W area, the mean value TG in the reanalyzes extends from 28.4°C to 29.4°C, the range in the data based on observations is from 29.5°C to 29.9°C. MPAS shows, with 28.7°C, a cold bias of −0.6°C in relation to the mean of the entirety of the reference data, of −0.4°C in relation to the mean value of the reanalysis products, and −1.1°C to the observational reference. The corresponding biases in the SAH_W area are −0.6°, −0.3°, −1.2°C, and in the GUI_C area, −0.9°, −0.5° and −1.6°C.

These results are comparable to the findings from previous simulation experiments. For instance, Hernandez-D´ıaz *et al*. (2013) found, over West Africa, biases in the simulations with the Canadian Regional Climate Model (CRCM5) in the range from −2°C to 2°C. Gbobaniyi *et al*. (2014) found, with the WRF model, biases of 0.8°C over West Africa, of 0.8°C over Guinea, and 1.6°C over the Sahel during the JAS (July, August, September) period. With the RCA4 model, Nikiema *et al*. (2017) reported biases of 1.2°C over WA, 1° C over Guinea and 1.2°C over the Sahel. Kim *et al*. (2014) concluded from the CORDEX-Africa experiment with 10 regional climate models, seasonal (JJAS) biases ranging from −0.5°C to 0.8°C over West Africa. Dosio *et al*. (2015) found in simulations with the COSMO-CLM model cold biases up to 3°C in the Guinea region and the southern Sahel. Careto *et al*. (2018) reported in CORDEX-Africa experiments cold biases in most of Africa for all RCMs, with the largest biases over the Sahel. With the MPAS model, Maoyi and Abiodun (2021) found a cold bias up to 2°C over the Indian Ocean and cold biases up to 1.2°C within the southern African countries. They attributed the error primarily to the coarser resolution of 240 km applied in the simulations.

Figures 4.14 to 4.15 depict boxplots of the mean daily maximum temperatures TX and TXx, for the reference data and the MPAS simulations. The corresponding area mean values are shown in Table 4.1. Compared to the mean values, the cold biases are larger. In the SAH_W area, a cold bias of −1.4°C compared to the mean of all the reference data is present for TX. It is −2.2°C for TXx. The cold biases related to the reanalyzes are smaller. However, it has be considered that NCEP-2 has a much lower resolution. Related to the observations, the MPAS cold biases are larger, at −2.1°C and −2.5°C, respectively. The results obtained for the SAH_E and GUI_C areas are similar. However, the biases are larger when only the observational reference is considered.

The estimated number of tropical nights is, in SAH_W and SAH_E, within the range of the reference data (Figure 4.14) and only in the GUI_C area is TR, with 10 days larger, underestimated. When compared to observations only, biases ranging from −12 to −20 days are present. This is about 10% to 80%. The same findings apply to the number of summer days SU (Figure 4.15), where this number is slightly underestimated, by five days (14%) in the area SAH_W and by fifteen days (33%) in SAH_E. The number of summer days in the GUI_C area is very small and therefore not considered here.

Biases in the percentiles TN90p and TX90 reach values of -33% and -53% in SAH_W, -19% and -7% in SAH_E and +7% and -46% in GUI_C when compared to the mean values of the reference data. The biases are larger in SAH_E and GUI_C and smaller in SAH_W when the reference are observations only. Finally, the largest biases, reaching -66% in 66% SAH_W and -86% in GUI_C, are found for the heat wave duration index HWDI. In SAH_E, this bias is, at 10%, rather small.

Table 4.1. Mean values of temperature indices over the investigation areas for the JJA season, both observed and simulated.

Area		TG (°C)	TX (°C)	TXx (°C)	TR (Days)	SU (Days)	TN90p (%)	TX90p (%)	HWDI (Days)
SAH_W	ERA5	29.5	34.3	40.3	51.6	41.1	14.2	20.1	10.7
	JRA-55	29.3	33.2	40.5	52.5	31.1	29.8	34.2	40.8
	NCEP-2	28.6	32.4	40.5	50.2	29.8	5.2	57.4	34.4
	MERRA-2	29.6	34.7	41.3	49.0	41.9	15.0	20.2	18.4
	CPC	30.0	34.5	41.2	58.7	40.7	15.5	15.6	18.6
	CRU	29.5	35.0	-	-	-	15.4	-	-
	CHIRTS	30.4	35.0	41.1	68.1	43.5	15.3	12.8	6.6
	MPAS_A	28.8	33.1	38.5	51.0	33.9	13.8	11.5	8.5
	MPAS_B	28.4	32.6	38.4	48.7	30.5	7.5	13.8	9.3
	MPAS	28.6	32.9	38.5	49.8	32.2	10.7	12.7	8.9
SAH_E	ERA5	29.5	34.9	40.4	46.4	49.0	21.0	27.3	14.3
	JRA-55	28.6	32.9	39.4	39.4	34.8	46.0	54.1	40.6
	NCEP-2	28.4	32.7	40.7	41.3	33.9	17.2	76.4	55.1
	MERRA-2	30.1	36.0	41.6	48.2	54.7	26.7	32.4	23.5
	CPC	29.9	35.3	42.0	52.8	47.7	26.9	20.7	24.9
	CRU	29.9	36.4		-	-	-	-	-
	CHIRTS	31.7	37.1	42.6	78.5	61.9	19.4	19.2	9.5
	MPAS_A	28.8	33.2	38.7	49.7	33.6	25.3	22.1	18.1
	MPAS_B	28.7	32.7	38.0	55.7	28.8	19.2	21.1	15.3
	MPAS	28.7	33.0	38.4	52.7	31.2	22.3	21.6	16.7

GUI_C	ERA5	25.1	28.4	31.8	5.7	0.2	8.4	14.9	0.4
	JRA-55	25.1	28.5	32.3	14.7	1.8	13.1	18.0	9.7
	NCEP-2	23.9	25.8	31.7	8.0	0.1	4.2	55.0	9.0
	MERRA-2	25.1	28.7	32.2	5.0	0.7	9.2	19.7	7.2
	CPC	25.7	28.9	33.4	19.2	0.2	15.4	19.4	7.7
	CRU	25.4	29.2	-	-	-	-	-	-
	CHIRTS	26.3	29.7	33.4	23.2	0.2	16.0	13.4	0.2
	MPAS_A	24.1	27.3	30.5	1.7	0.0	12.2	15.4	1.1
	MPAS_B	23.8	26.7	29.6	1.8	0.0	10.6	9.9	0.0
	MPAS	24.0	27.0	30.1	1.8	0.0	11.4	12.7	0.6

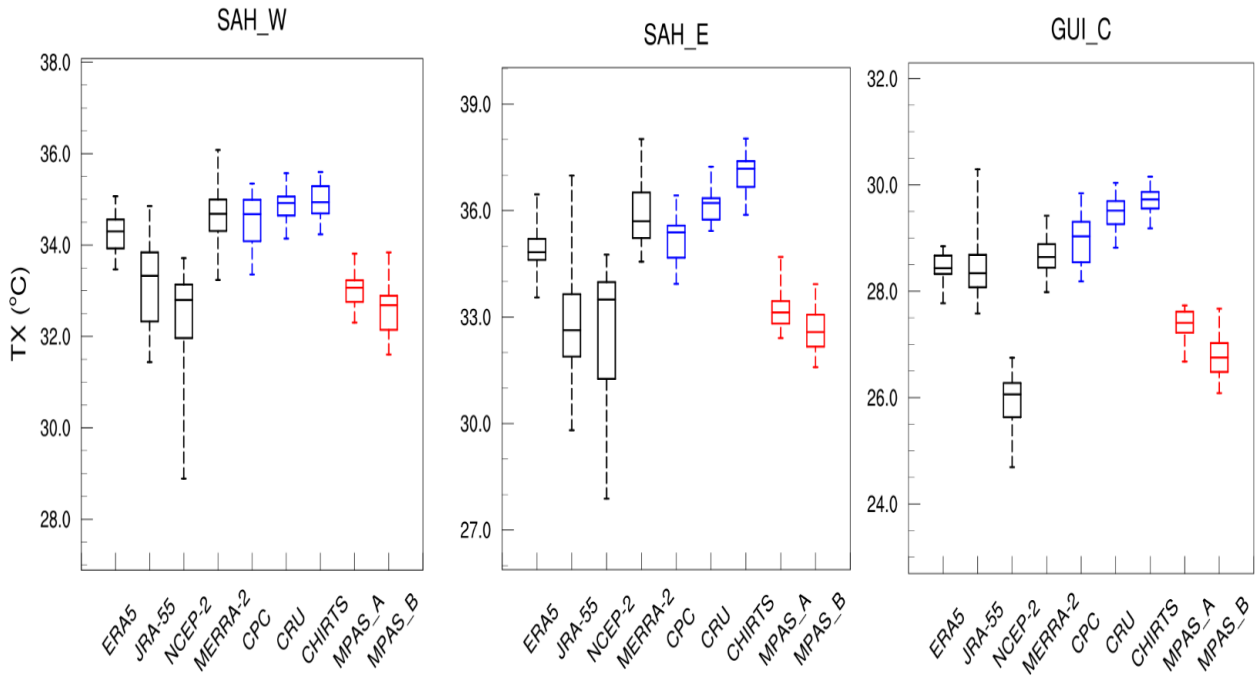

Figure 4.14: Boxplots of mean daily maximum temperature TX for the reference data and MPAS simulation in the investigation areas SAH_W, SAH_E and GUI_C and the summer season (JJA).

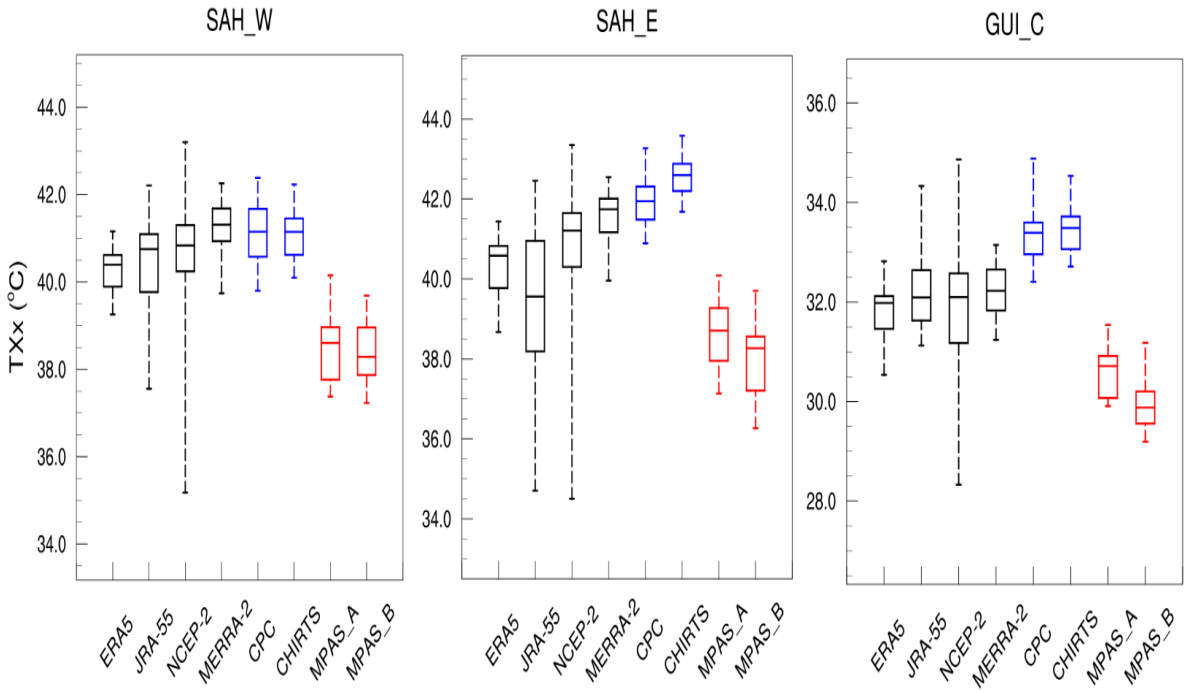

Figure 4.15: Boxplots of TXx for the reference data and MPAS simulation in the investigation areas SAH_W, SAH_E and GUI_C and the summer season (JJA)..

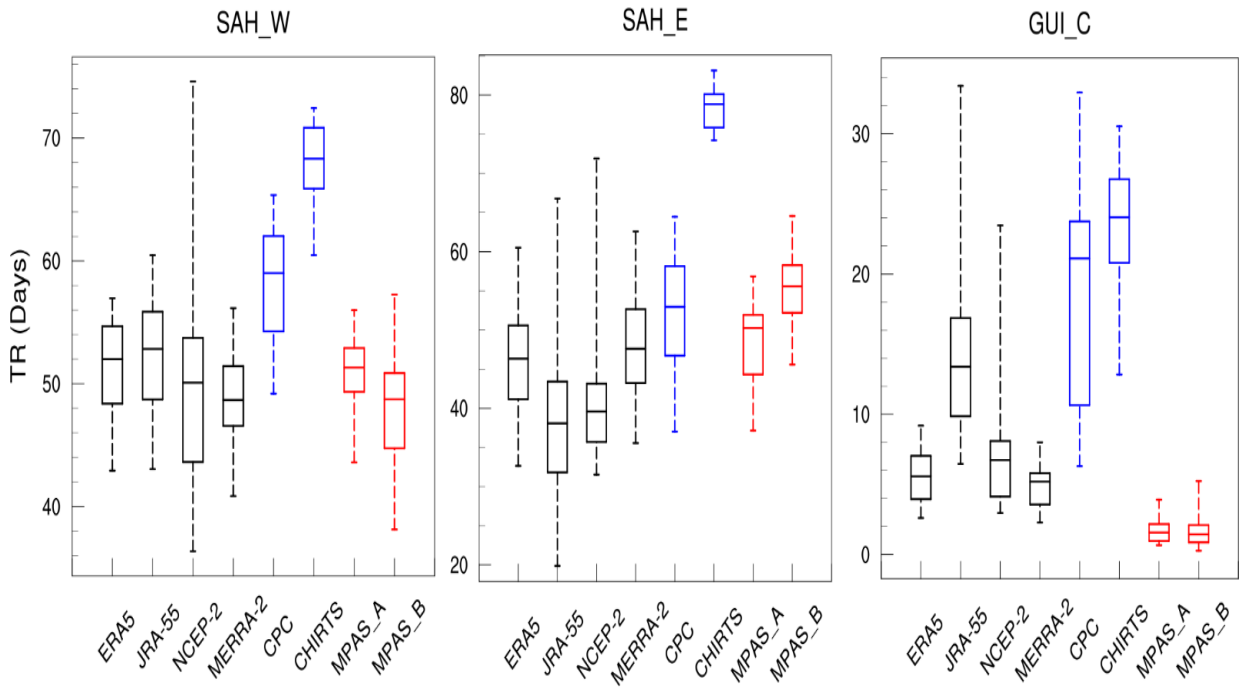

Figure 4.16: Boxplots of TR for the reference data and MPAS simulation in the investigation areas SAH_W, SAH_E and GUI_C and the summer season (JJA).

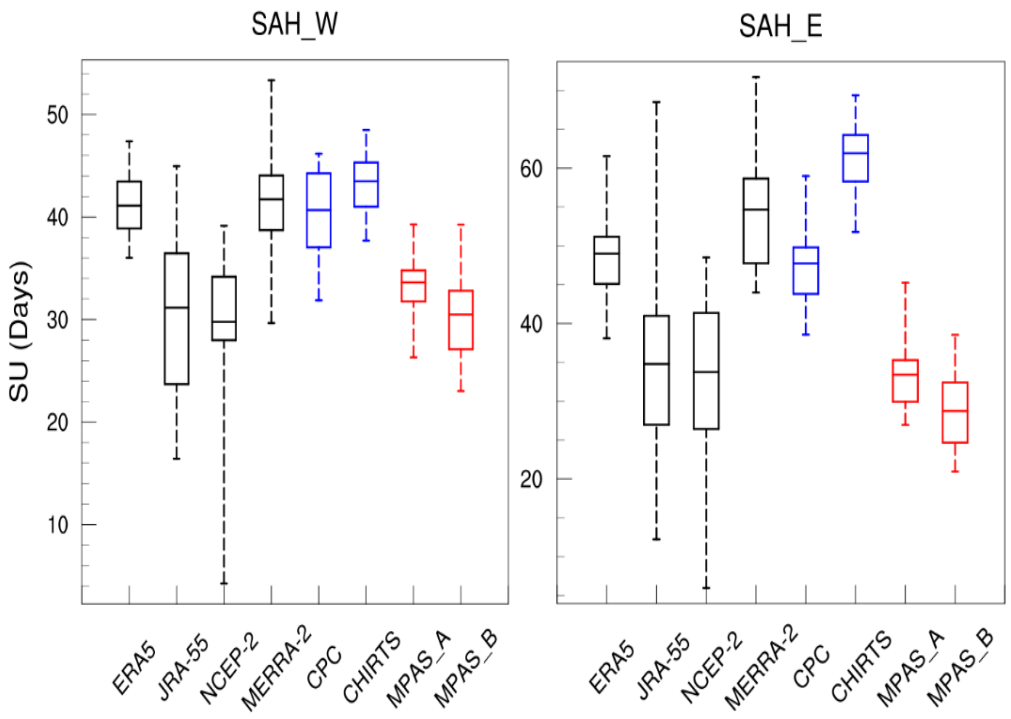

Figure 4.17: Boxplots of SU for the reference data and MPAS simulatio in the investigation areas SAH_W, SAH_E and GUI_C and the summer season (JJA).

In summary, it can be concluded that there is moderate to partly large biases in the summer area mean values of the investigated indices. These are in general cold biases and underestimations of the reference data. The biases are larger when only observational reference is considered. On the other hand, the ranges in the MPAS simulations and in the observations are similar. Lower biases are found in comparison to the reanalyses, which on the other hand reveal much higher ranges. MPAS reaches, when biases in percent of the reference are considered, the lowest biases in the SAH_W area in five of the investigated indices. Limiting this comparison to the reference from observations yields the lowest biases in four indices SAH_E and four in SAH_W. In the complex coastal area GUI_C, MPAS simulations reveal the highest biases. As in the CORDEX experiments (Kim *et al*., 2014), the biases simulated for West Africa are generally smaller than for the eastern part of the Sahel. This might however be related to the lower density of monitoring stations in this region (Masunaga *et al*., 2019). Dosio (2017) found, regarding the summer mean temperature (TG), large discrepancies between the individual simulations, with the model spread ranging from 3.5° C over the coast of Guinea, to 7° C, over SAH_E.

Despite the deficiencies, the general applicability of MPAS to climate simulations can be concluded here. Also, results obtained from the two procedures employed for initializing the model, MPAS_A and MPAS_B are very similar (Table4) and demonstrate the equivalence of these approaches to initialization.

4.3.1.3 Regional patterns and differences in temperature indices

Large biases are found at regional scales. Figure 4.18 shows the maps of the MPAS simulated mean maximum temperature (TX) and differences (Figure 4.19) between

MPAS, the mean values of the MPAS_A and MPAS_B experiments, and the mean of the applied reference data. All the datasets show a similar pattern for the spatial distraction of TX. This pattern shows an increase in TX from south to north. The north Sahel (Sahara) experiences high temperatures. MPAS reveals a notable cold bias throughout the considered region. Only in the Volta region and Western Sahara there are small positive biases. In comparison with the reanalyses, the biases are generally lower, reveal however similar values with MERRA-2 and CHIRTS. The results with JRA-55 and NCEP-2 differ and show also positive biases. The smallest differences occur with the ERA5 reference. Considering the biases in the observations resulting from the rather low station density in some areas and coarser resolution of the other reanalysis data, it can be concluded that MPAS performs reasonablye. The shortcomings in simulating TX in MPAS may also be related to the resolution (60 km) compared with the other datasets which have low resolution.

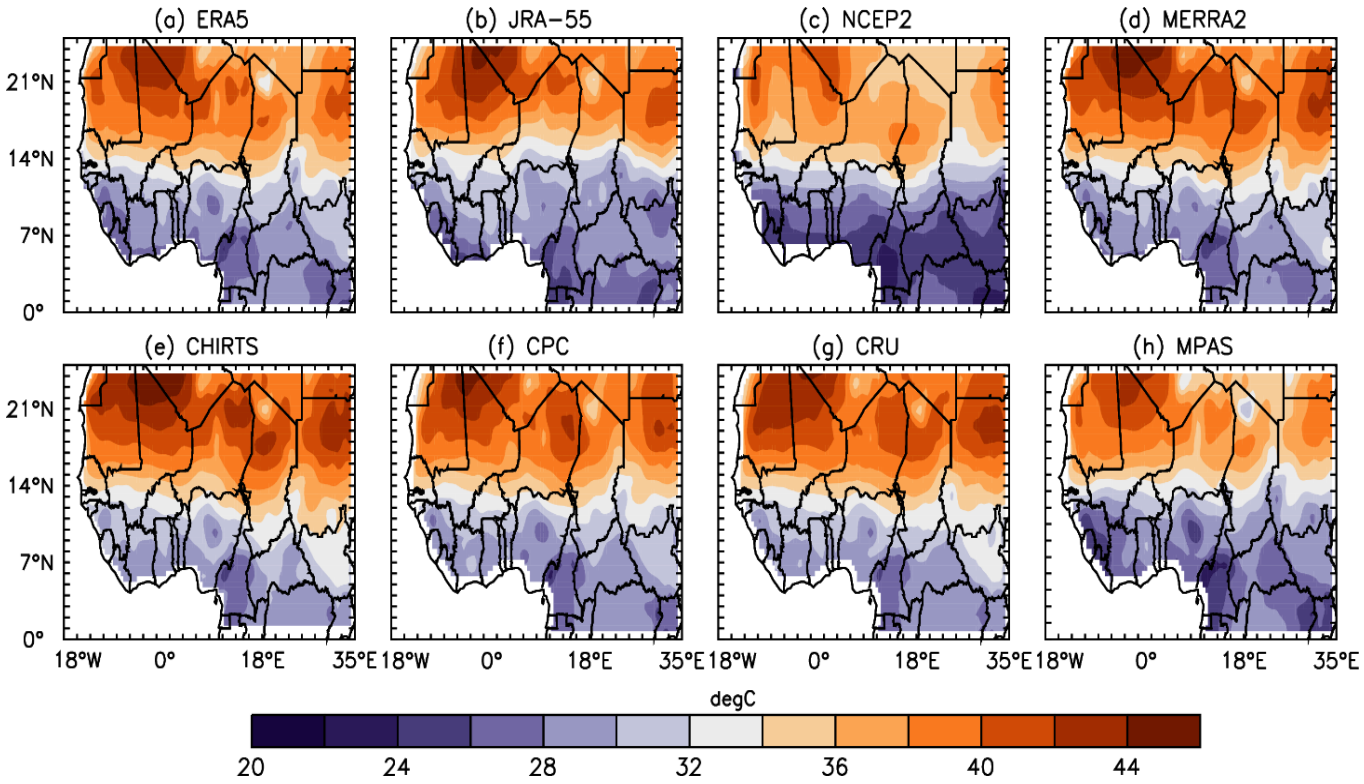

Figure 4.18: Spatial distribution of TX for Simulated MPAS and reference data.

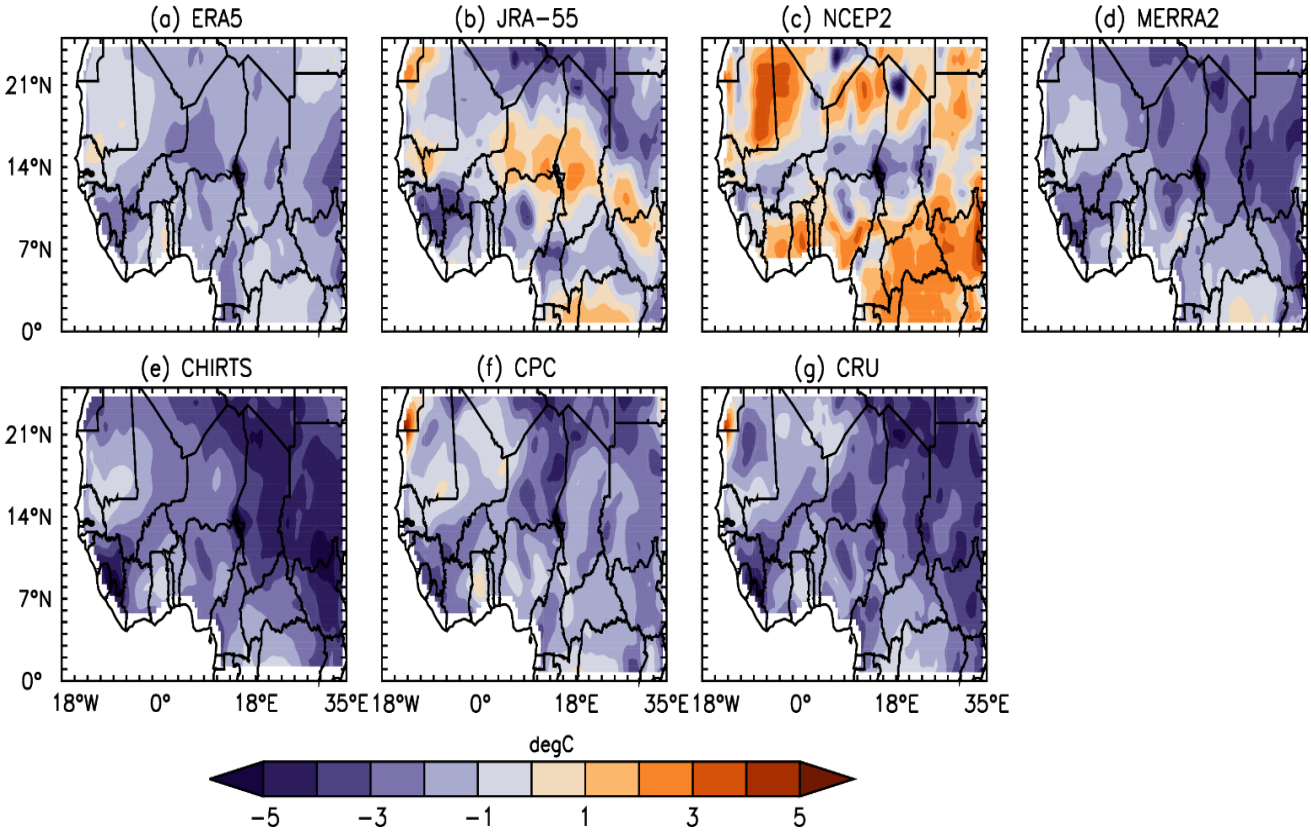

Figure 4.19: Simulated MPAS TX differences between the MPAS and reference data.

Figure 4.20 and Figure 4.21 show, respectively, the regional patterns and differences between MPAS of occurrence of warm days TX90p (warm days) during JAS season. The regional pattern of the extreme temperature threshold (90th percentile of daily maximum temperature: TX90p) with the reanalyzes is different. ERA5 and MERRA-2 show the lowest extreme, while JRA-55 and NCEP-2 show the highest extreme. All the reanalyzes show the highest TX90p over the Sahel and the lowest over the Gulf of Guinea. The spatial pattern with the observed data and MPAS is quite similar and shows the smallest TX90p, in comparison with the reanalyses. In comparison with the observations data, MPAS underestimates the occurrence of warm days throughout the region. MPAS shows the most significant negative bias in comparison with JRA-55 and NCEP2. This may be related to the higher resolution of those datasets. MPAS reveals smallest biases in the central Sahel in comparison with ERA5 and reveals negative biases in the South-East of the region in comparison with MERRA2. Compared with the observations, MPAS reveals more negligible bias; only positive bias is simulated in the northern Sahara.

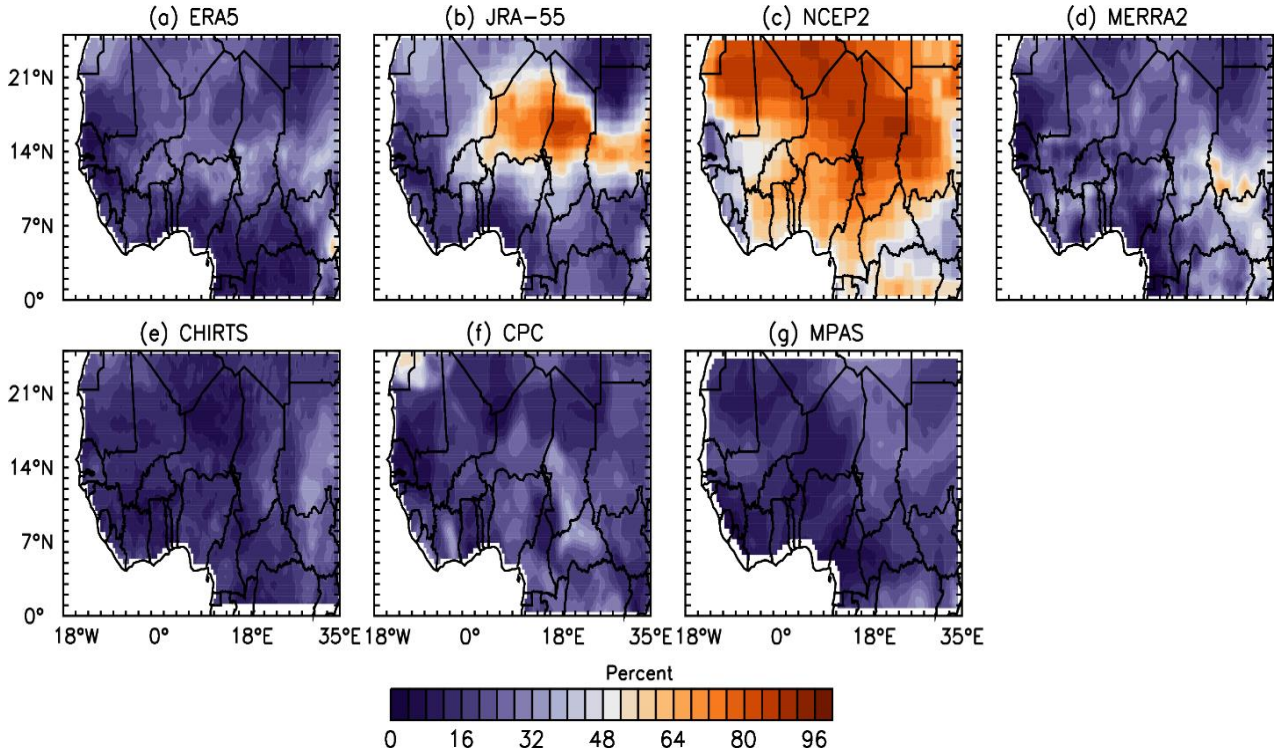

Figure 4.20: Spatial distribution of 90 percentiles of TX (TX90p) for Simulated MPAS and reference data.

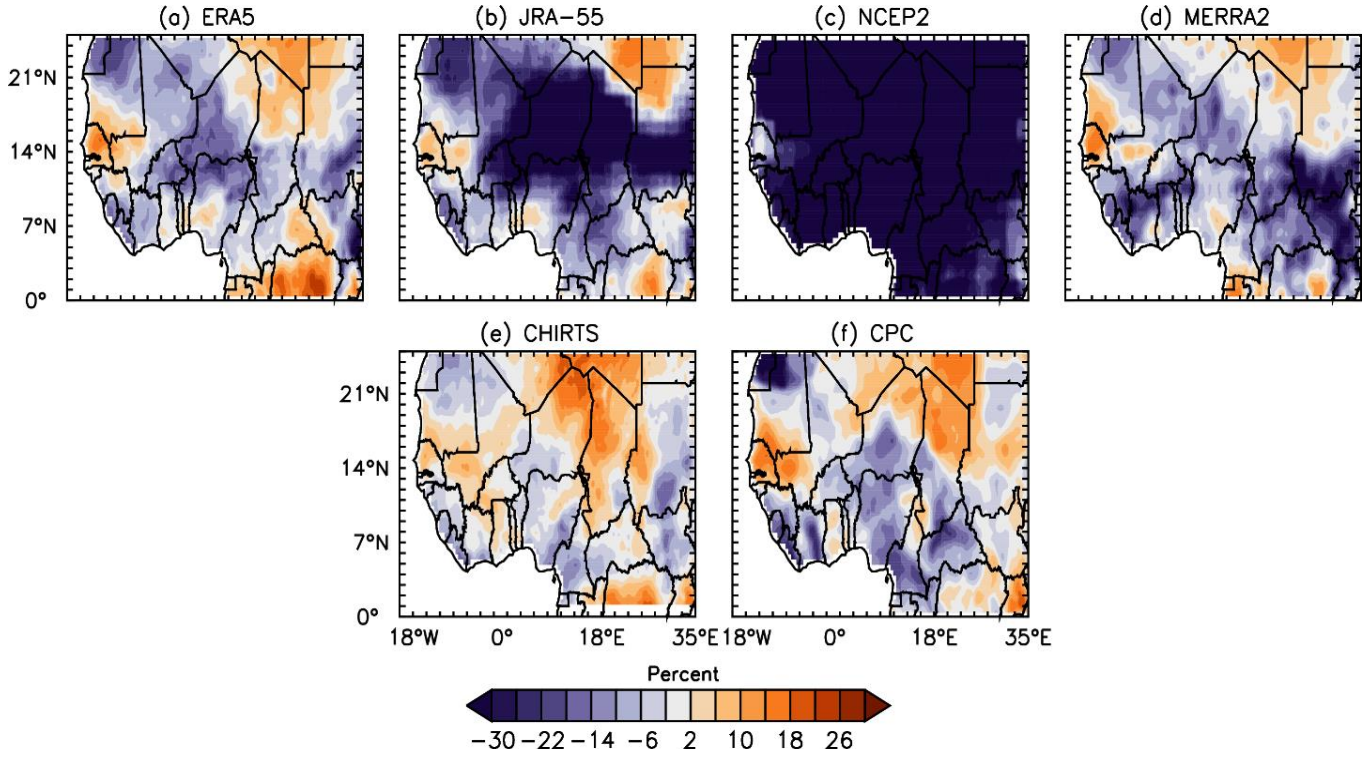

Figure 4.21: Simulated TX90p differences between the MPAS and reference data.

Figure 4.22 and Figure 4.23 show, respectively, the regional and seasonal patterns and differences between MPAS of occurrence of warm nights TN90p (warm nights). The regional pattern of the extreme temperature threshold (90th percentile of daily minimum temperature: TN90p) with the reanalyzes is similar except for JRA-55, which shows higher TN90p over Central Sahel. The spatial pattern with the observed data and MPAS is quite similar and shows the smallest TN90p in comparison with CPC which shows higher warm nights in the south of Sahel East. However, MPAS reveals large biases throughout the considered region. In comparison with the reanalyses, MPAS shows a negative bias over the region. MPAS reveals the smallest biases in the Sahelian zone in comparison with ERA5 and MERRA2. However, MPAS shows larger biases in the Sahelian and the Saharan zones in comparison with JRA-55. In comparison with the observed data, MPAS reveals smaller biases over the Sahelian zone and larger negative biases in the Guinea in comparison with both CHIRTS and CPC.

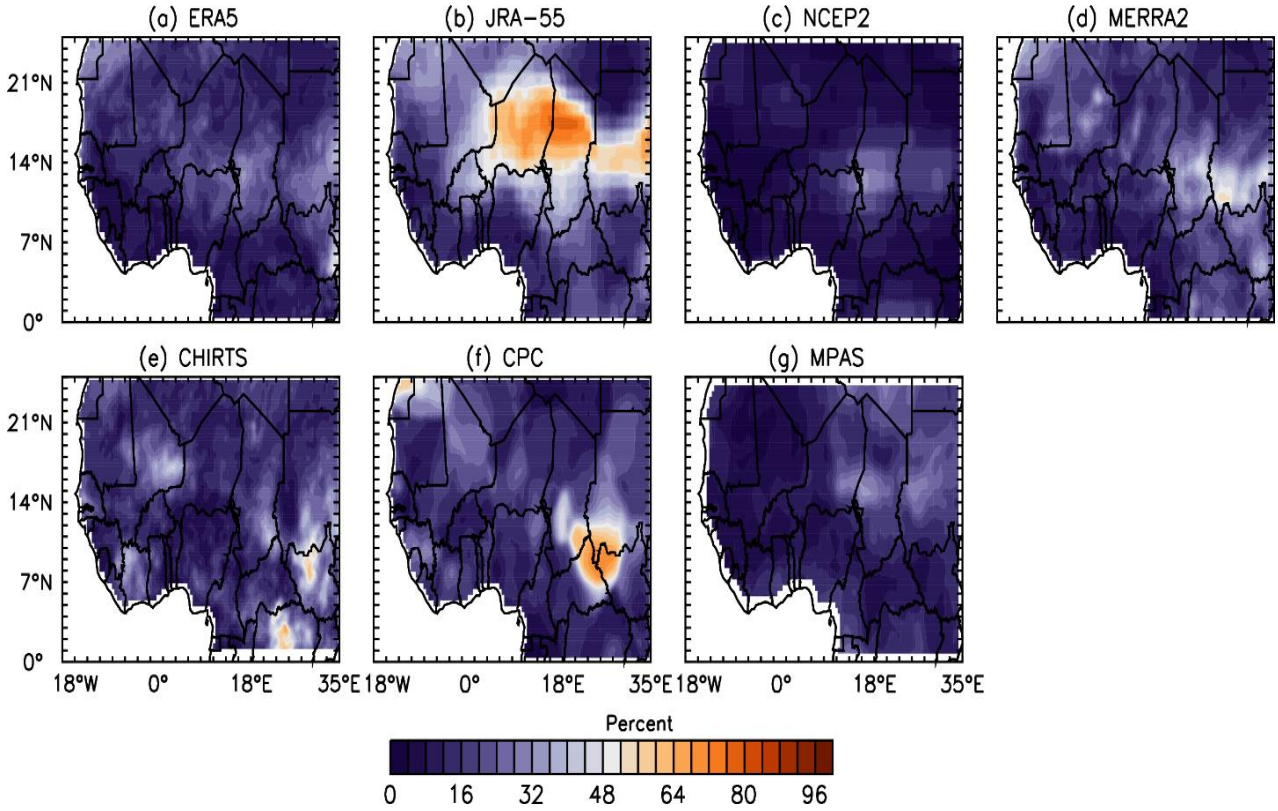

Figure 4.22: Spatial distribution of 90 percentiles of TN (TN90p) for Simulated MPAS and reference data .

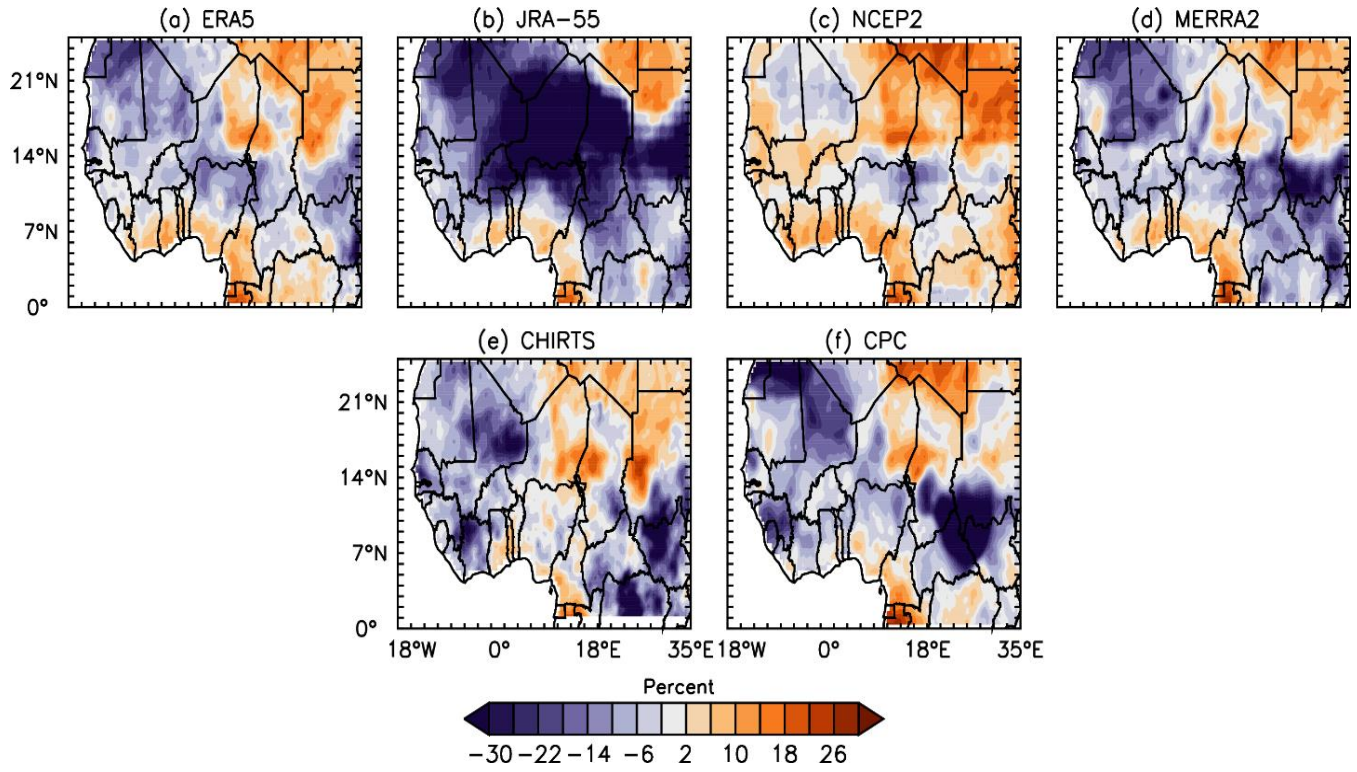

Figure 4.23: Simulated TN90p differences between the MPAS and reference data.

Figure 4.24 and Figure 4.25 show, respectively the regional seasonal patterns and differences between MPAS and different datasets of the number of summer days (SU) with daily maximum temperature when TX > 35° C. Concerning the regional pattern, all datasets show that the number of summer days increases from south to north as temperature increase also from south to north. Patterns of the differences in SU are similar in the Sahel, showing large underestimations, especially in the eastern part. Positive biases are found in the hot northern part of the Sahel and Saharan zones, while in WA the biases are rather small. Dosio (2016) argued from the results of the CORDEX-Europe experiment that the underestimation of the number of summer days SU is the consequence of the underestimation of the daily maximum temperature TX. The biases in the southern parts of the investigated area are smaller. However, the number of observed SU days is small there. The underestimation of the number of summer days in MPAS is because of the cold biases in simulating the maximum temperature (Table 4.1).

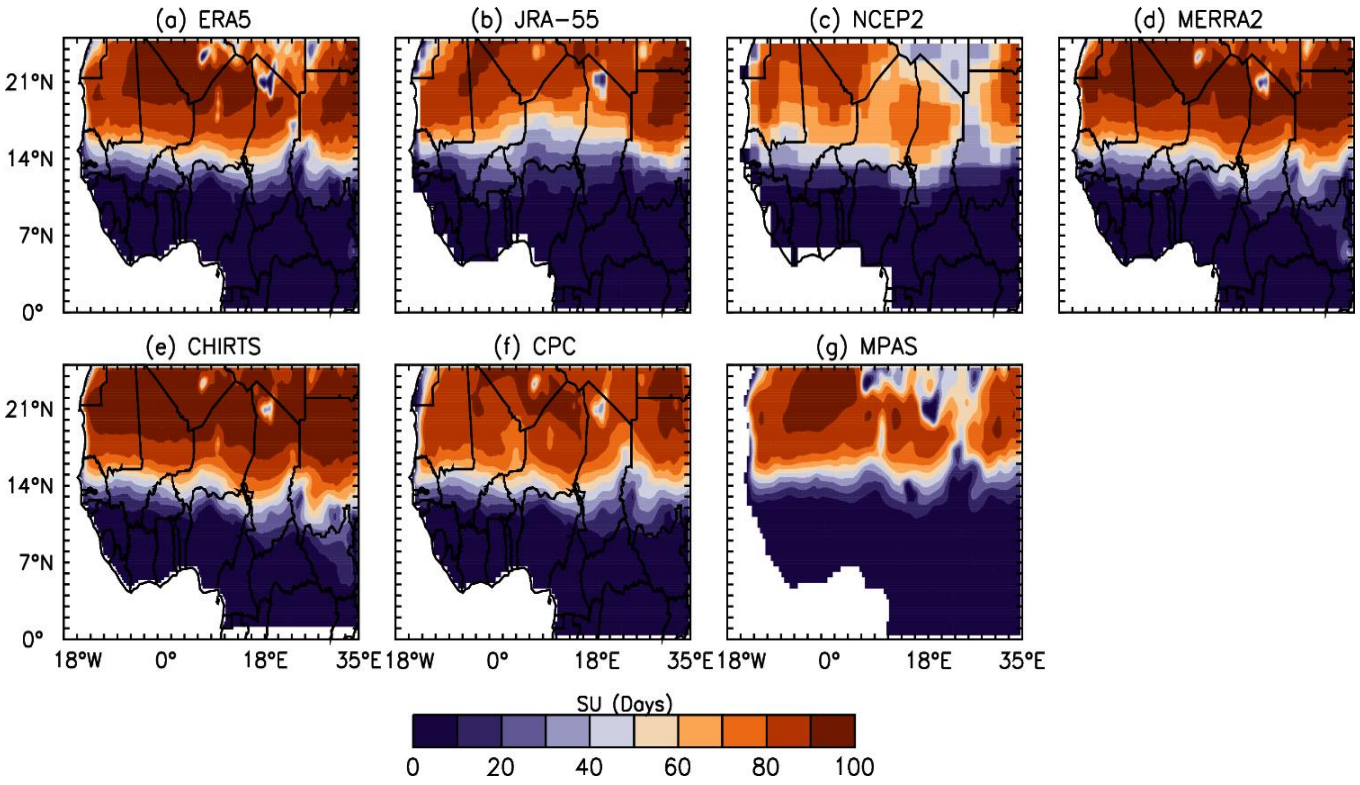

Figure 4.24: Spatial distribution of SU for Simulated MPAS and reference data.

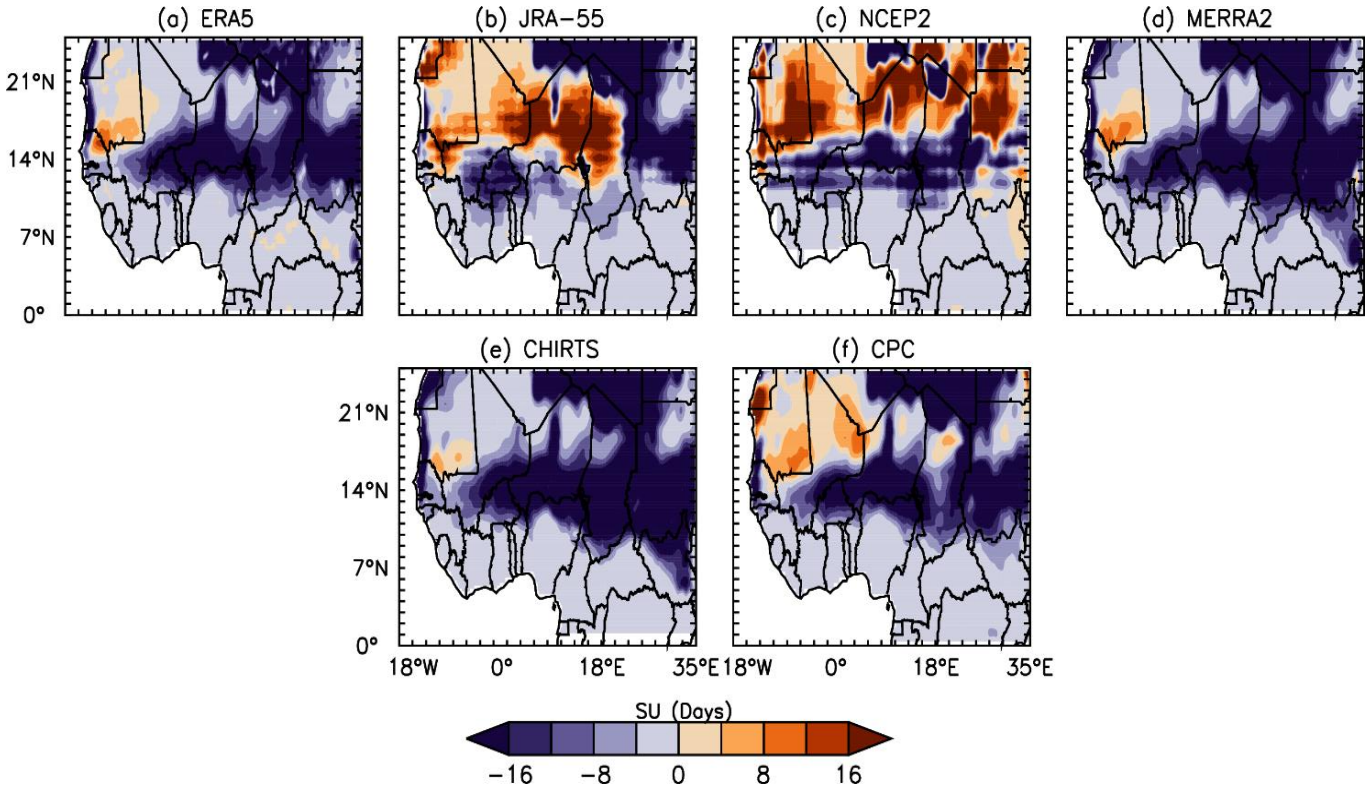

Figure 4.25: Simulated MPAS SU differences between the MPAS and reference data.

.

Figure 4.26 and Figure 4.27 show respectively the regional seasonal patterns and differences between MPAS and different datasets of the number of simulated heat wave duration index (HWDI). All the datasets show an increase in the HWDI from south to north, which does not contradict the increase in the temperature into the same direction. Only NCEP-2 shows smaller HWDI among the reanalysis. In comparison with CPC MPAS shows smaller HWDI, while a positive bias dominates in comparison with the CHIRTS. Differences between JRA-55 and NCEP-2 are mostly negative. With ERA5 and MERRA-2, positive biases dominate the northern part. In the southern part, the biases are rather negative and larger with the JRA-55 reanalysis. The largest discrepancies seem to occur around the latitude of 15°N. Compared to the reanalyzes, the underestimation of the HWDI in MPAS is strongly related to the cold biases in the simulation of the TX of MPAS.

.

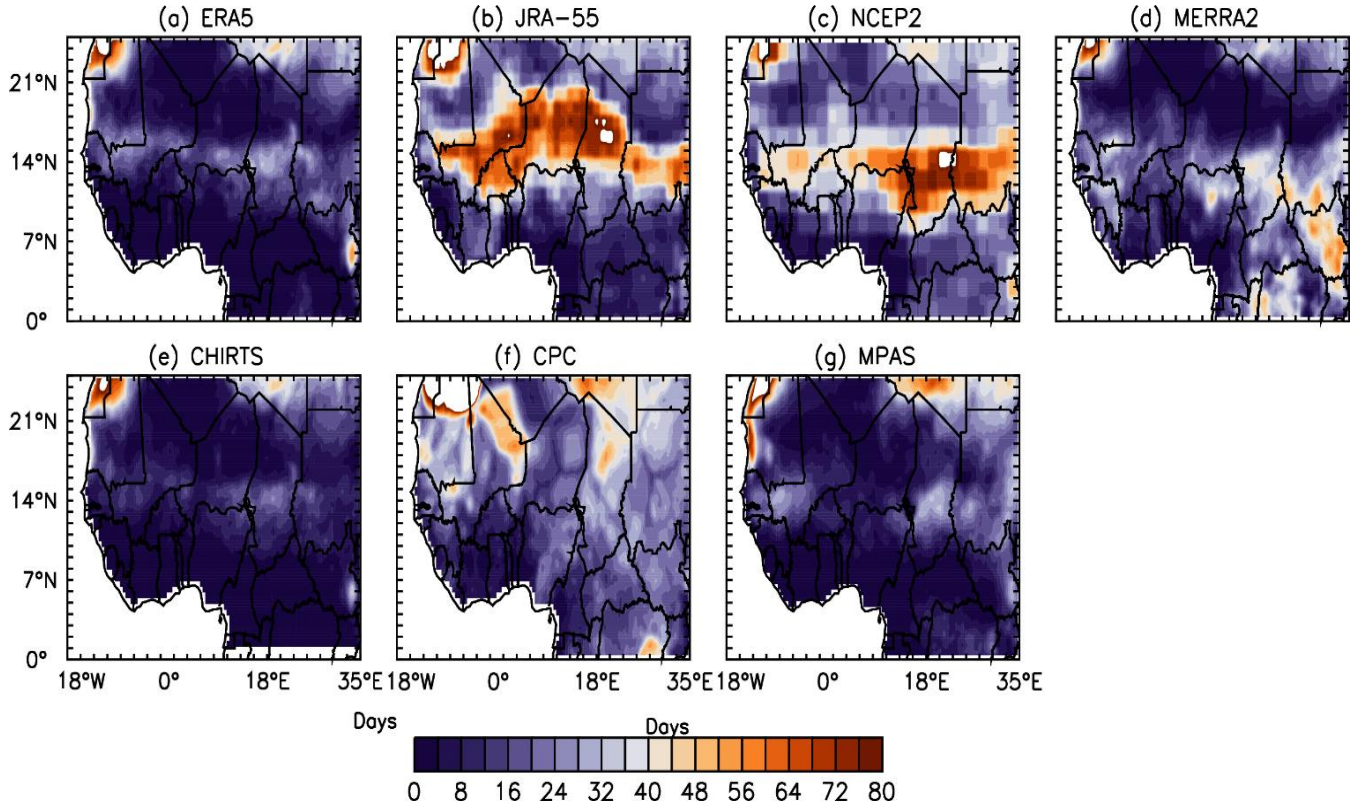

Figure 4.26: Spatial distribution of HWDI for Simulated MPAS and reference data.

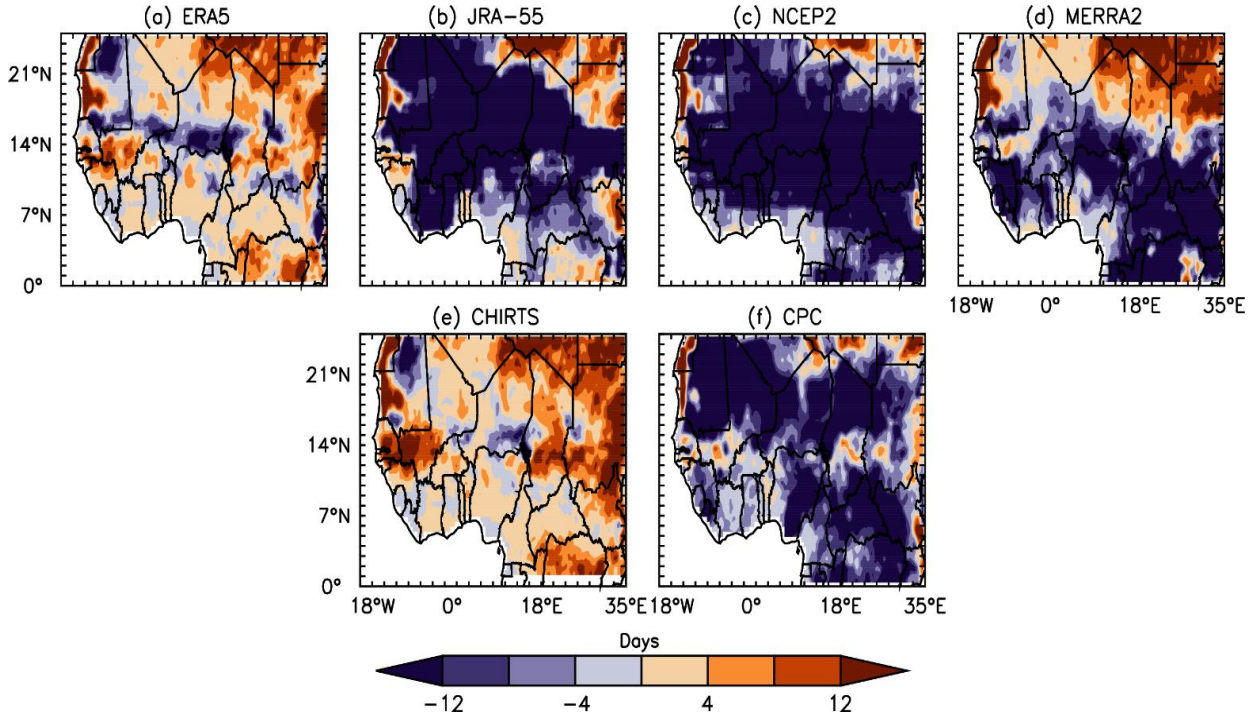

Figure 4.27: Simulated HWDI differences between the MPAS and reference data.

.

Figure 4.28 and Figure 4.29 depicts respectively the regional seasonal patterns and differences between MPAS and the different datasets of the number of Tropical nights (TR) with daily minimum temperature TN > 24° C. The regional pattern in comparison to all datasets show that the number of numbers of tropical nights increases from south to north as the evolution of temperature which also increases in the same direction. All the reanalysis shows larger TR in the eastern and northern parts of Sahel except NCEP-2 which shows a few days of TR. The TR is higher in CHIRTS than in CPC for the observed dataset. MPAS simulates the spatial pattern closer to the reanalyses. However, differences between MPAS and all datasets are similar in the Sahel, showing large underestimations, especially in the western and southern parts. Positive biases are found in the hot northern part of the Sahel and Sahara zones, while the biases are relatively small in WA. Dosio (2016) argued from the results of the CORDEX-Europe experiment that the underestimation of the number of tropical nights TR is the consequence of the underestimation of daily minimum temperature TN. The biases in the northern parts of the investigated area are smaller. However, the number of observed TR days is small there.

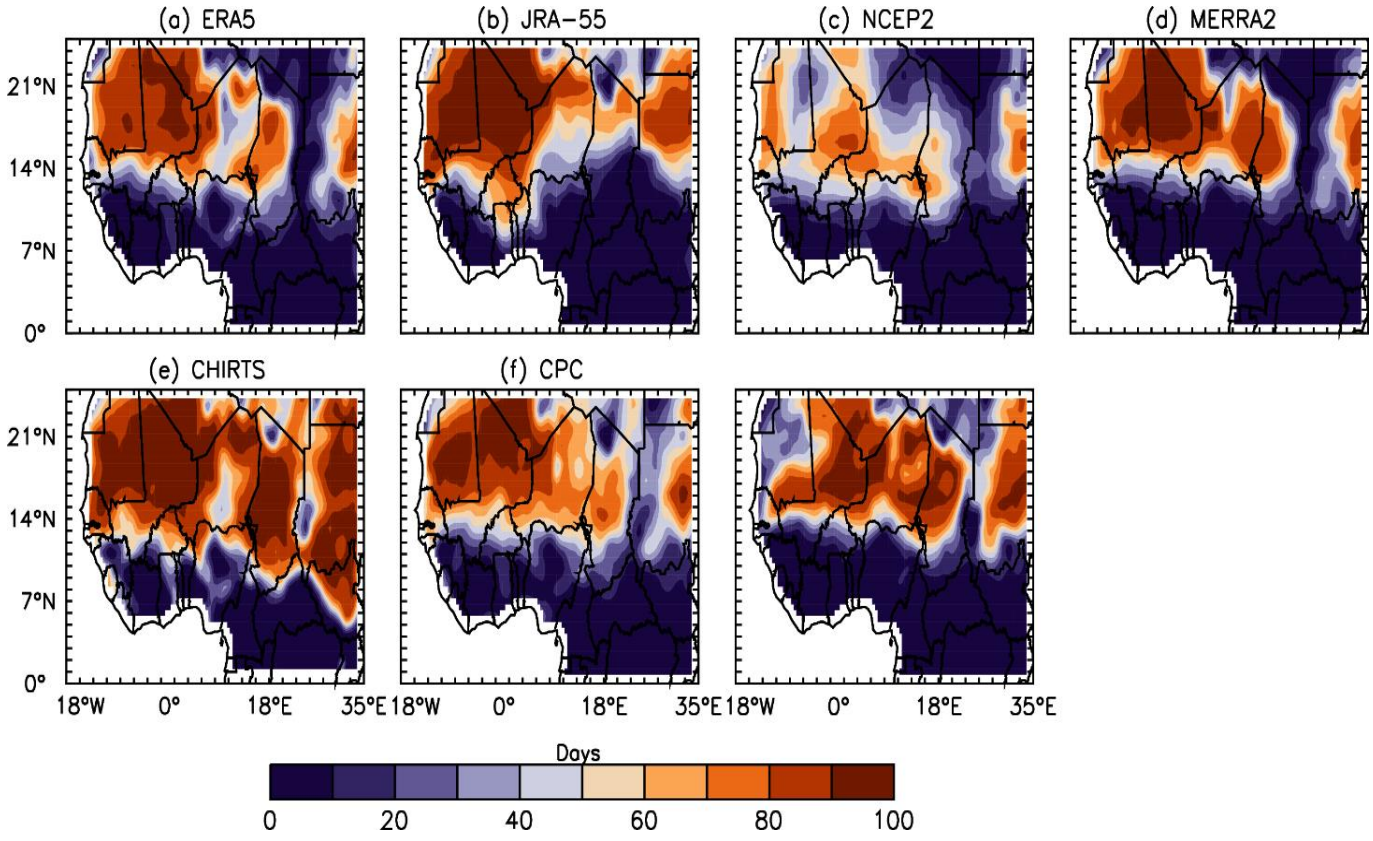

Figure 4.28: Spatial distribution of TR for Simulated MPAS and reference data.

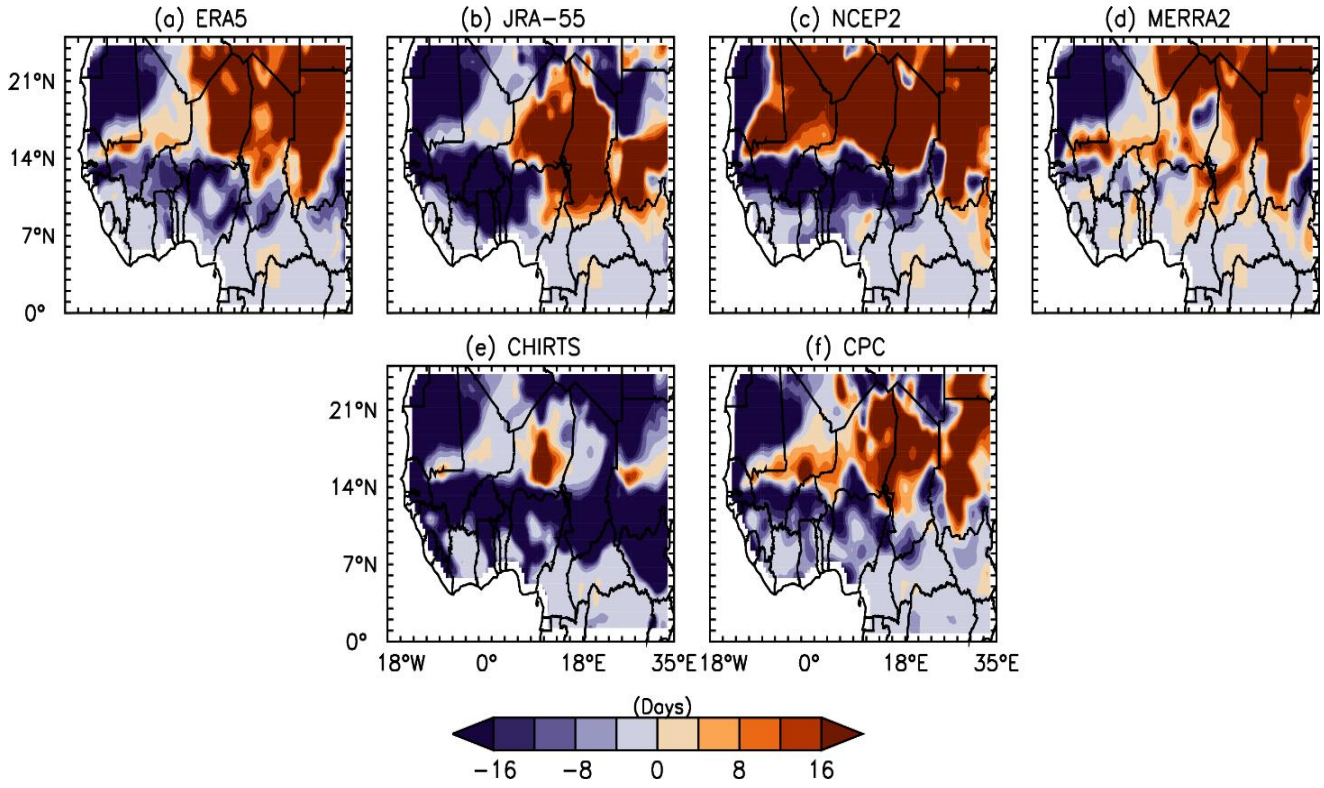

Figure 4.29: Simulated TR differences between the MPAS and reference data.

Summarizing the regional findings, it can be concluded that a cold bias in the TX is evident. It dominates the results obtained for the related temperature indices. Due to large differences between the single reference data, those results are less clear

The cold biases in MPAS may contribute to dry biases in the simulated rainfall, as the temperature gradient is the origin of jets, which in turn transport moisture, and the development of rainfall over the Sahel (Grist & Nicholson, 2001). In addition, the deficiencies in precipitation may also be related to the fact that the MPAS underestimates the number of summer days. SU can affect the convection and regional precipitation recycling (Arnault *et al*., 2016) over WA and the Sahel. Nicholson and Webster (2007) argued that the reduction in the number of mesoscale convective systems negatively influences the formation of rainfall over the Sahel.

4.3.2 Precipitations indices

Figure 4.30 shows the distributions of the area mean summer (JJA) daily rainfall RR in the investigated area SAH_W, SAH_E, and GUI_C for both reference data and the performed MPAS simulations. It reveals that the results obtained with MPAS are well in range in the SAH_E, with only slight differences between the different simulation approaches of MPAS_A and MPAS_B. However, in the SAH_W and GUI_C, MPAS underestimates the distributed rainfall.

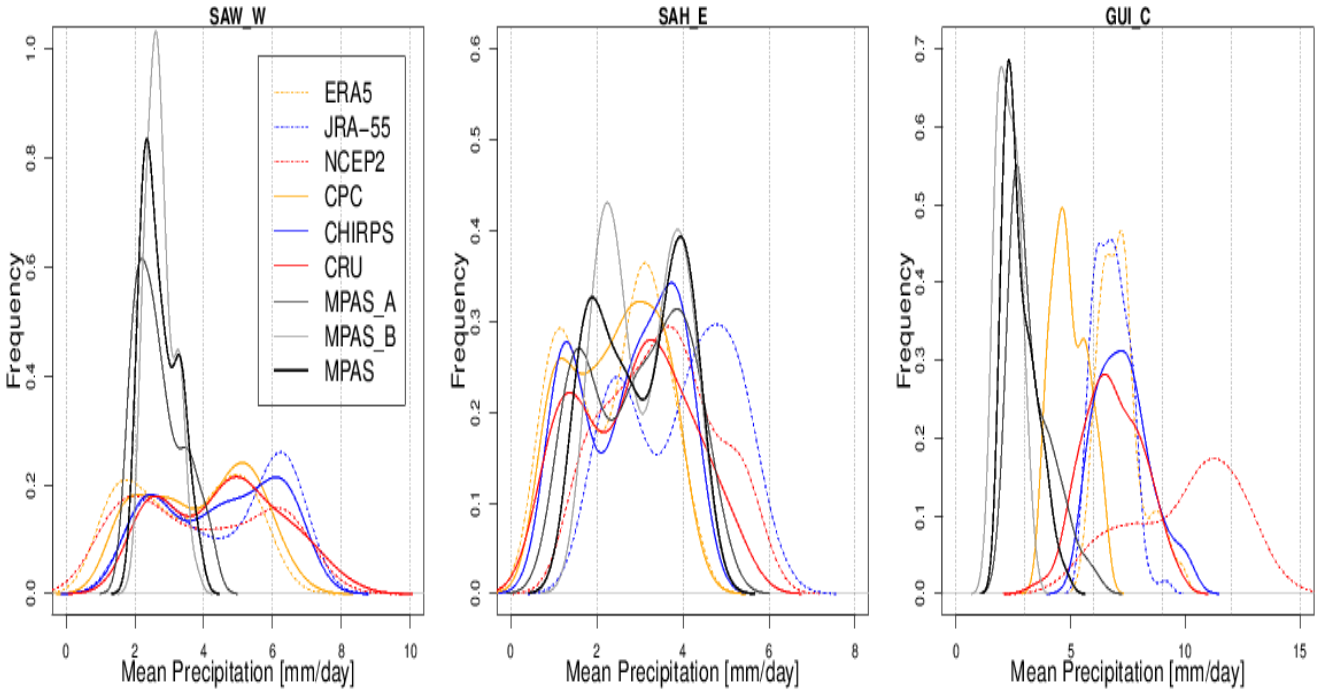

Figure 4.30: Distribution of the area mean summer (JJA) daily rainfall RR in the investigated area SAH_W, SAH_E and GUI_C.

4.3.2.1 Area mean values of precipitation indices

Table 4.2 shows the results for the investigated precipitation indices in the investigation areas SAH_W and SAH_E in comparison with observational reference from satellite, gauge and reanalysis products as presented by Dosio *et al*. (2021b). It reveals an underestimation of the observed amount of daily precipitation RR in the SAH_W area by 1.6 mm/d or 38%, and is outside the range of the observational datasets. In SAH_E MPAS slightly overestimates the observations, by 4%, and is well within the range of the reference data. Only small biases are present in the number of rainy wet days (RR1) with precipitation of at least 1 mm in the area SAH_W. The shortcoming here is the low precipitation intensity on wet days. Also, an underestimation on the order of 40% is present for the area mean maximum daily rain Rx1day. In SAH_E, RR1 is overestimated by 37% and the maximum daily rain is underestimated by 31%. The investigations of Dosio *et al*. (2021a) based on CMIP5, CIMIP6 global models and CORDEX experiments found a large spread between the models. The MPAS results are within the range of those findings. However, it has to be concluded that it has a significant dry bias for West Africa.

Figures 4.31 to 4.32 depict boxplots of a number of wet days RR1 and maximal daily rainfall (Rx1day). For the reference data and the MPAS simulations. Corresponding area mean values are shown in Table 4.2. In the SAH_W area, MPAS simulates positive bias for RR1 up to 3.7 days compared to the mean of all the reference data. Results are similar in the SAH_W. The bias is smaller (2.9 days) in the reanalysis than in the observed dataset (5 days). For Rx1day, MPAS shows negative bias up to -14.5 mm/day compared to the mean of all the reference data and does not show any difference when compared to both the reanalysis and observed dataset. Results obtained over SAH_E give a larger positive bias than in SAH_W for RR1 in comparison with all the datasets, 11.5 days, 8.5 days, and 16.2 days respectively. The negative bias is smaller in SAH_W. However, over the GUI_C, MPAS gives the largest negative bias than in SAH_E and SAH_W for both RR1 and Rx1day.

Table 4.2. Mean values of precipitation indices over the investigation areas for the JJA season, both observed and simulated.

Area	RR (mm/day)	RR1 (days)	RX1day (mm/day)
SAH_W			
ERA5	3.4	38.1	35.0
JRA-55	4.5	48.5	27.5
NCEP-2	3.8	28.4	46.1
CPC	3.8	33.0	42.5
CRU	4.6	-	-
GPCC	4.3	-	-
CHIRPS	4.4	39.4	31.3
S	**3.7–4.6–7.0**	**32.8–39.3–47.6**	**22.0–41.3–68.1**
G	**3.9–4.3–4.6**	**33.8–40.3–49.6**	**29.1–39.3–46.2**
R	**2.8-4.1-5.2**	**23.8-47.2-63.6**	**25.7-33.5-43.1**
MPAS_A	2.6	41.4	21.6
MPAS_B	2.7	42.7	22.4
MPAS	2.7	41.2	22.0
SAH_E			
ERA5	2.3	33.1	20.0
JRA-55	3.9	48.0	20.0
NCEP-2	3.4	25.5	42.7
CPC	2.1	24.2	29.6
CRU	2.8	-	-
GPCC	2.7	-	-
CHIRPS	2.7	31.5	21.7

S	**2.1-2.9-4.7**	**22.1-29.5-37.5**	**18.2–29.8–51.5**
G	**2.5–2.8–3.1**	**25.9–31.2–38.8**	**23.3–31.0–40.5**
R	**2.4-3.1-3.7**	**25.9-41.5-49.1**	**16.7-28.1-44.1**
MPAS_A	2.9	40.6	21.6
MPAS_B	3.0	47.4	21.0
MPAS	3.0	44.0	21.3
GUI_C			
ERA5	7.6	76.4	54.0
JRA-55	7.4	72.0	32.7
NCEP-2	10.8	63.7	88.3
CPC	5.1	40.0	52.4
CRU	7.3	-	-
GPCC	7.1	-	-
CHIRPS	7.5	44.1	54.7
MPAS_A	2.8	50.6	10.0
MPAS_B	2.9	40.0	13.5
MPAS	2.9	45.3	11.8

Nb: S, G and R denote minimum, mean and maximum values of observational datasets for satellite (S), gauge (G) and reanalysis (R) products as presented by Dosio, Pinto, et al. (2021).

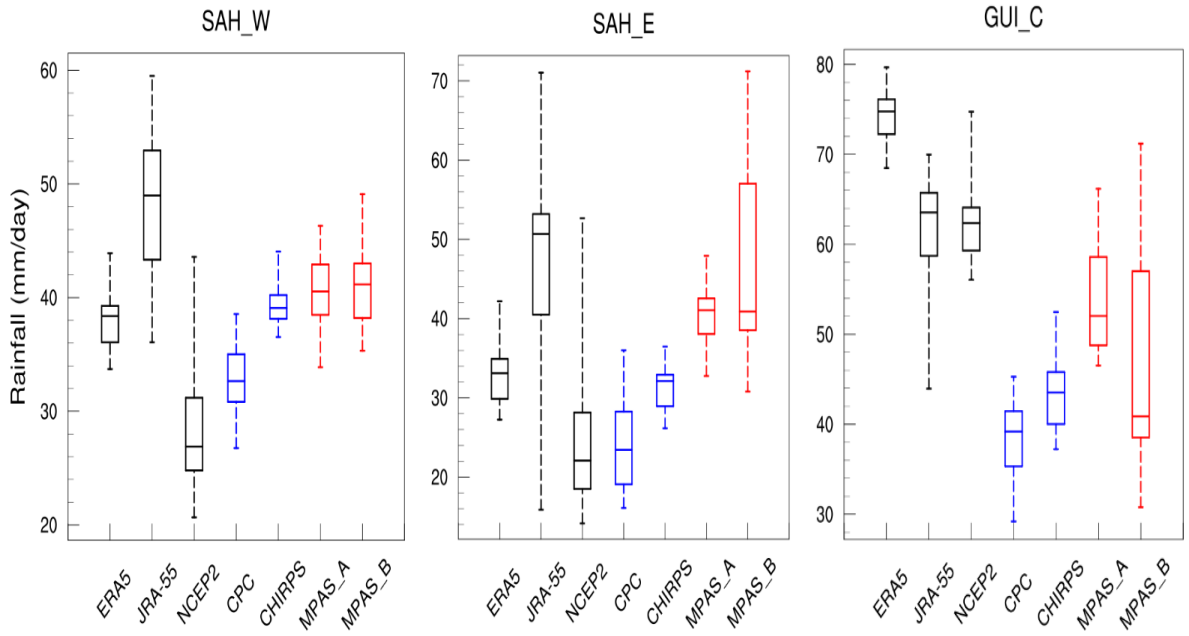

Figure 4.31: Boxplots of number of wet days RR1 when RR >= 1 mm for the reference data and MPAS simulation in the investigation areas SAH_W, SAH_E and GUI_C and the summer season (JJA).

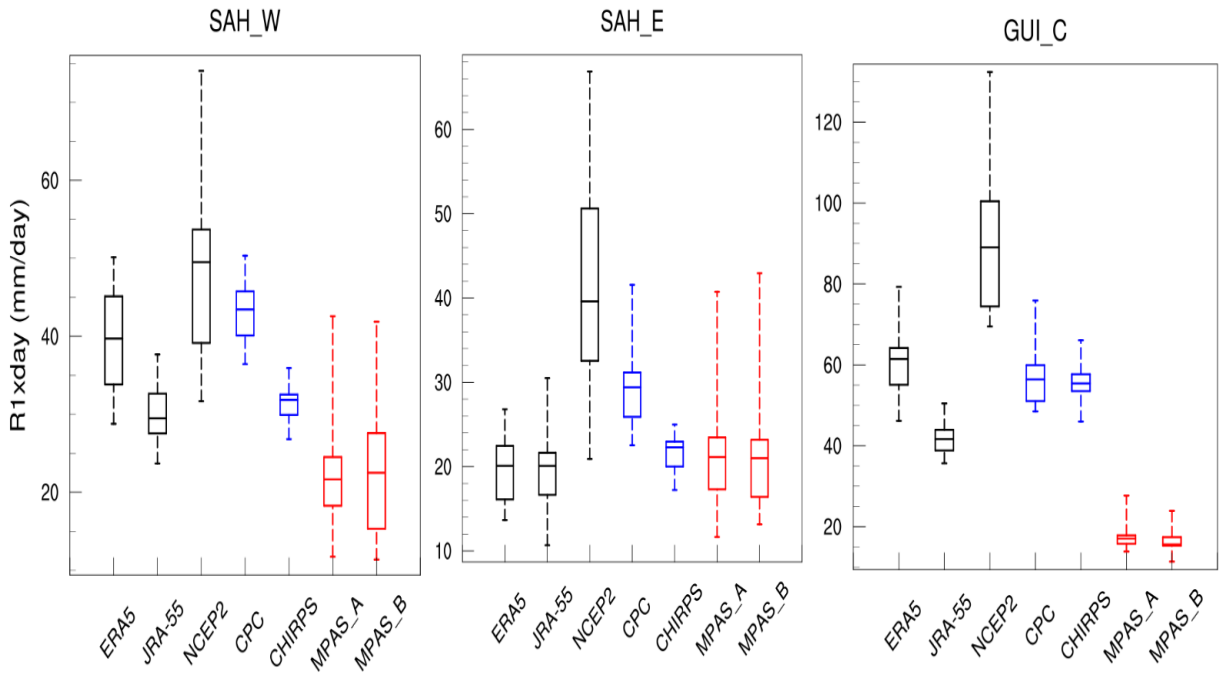

Figure 4.32: Boxplots of maximal daily RR (R1xday) for the reference data and MPAS simulation in the investigation areas SAH_W, SAH_E and GUI_C and the summer season (JJA).

4.3.2.2 Regional differences in precipitation indices

Figure 4.33 and Figure 4.34 depicts respectively the regional seasonal patterns and differences between MPAS as the mean value of the MPAS_A and MPAS_B experiments and the applied reference data during JJA season of the number of wet days (RR1) when RR > 1mm. The regional pattern of all datasets shows that the number of wet days decreases from south to north as the evolution of rainfall also decreases in this direction. The RR1 is larger over the Gulf of Guinea in the reanalyzes than in observed data. However, MPAS shows the RR1 in the Eastern Sahel closer to CHIRPS. MPAS underestimates RR1 over the Sahelian zone in comparison with ERA5 and NCEP2 while overestimating in the coastal area. Only results with JRA-55 overestimate the RR1 over the Sahelian zone. Smaller biases are shown over the northern part in comparison to all the datasets. The biases in the observed data might be impacted by the low station density in some zones and the low resolution of the reanalysis data therefore, MPAS performs realistically well.

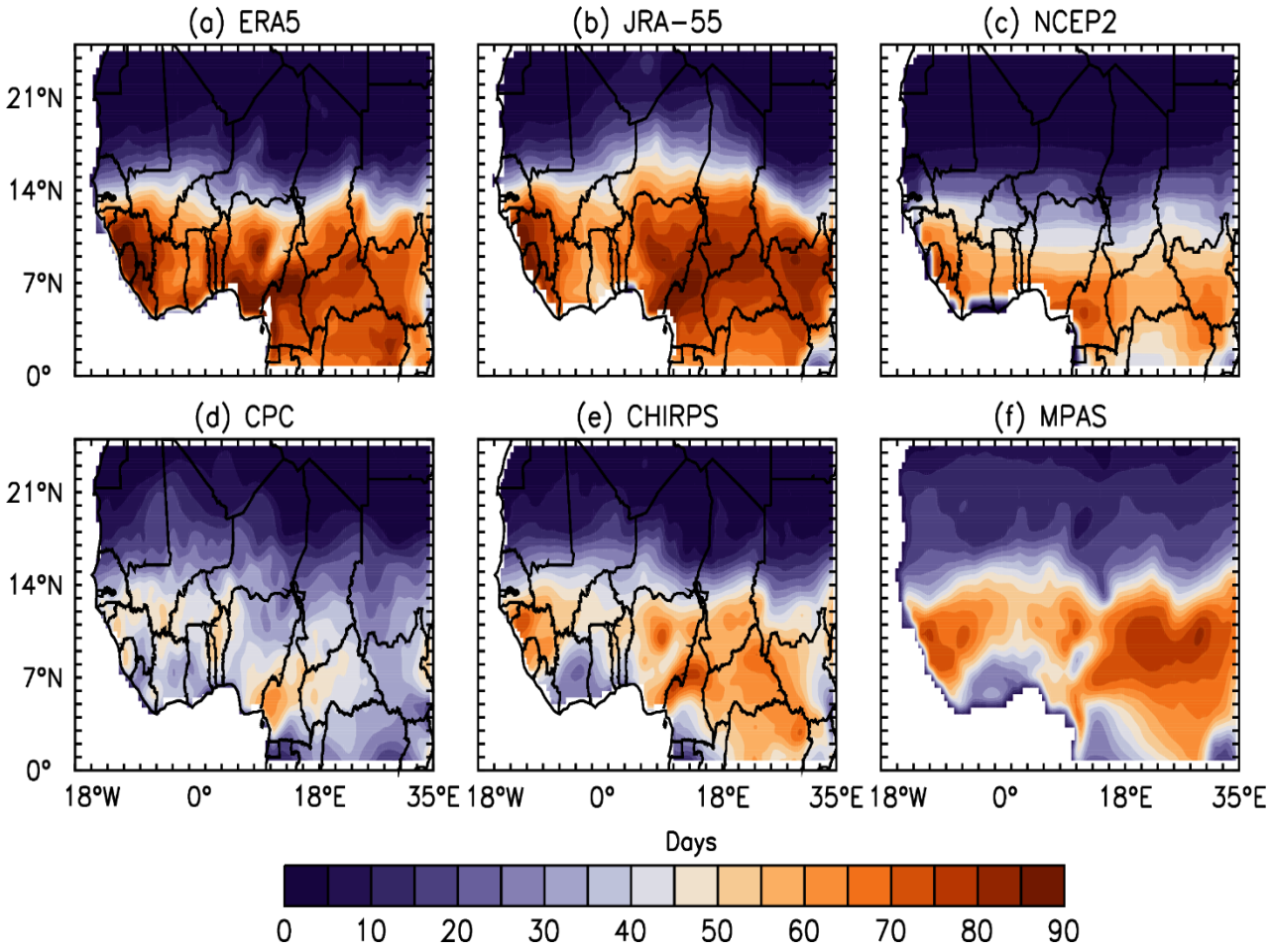

Figure 4.33: Spatial distribution of RR1 for Simulated MPAS and reference data.

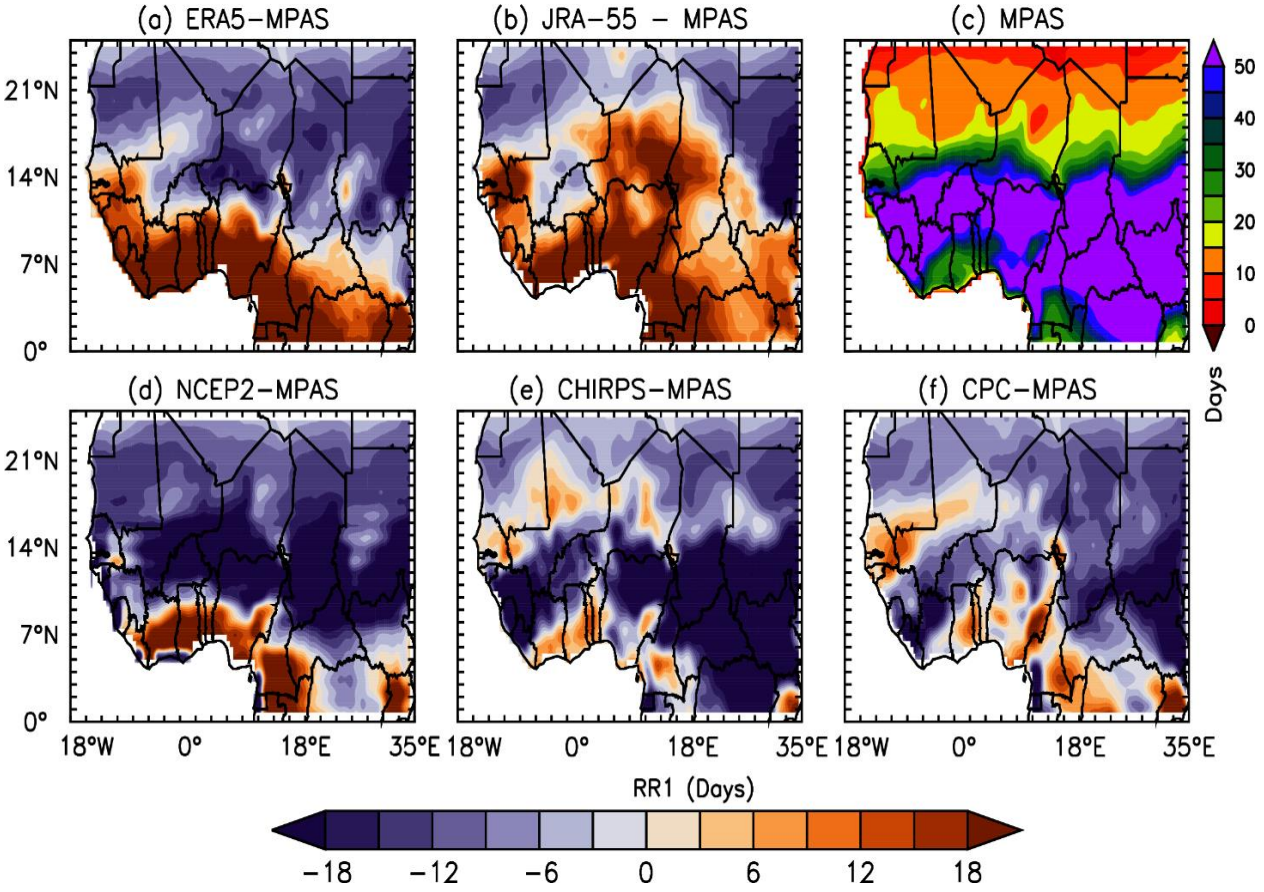

Figure 4.34: Simulated RR1 differences between the MPAS and reference data.

Figure 4.36 shows the maps of the MPAS simulated spatial distribution of maximum rainfall days (RX1day) and differences (Figure 4.37) between MPAS as the mean value of the MPAS_A and MPAS_B experiments and the mean of the applied reference data. All the datasets show that the RX1day decreases from south to north. in agreement with what has been shown in the area mean values (Table 4.2). Larger biases are found at regional scales. In comparison with the reanalysis, MPAS reveals a notable dry bias throughout the region. Only NCEP-2 shows the highest RX1day over the Gulf of Guinea. Only in the eastern and central Sahel, there are small wet biases, but results show strong dry bias in comparison with NCEP2. In comparison with the observed, dry biases are generally present, revealing similar patterns. Only CPC shows higher RX1day than CHIRPS, while MPAS shows underestimation over the Gulf of Guinea Generally, results reveal a slight wet bias in the eastern Sahel.

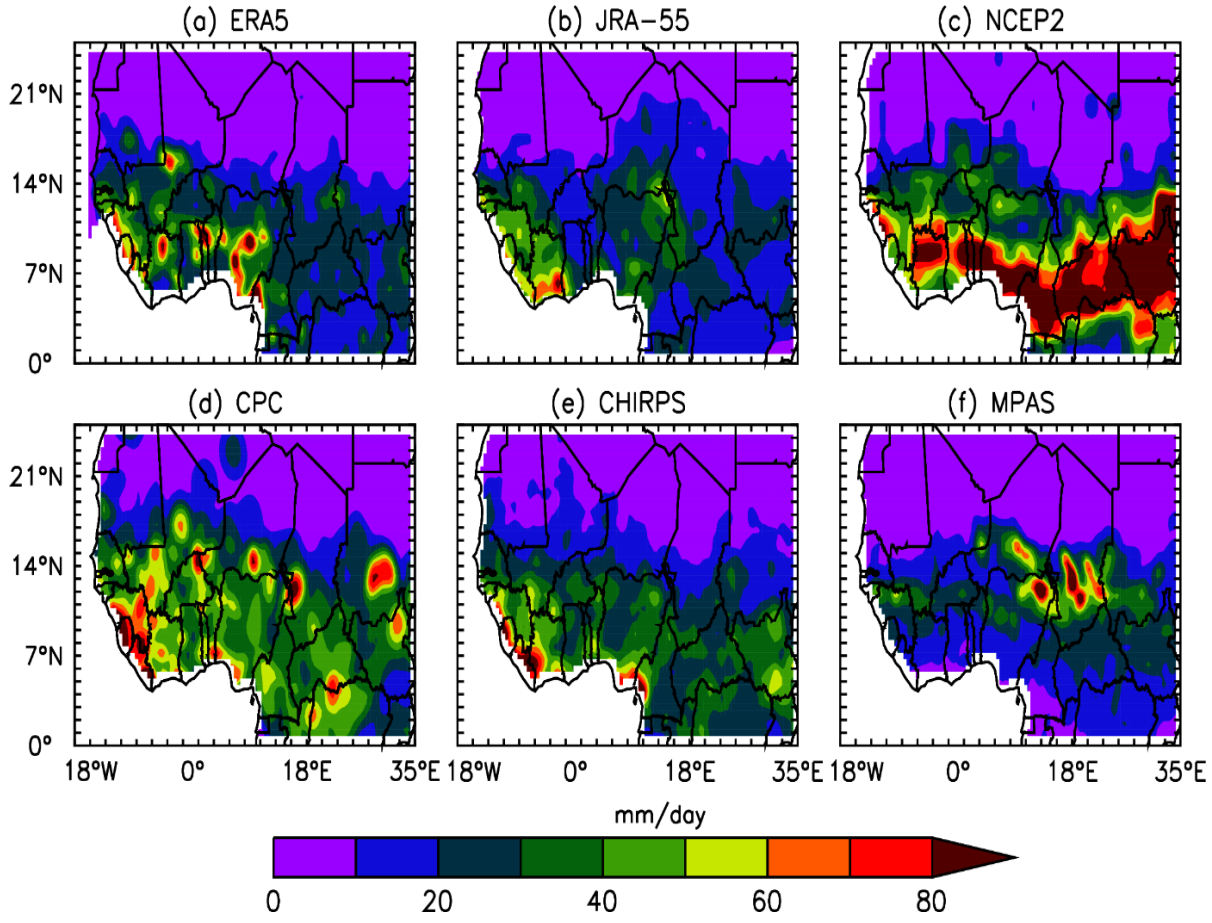

Figure 4.35: Spatial distribution of RX1day for Simulated MPAS and reference data.

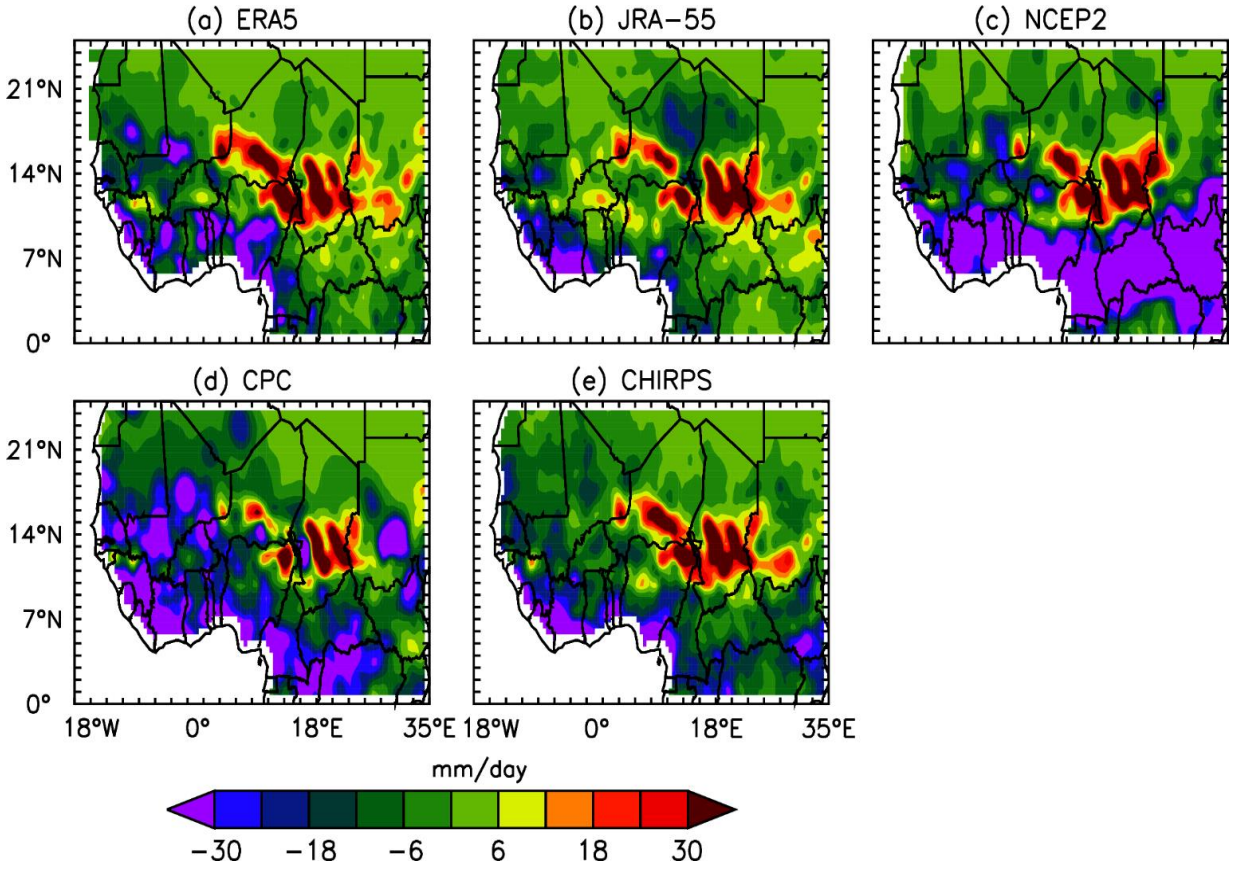

Figure 4.36: Simulated RX1day differences between the MPAS and reference data.

Various reasons have been discussed explaining the obvious deficiencies of the climate models in reproducing observed temperature and precipitation characteristics in WA and the Sahel. They are related to a misplacement of the center of the monsoon and the underestimation of its intensity and to the northern shift of the West African Heat Low (Panitz *et al*., 2014), errors in the simulation of the lateral terrestrial water flow and its contribution to land surface evaporation (Arnault *et al*., 2021), as well as underestimation of the surface short-wave radiation and latent heat flux, cloudiness, surface water and the surface albedo (Sylla *et al*., 2009; Diallo *et al*., 2017; Dieng *et al*., 2017). In applications of the WRF model together with the Noah-LSM, Glotfelty *et al*. (2021) identified the satellite derived albedo climatology as a source of additional errors. Careto *et al*. (2018) linked higher temperatures to evaporative stress and strong soil moisture temperature coupling in some areas. For the Sahel, however, they stated that precipitation regimes are more important. Finally, as pointed out by Heinzeller *et al*. (2018), the choice of physical parametrizations can greatly influence the model's capabilities, especially the accuracy of the surface temperature and precipitation.

In summary, it can be stated that the MPAS global static 60-km mesh approach does not provide higher fidelity than the regional climate models. However, the ability of MPAS to apply variable meshes in a regional refinement and to run in convection permitting mode opens possibilities for improvements, as shown by Heinzeller *et al*. (2016).

CHPAPTER FIVE

5.0 CONCLUSION AND RECOMMENDATION

5.1 Conclusion

5.1.1 WAM rainfall pattern

MPAS gives a realistic representation of the WAM rainfall pattern, which follows the displacement of the ITCZ. Most notably, MPAS correctly places the ITZC as in ERA5 and shows that the rainfall decreases northward in good agreement with the observed data. Furthermore, MPAS performs better than all the CMIP6 datasets during DFF and MAM seasons. However, MPAS struggles to capture the maxima of orographic rainfall (Guinea Highlands, Cameroun Mountains, Jos Plateau) compared to observed data and the reanalysis.

5.1.2 Seasonal cycle of WAM

MPAS reproduces the main phases of the WAM as in the observed datasets. The simulated onset is from March to June in MPAS, characterized by the northward extension of the rain belt from the coast. The simulated peak is characterized by a northward (10° N - 14° N) jump of the rain-belt and the end of the rainfall south of 6°N, occurring from June to September in MPAS as in the observations. In addition, MPAS simulates the bimodality of rainfall over the Guinea and the unimodality over the Savana and Sahel as in the observations. There are substantial dry biases in the MPAS simulations of the monsoon peak. The error, which ranges between -1 to -5 mm/day, is out of range of the uncertainty in the observed data (-1mm/day). Compared to CMIP6 models, MPAS shows larger biases in the simulation of the WAM rainfall.

MPAS performs well in simulating the annual cycle of zonal wind at 700 hPa. The monsoon flow is well captured around Guinea, and the model shows the different phases of the flow, for instance, the ascendence from March to June, the peak in August, and the southward retreat from September to October.

However, over Sahel, MPAS captures southeast winds from January to March and October to December with high intensity. MPAS also fails to capture the strength of monsoon during the peak period of August over Sahel and Savana compared to ERA5. In addition, MPAS weakly simulates the annual cycle of the zonal wind more than all the CMIP6 models when referring to ERA5. The underestimation of the monsoon flow and the overestimation of harmattan may explain MPAS's struggles to capture the peak of monsoon rainfall over West Africa.

5.1.3 WAM rainfall producing system

MPAS captures well the low-level monsoon flow as in ERA5. The northward extension is well represented in agreement with ERA5. The core of the AEJ is around 15°N and 600 hPa in the reanalysis and all the CMIP6 models. The absence of MPAS output at 600 hPa pressure level weakens the analysis of the AEJ in the model. MPAS simulates the strength of the TEJ (200hPa) quite well as in ERA5. However, MPAS overestimates the low-level monsoon flow and fails to locate the TEJ as in ERA5.

MPAS underestimates the vertical velocity of all the shallower zones compared to ERA5. All the CMIP6 models show an overestimation of the vertical motion. Hence, the convection activities are more substantial in MPAS compared to ERA5. Overall, the dry

biases in MPAS may be linked to the weak representation of the convective activities over the Sahel, Savana, and Guinea Coast.

5.1.4 Simulation of thermal activities during summer

MPAS fails to locate the temperature gradient farther north than ERA5 does. In contrast with ERA5, MPAS simulates the temperature gradient at almost the exact location in the north through all the months. The misplacement of the gradient in MPAS can influence the atmospheric circulation in the Sahelian zone, as the temperature gradient is responsible for the formation of the jet.

MPAS simulates the magnitude of the thermal wind as in ERA5 but less extended eastward and northward as ERA5 does. However, for the thermal wind between 700 and 925 hPa, MPAS shows the opposite of the thermal wind between 500 and 925 hPa, where MPAS simulates a smaller area of the thermal activities; this may influence the formation of the wind shear, hence the easterly jets, and may cause MPAS to simulate a weaker AEJ that may contribute to the dryness in MPAS over the investigated area.

Summarizing, several reasons can be linked to the model error leading to the dry bias in the model outputs. These reasons include the resolution used, the weak representation of the jets during summer, the cold bias and the temperature gradient over the continent, and the smaller representation of the thermal activities. Further study is needed to improve the simulation; for instance, using variable resolution or sensitivity to SST can be a solution to improve MPAS results obtained from the regular grid.

5.1.5 Simulation of temperature extreme, heat waves, and precipitation indices

The results reveal moderate cold biases in the range from -0.6°to -0.9° C for the daily mean temperature and increase to -1.4°–-2.0° C for the area mean of the daily maximum temperature TX and to -2.2°–-2.7° C for TXx as the maximum of TX. The bias in the number of tropical nights TN ranges from +3 to -10 days. An underestimation by up to 50% is also present in the number of summer days SU with TX > 35°C. The percentage of days when TN > the 90th percentile TN90p as well as the percentage of days when TX > the 90th percentile TX90p reveal underestimations by up to 50%, and the heat wave duration index HWDI is underestimated by 10%–60%. Compared to the reanalyses, the biases revealed by the MPAS simulations are generally smaller than with the measured observational reference. Because of the present and reported deficiencies in the observed data for the Sahel, the shortcomings in the MPAS simulations are in reality most likely smaller.

Regional biases are to a large extent negative. Regarding temperatures, the smallest biases occur in West Africa. The smallest biases in precipitation occur in the eastern part. However, the underestimation in the first case and the overestimation in the second reveal that improvements of the model regarding its physics, land–surface scheme, and land surface input data are required for an adequate simulation of the WA and Sahelian climate.

The results obtained from the two model initialization procedures used are very similar and demonstrate the equivalence of the two approaches. Compared to long term runs, selections of the initialization years in relation to the spread of mean SST temperatures in the Gulf of Guinea extremely reduce the demand on the CPU, especially when only short terms, such as months or specific seasons, are considered.

Shortcomings in the reproduction of temperatures and precipitation found in the present investigation indicate that the global approach does not provide higher fidelity than regional climate models. Kim *et al*. (2014) showed that in CORDEX- Africa, multi model ensembles generally outperformed the single ensembles. In such ensemble approaches, MPAS simulations can be applied as an adequate member.

5.2 RECOMMENDATIONS

One of the significant challenges in conducting research in West Africa is the scarcity of a dense observational network. This research needs a dense observation network to perform a more solid evaluation of the MPAS model output. However, this evaluation was limited as the observed data were verified against satellite and reanalysis products. Hence, there is a need to spread the current observations networks to perform a trustier model validation at a larger temporal and spatial scale, particularly for extreme climate variables like rainfall.

Mainly, the error in the model's output originates from the model components, such as the dynamics, physics, and other less-considered model elements, as well as modification in the model program of initialization datasets. Therefore, it is recommended that the MPAS model development community work on the MPAS model physics for better atmospheric feature (WAM) representation and reduction of the biases in the model results.

Adding more pressure levels in the diagnostics files is recommended to facilitate the comparison to the reanalysis datasets. This addition of variables includes the zonal wind, meridional wind, vertical velocity, and temperature at different pressure levels.

It is also recommended to evaluate MPAS using variable resolution (stretch grid) in simulating temperature and precipitation indices during the boreal summer monsoon at higher resolution.

It is essential also to continue assessing the model over Africa in general and over West Africa particularly, because it is a promising tool with multi purposes (variable resolution, uniform resolution) that can revolute the climate modeling science in next coming years.

REFERENCES

Abatan, A. A. (2011). West African extreme daily precipitation in observations and stretched-grid simulations by CAM-EULAG. Iowa State University.

Abiodun, B. J., Gutowski, W. J., Abatan, A. A., & Prusa, J. M. (2011). CAM-EULAG: A non-hydrostatic atmospheric climate model with grid stretching. *Acta Geophysica*, *59*(6), 1158-1167.

Abiodun, B. J., Pal, J. S., Afiesimama, E. A., Gutowski, W. J., & Adedoyin, A. (2010). Modelling the impacts of deforestation on monsoon rainfall in West Africa. In IOP Conference Series: Earth and Environmental Science (Vol. 13, No. 1, p. 012008). IOP Publishing.

Abiodun, B. J., Salami, A. T., Matthew, O. J., & Odedokun, S. (2013). Potential impacts of afforestation on climate change and extreme events in Nigeria. Climate dynamics, 41(2), 277-293.

Adeniyi, M. O., & Oyekola, S. O. (2017). Assessment of heat and cold wave events over West Africa using three regional climate models. Annals of Geophysics, 60(3), A0322-A0322.

Afiesimama, E. A., Pal, J. S., Abiodun, B. J., Gutowski, W. J., & Adedoyin, A. (2006). Simulation of West African monsoon using the RegCM3. Part I: model validation and interannual variability. Theoretical and Applied Climatology, 86(1), 23-37.

Ahmed, K. F., Wang, G., Yu, M., Koo, J., & You, L. (2015). Potential impact of climate change on cereal crop yield in West Africa. https://doi.org/10.1007/s10584-015-1462-7

Ajibola, F. O., Zhou, B., Tchalim Gnitou, G., & Onyejuruwa, A. (2020). Evaluation of the performance of CMIP6 HighResMIP on West African precipitation. Atmosphere, 11(10), 1053.

Akinsanola, A. A., Ajayi, V. O., Adejare, A. T., Adeyeri, O. E., Gbode, I. E., Ogunjobi, K. O., ... & Abolude, A. T. (2018). Evaluation of rainfall simulations over West Africa in dynamically downscaled CMIP5 global circulation models. Theoretical and applied climatology, 132(1), 437-450

Akinsanola, A. A., Ogunjobi, K. O., Ajayi, V. O., Adefisan, E. A., Omotosho, J. A., & Sanogo, S. (2017). Comparison of five gridded precipitation products at climatological scales over West Africa. Meteorology and Atmospheric Physics, 129(6), 669-689.

Alexander, L. V., Zhang, X., Peterson, T. C., Caesar, J., Gleason, B., Klein Tank, A. M. G., ... & Vazquez-Aguirre, J. L. (2006). Global observed changes in daily climate extremes of temperature and precipitation. *Journal of Geophysical Research: Atmospheres*, *111*(D5).

Avila, L. A., & Pasch, R. J. (1992). Atlantic tropical systems of 1991. Monthly Weather Review, 120(11), 2688-2696.

Barry, A. A., Caesar, J., Tank, A. M. G. K., Aguilar, E., Mcsweeney, C., Ahmed, M., Nikiema, M. P., Narcisse, K. B., Sima, F., Stafford, G., Touray, L. M., Ayilari-naa, J.

A., Mendes, C. L., Tounkara, M., Gar-glahn, E. V. S., Coulibaly, M. S., Dieh, M. F., Oyegade, J. A., Sambou, E., & Laogbessi, E. T. (2018). West Africa climate extremes and climate change indices. https://doi.org/10.1002/joc.5420

Becker, A., Finger, P., Meyer-Christoffer, A., Rudolf, B., Schamm, K., Schneider, U., & Ziese, M. (2013). A description of the global land-surface precipitation data products of the Global Precipitation Climatology Centre with sample applications including centennial (trend) analysis from 1901–present. *Earth System Science Data*, *5*(1), 71-99.

Bernstein, L., Bosch, P., Canziani, O., Chen, Z., Christ, R., & Riahi, K. (2008). IPCC, 2007: climate change 2007: synthesis report.

Besler, H. (1984). Indicators for stability and mobility of sands. Travaux de l'Institut de Géographie de Reims, 59(1), 105-109.

Biasutti, M., & Giannini, A. (2006). Robust Sahel drying in response to late 20th century forcings. Geophysical Research Letters, 33(11).

Broxton, P. D., Zeng, X., Sulla-Menashe, D., & Troch, P. A. (2014). A global land cover climatology using MODIS data. Journal of Applied Meteorology and Climatology, 53(6), 1593-1605. Bryson, R. A. (1973). Drought in Sahelia. Who or what is to blame? Ecologist, 3(10),

Bucchignani, E., Mercogliano, P., Panitz, H. J., & Montesarchio, M. (2018). Climate change projections for the Middle East–North Africa domain with COSMO-CLM at different spatial resolutions. *Advances in Climate Change Research*, *9*(1), 66-80.

Bucchignani, E., Montesarchio, M., Cattaneo, L., Manzi, M. P., & Mercogliano, P. (2014). Regional climate modeling over China with COSMO-CLM: Performance assessment and climate projections. *Journal of Geophysical Research: Atmospheres*, *119*(21), 12-151.

Burpee, R. W. (1972). The origin and structure of easterly waves in the lower troposphere of North Africa. Journal of the Atmospheric Sciences, 29(1), 77-90

Burpee, R. W. (1974). Characteristics of North African easterly waves during the summers of 1968 and 1969. Journal of Atmospheric Sciences, 31(6), 1556-1570.

Cadet, D. L., & Houston, S. H. (1984). Precipitable water over Africa and the Eastern/Central Atlantic Ocean during the 1979 summer. Journal of the Meteorological Society of Japan. Ser. II, 62(5), 761-774.

Caniaux, G., Giordani, H., Redelsperger, J. L., Guichard, F., Key, E., & Wade, M. (2011). Coupling between the Atlantic cold tongue and the West African monsoon in boreal spring and summer. Journal of Geophysical Research: Oceans, 116(C4).

Cardoso, R. M., Soares, P. M., Lima, D. C., & Miranda, P. (2019). Mean and extreme temperatures in a warming climate: EURO CORDEX and WRF regional climate high-resolution projections for Portugal. *Climate Dynamics*, *52*(1), 129-157.

Centre, O. H. L., Franche-comt, B., Universit, O., York, N., Universit, O. M. E., Alpes, G., Umr, L., Locean, A., & Universit, S. (2017). Characterization of Heat Waves in the Sahel and Associated Physical Mechanisms. https://doi.org/10.1175/JCLI-D-16-0432.1

Chagnaud, G., Gallée, H., Lebel, T., Panthou, G., & Vischel, T. (2020). A boundary forcing sensitivity analysis of the West African monsoon simulated by the modele atmospherique regional. Atmosphere, 11(2), 191.

Charney, J., Quirk, W. J., Chow, S. H., & Kornfield, J. (1977). A comparative study of the effects of albedo changes on drought in semi–arid regions. Journal of the atmospheric sciences, 34(9), 1366-1385.

Clough, S. A., Shephard, M. W., Mlawer, E. J., Delamere, J. S., Iacono, M. J., Cady-Pereira, K., ... & Brown, P. D. (2005). Atmospheric radiative transfer modeling A summary of the AER codes. Journal of Quantitative Spectroscopy and Radiative Transfer, 91(2), 233-244.

Cook, K. H. (1999). Generation of the African easterly jet and its role in determining West African precipitation. Journal of climate, 12(5), 1165-1184.

Cook, K. H. (2008). The mysteries of Sahel droughts. *Nature Geoscience*, *1*(10), 647-648.

Cook, K. H., & Vizy, E. K. (2006). Coupled model simulations of the West African monsoon system: Twentieth-and twenty-first-century simulations. Journal of climate, 19(15), 3681-3703.

Coumou, D., & Rahmstorf, S. (2012). A decade of weather extremes. Nature climate change, 2(7), 491-496.

Coumou, D., Rahmstorf, S. A decade of weather extremes. *Nature Clim Change* **2**, 491–496 (2012). https://doi.org/10.1038/nclimate1452

Couvreux, F., Rio, C., Guichard, F., Lothon, M., Canut, G., Bouniol, D., & Gounou, A. (2012). Initiation of daytime local convection in a semi-arid region analysed with high-resolution simulations and AMMA observations. Quarterly Journal of the Royal Meteorological Society, 138(662), 56-71.

Dai, A., Trenberth, K. E., & Qian, T. (2004). A global dataset of Palmer Drought Severity Index for 1870–2002: Relationship with soil moisture and effects of surface warming. Journal of Hydrometeorology, 5(6), 1117-1130.

Danielson, J. J., & Gesch, D. B. (2011). Global multi-resolution terrain elevation data 2010 (GMTED2010) (p. 26). Washington, DC, USA: US Department of the Interior, US Geological Survey.

Davis, C. A., Ahijevych, D. A., Wang, W., & Skamarock, W. C. (2016). Evaluating medium-range tropical cyclone forecasts in uniform-and variable-resolution global models. Monthly Weather Review, 144(11), 4141-4160.

Davis, R.E.; Novicoff, W.M. The Impact of Heat Waves on Emergency Department Admissions in Charlottesville, Virginia, U.S.A. Int. J. Environ. Res. Public Health 2018, 15, 1436. https://doi.org/10.3390/ijerph15071436

Diallo, I., Sylla, M. B., Giorgi, F., Gaye, A. T., & Camara, M. (2012). Multimodel GCM-RCM ensemble-based projections of temperature and precipitation over West Africa for the early 21st century. International Journal of Geophysics, 2012.

Diasso, U., & Abiodun, B. J. (2015). Drought modes in West Africa and how well CORDEX RCMs simulate them. https://doi.org/10.1007/s00704-015-1705-6

Diedhiou, A., Janicot, S., Viltard, A., & de Felice, P. (1998). Evidence of two regimes of easterly waves over West Africa and the tropical Atlantic. Geophysical Research Letters, 25(15), 2805-2808.

Diedhiou, A., Janicot, S., Viltard, A., De Felice, P., & Laurent, H. (1999). Easterly wave regimes and associated convection over West Africa and tropical Atlantic: Results from the NCEP/NCAR and ECMWF reanalyses. Climate Dynamics, 15(11), 795-822.

Dieng, D., Cannon, A. J., Laux, P., Hald, C., Adeyeri, O., Rahimi, J., ... & Kunstmann, H. (2022). Multivariate bias-correction of high-resolution regional climate change simulations for West Africa: performance and climate change implications. *Journal of Geophysical Research: Atmospheres*, *127*(5), e2021JD034836.

Dieng, D., Smiatek, G., Bliefernicht, J., Heinzeller, D., Sarr, A., Gaye, A. T., & Kunstmann, H. (2017). Evaluation of the COSMO-CLM high-resolution climate simulations over West Africa. *Journal of Geophysical Research: Atmospheres*, *122*(3), 1437-1455.

Dilley, M., & Heyman, B. N. (1995). ENSO and disaster: Droughts, floods and El Niño/Southern Oscillation warm events. *Disasters*, *19*(3), 181-193.

Donkin, P. T., & Abiodun, B. J. (2022). Capability and sensitivity of MPAS-A in simulating tropical cyclones over the South-West Indian Ocean. Modeling Earth Systems and Environment, 1-16.

Dosio, A. (2016). Projections of climate change indices of temperature and precipitation from an ensemble of bias-adjusted high-resolution EURO-CORDEX regional climate models. *Journal of Geophysical Research: Atmospheres*, *121*(10), 5488-5511.

Dosio, A. (2017). Projection of temperature and heat waves for Africa with an ensemble of CORDEX Regional Climate Models. Climate Dynamics, 49(1), 493–519. https://doi.org/10.1007/s00382-016-3355-5

Dosio, A., Jury, M. W., Almazroui, M., Ashfaq, M., Diallo, I., Engelbrecht, F. A., & Tamoffo, A. T. (2021). Projected future daily characteristics of African precipitation based on global (CMIP5, CMIP6) and regional (CORDEX, CORDEX-CORE) climate models. *Climate Dynamics*, *57*(11), 3135-3158.

Dosio, A., Pinto, I., Lennard, C., Sylla, M. B., Jack, C., & Nikulin, G. (2021). What Can We Know About Recent Past Precipitation Over Africa? Daily Characteristics of African Precipitation From a Large Ensemble of Observational Products for Model Evaluation. Earth and Space Science, 8(10). https://doi.org/10.1029/2020EA001466

Druyan, L. M., Feng, J., Cook, K. H., Xue, Y., Fulakeza, M., Hagos, S. M., & Ibrah, S. S. (2010). The WAMME regional model intercomparison study. Climate Dynamics, 35(1), 175-192.

Eltahir, E. A. B., & Gong, C. (1995). Ocean-Atmosphere-Land Interactions and Rainfall in the Sahel. EOS, Transactions of the American Geophysical Union, 74(46), F91.

Endris, H. S., Omondi, P., Jain, S., Lennard, C., Hewitson, B., Chang'a, L., & Tazalika, L. (2013). Assessment of the performance of CORDEX regional climate models in simulating East African rainfall. *Journal of Climate*, *26*(21), 8453-8475.

Engdaw, M. M., Ballinger, A. P., Hegerl, G. C., & Steiner, A. K. (2022). Changes in temperature and heat waves over Africa using observational and reanalysis data sets. *International Journal of Climatology*, 42(2), 1165– 1180. https://doi.org/10.1002/joc.7295

FAO. (2009). Food and Agricultural Organization of the United Nations, FAO Statistical

Fasullo, J., & Webster, P. J. (2003). A hydrological definition of Indian monsoon onset and withdrawal. Journal of Climate, 16(19), 3200-3211

Flaounas, E., Janicot, S., Bastin, S., Roca, R., & Mohino, E. (2012). The role of the Indian monsoon onset in the West African monsoon onset: observations and AGCM nudged simulations. Climate dynamics, 38(5), 965-983

Flohn, H. (1964). Investigations on the tropical easterly jet. Dümmlers Vlg.

Fontaine, B., Trzaska, S., & Janicot, S. (1998). Evolution of the relationship between near global and Atlantic SST modes and the rainy season in West Africa: statistical analyses and sensitivity experiments. Climate Dynamics, 14(5), 353-368.

Fox-Rabinovitz, M., Côté, J., Dugas, B., Déqué, M., & McGregor, J. L. (2006). Variable resolution general circulation models: Stretched-grid model intercomparison project (SGMIP). Journal of Geophysical Research: Atmospheres, 111(D16).

Fox-Rabinovitz, M., Cote, J., Dugas, B., Deque, M., McGregor, J. L., & Belochitski, A. (2008). Stretched-grid Model Intercomparison Project: decadal regional climate simulations with enhanced variable and uniform-resolution GCMs. Meteorology and atmospheric physics, 100(1), 159-178.

Funk, C., Peterson, P., Landsfeld, M., Pedreros, D., Verdin, J., Shukla, S., & Michaelsen, J. (2015). The climate hazards infrared precipitation with stations—a new environmental record for monitoring extremes. *Scientific data*, *2*(1), 1-21.

Funk, C., Peterson, P., Peterson, S., Shukla, S., Davenport, F., Michaelsen, J., & Mata, N. (2019). A high-resolution 1983–2016 T max climate data record based on infrared temperatures and stations by the Climate Hazard Center. *Journal of Climate*, *32*(17), 5639-5658.

Gaye, A., Viltard, A., & De Felice, P. (2005). Squall lines and rainfall over Western Africa during summer 1986 and 87. *Meteorology and Atmospheric Physics*, *90*(3), 215-224.

Gbobaniyi, E., Sarr, A., Sylla, M. B., Diallo, I., Lennard, C., Dosio, A., & Lamptey, B. (2014). Climatology, annual cycle and interannual variability of precipitation and temperature in CORDEX simulations over West Africa. International Journal of Climatology, 34(7), 2241-2257.

Gbode, I. E., Akinsanola, A. A., & Ajayi, V. O. (2015). Recent changes of some observed climate extreme events in Kano. International Journal of Atmospheric Sciences, 2015.

Gelaro, R., McCarty, W., Suárez, M. J., Todling, R., Molod, A., Takacs, L., & Zhao, B. (2017). The modern-era retrospective analysis for research and applications, version 2 (MERRA-2). *Journal of climate*, *30*(14), 5419-5454.

Giannini, A., Saravanan, R., & Chang, P. (2003). Oceanic forcing of Sahel rainfall on interannual to interdecadal time scales. Science, 302(5647), 1027-1030.

Giannini, Alessandra. (2007). Sahel Drought and Global Climate Change. Panel contribution to the Population-Environment Research Network Cyberseminar on Population-Development-Environment Linkages in the Sudano-Sahelian Zone of West Africa.

Giorgi, F., & Mearns, L. O. (1999). Introduction to special section: Regional climate modeling revisited. Journal of Geophysical Research: Atmospheres, 104(D6), 6335-6352.

Goldie, J., Alexander, L., Lewis, S.C. *et al.* Changes in relative fit of human heat stress indices to cardiovascular, respiratory, and renal hospitalizations across five Australian urban populations. *Int J Biometeorol* **62**, 423–432 (2018). https://doi.org/10.1007/s00484-017-1451-9

Grist, J. P., & Nicholson, S. E. (2001). A study of the dynamic factors influencing the rainfall variability in the West African Sahel. Journal of climate, 14(7), 1337-1359.

Grist, J. P., Nicholson, S. E., & Barcilon, A. I. (2002). Easterly waves over Africa. Part II: Observed and modeled contrasts between wet and dry years. Monthly Weather Review, 130(2), 212-225.

Grodsky, S. A., Carton, J. A., & Nigam, S. (2003). Near surface westerly wind jet in the Atlantic ITCZ. Geophysical Research Letters, 30(19)

Guha-Sapir, D., & van Panhuis, W. G. (2009). Health impact of the 2004 Andaman Nicobar earthquake and tsunami in Indonesia. Prehospital and disaster medicine, 24(6), 493-499.

Guha-Sapir, D., Hargitt, D., & Hoyois, P. (2004). Thirty years of natural disasters 1974-2003: The numbers. Presses univ. de Louvain.

Hagos, S. M., & Cook, K. H. (2007). Dynamics of the West African monsoon jump. Journal of Climate, 20(21), 5264-5284.

Hagos, S. M., & Cook, K. H. (2008). Ocean warming and late-twentieth-century Sahel drought and recovery. *Journal of Climate*, *21*(15), 3797-3814.

Haile, M. (2005). Weather patterns, food security and humanitarian response in sub-Saharan Africa. *Philosophical Transactions of the Royal Society B: Biological Sciences*, *360*(1463), 2169-2182.

Hall, N. M., & Peyrillé, P. (2006, December). Dynamics of the West African monsoon. In Journal de Physique IV (Proceedings) (Vol. 139, pp. 81-99). EDP sciences.

Harris, I., Osborn, T. J., Jones, P., & Lister, D. (2020). Version 4 of the CRU TS monthly high-resolution gridded multivariate climate dataset. *Scientific data*, *7*(1), 1-18.

Harris, L. M., Lin, S. J., & Tu, C. (2016). High-resolution climate simulations using GFDL HiRAM with a stretched global grid. Journal of Climate, 29(11), 4293-4314.

Heinzeller, D., Duda, M. G., & Kunstmann, H. (2016). Towards convection-resolving, global atmospheric simulations with the Model for Prediction Across Scales (MPAS) v3. 1: An extreme scaling experiment. Geoscientific Model Development, 9(1), 77-110.

Held, I. M., & Soden, B. J. (2006). Robust responses of the hydrological cycle to global warming. Journal of climate, 19(21), 5686-5699.

Hernández-Díaz, L., Laprise, R., Sushama, L. *et al.* Climate simulation over CORDEX Africa domain using the fifth-generation Canadian Regional Climate Model (CRCM5). *Clim Dyn* **40**, 1415–1433 (2013). https://doi.org/10.1007/s00382-012-1387-z

Hersbach, H., Bell, B., Berrisford, P., Hirahara, S., Horányi, A., Muñoz-Sabater, J., & Simmons, A. (2020). The ERA5 global reanalysis. Quarterly Journal of the Royal Meteorological Society. (In in print).Hoerling, M., Hurrell, J., Eischeid, J., & Phillips, A. (2006). Detection and attribution of twentieth-century northern and southern African rainfall change. Journal of climate, 19(16), 3989-4008.

Hong, J., Häkkinen, S. A. K., Paramonov, M., Äijälä, M., Hakala, J., Nieminen, T., & Petäjä, T. (2014). Hygroscopicity, CCN and volatility properties of submicron atmospheric aerosol in a boreal forest environment during the summer of 2010. Atmospheric Chemistry and Physics, 14(9), 4733-4748.

Hong, S. Y., & Lim, J. O. J. (2006). The WRF single-moment 6-class microphysics scheme (WSM6). Asia-Pacific Journal of Atmospheric Sciences, 42(2), 129-151.

Hourdin, F., Musat, I., Guichard, F. S., Ruti, P. M., Favot, F., Filiberti, M. A., & Gallée, H. (2010). AMMA-model intercomparison project. Bulletin of the American Meteorological Society, 91(1), 95-104.

Hoerling, M., Hurrell, J., Eischeid, J., & Phillips, A. (2006). Detection and attribution of twentieth-century northern and southern African rainfall change. Journal of climate, 19(16), 3989-4008.

Hulme, M. (2001). Climatic perspectives on Sahelian desiccation: 1973–1998. Global Environmental Change, 11(1), 19-29.

Hulme, M., & Tosdevin, N. (1989). The tropical easterly jet and Sudan rainfall: a review. Theoretical and applied climatology, 39(4), 179-187.

Iloeje, M. U., Van Vleck, L. D., & Wiggans, G. R. (1981). Components of variance for milk and fat yields in dairy goats. Journal of Dairy Science, 64(11), 2290-2293.

IPCC 2014 Climate Change 2014: Impacts, Adaptation, and Vulnerability: B. Regional Aspects. Contribution of Working Group II to the Fifth Assessment Report of the Intergovernmental Panel on Climate Change ed V R Barros *et al* (Cambridge: Cambridge University Press) p 88

Janicot, S. (1992). Spatiotemporal variability of West African rainfall. Part I: Regionalizations and typings. Journal of Climate, 5(5), 489-497.

Janicot, S. (1997, April). Impact of warm ENSO events on atmospheric circulation and convection over the tropical Atlantic and West Africa. In Annales Geophysicae (Vol. 15, No. 4, pp. 471-475). Copernicus GmbH.

Janicot, S., & Sultan, B. (2001). Intra-seasonal modulation of convection in the West African monsoon. Geophysical Research Letters, 28(3), 523-526.

Janicot, S., Moron, V., & Fontaine, B. (1996). Sahel droughts and ENSO dynamics. *Geophysical Research Letters*, *23*(5), 515-518.

Janicot, S., Thorncroft, C. D., Ali, A., Asencio, N., Berry, G., Bock, O., & Ulanovsky, A. (2008, September). Large-scale overview of the summer monsoon over West Africa during the AMMA field experiment in 2006. In Annales Geophysicae (Vol. 26, No. 9, pp. 2569-2595). Copernicus GmbH.

Jenkins, G. S., Gaye, A. T., & Sylla, B. (2005). Late 20th century attribution of drying trends in the Sahel from the Regional Climate Model (RegCM3). Geophysical Research Letters, 32(22).

Jury, M. R., & Nieves Jiménez, A. T. (2021). Tropical Atlantic dust and the zonal circulation. Theoretical and Applied Climatology, 143(3), 901-913.

Kanamitsu, M., Ebisuzaki, W., Woollen, J., Yang, S. K., Hnilo, J. J., Fiorino, M., & Potter, G. L. (2002). Ncep–doe amip-ii reanalysis (r-2). *Bulletin of the American Meteorological Society*, *83*(11), 1631-1644.

Kanamitsu, O., KURODA, Y., SAITO, H., & IKEDA, Y. (1970). A Mutant of Bacillus subtilis Appearing to Have a Temperature Sensitive Defect in the Ribosomes. The Journal of Biochemistry, 67(3), 353-361.

Karyampudi, V. M., and T. N. Carlson, 1988: Analysis and numerical simulations of the Saharan Air Layer and its effect on easterly wave disturbances. J. Atmos. Sci., 45, 3102–3136

Klein, C., Heinzeller, D., Bliefernicht, J., & Kunstmann, H. (2015). Variability of West African monsoon patterns generated by a WRF multi-physics ensemble. Climate Dynamics, 45(9), 2733-2755.

Klemp, J. B. (2011). A Terrain-following coordinate with smoothed coordinate surfaces. Monthly Weather Review, 139(7), 2163–2169. https://doi.org/10.1175/MWR-D-10-05046.1

Klutse, N. A. B., Quagraine, K. A., Nkrumah, F., Quagraine, K. T., Berkoh-Oforiwaa, R., Dzrobi, J. F., & Sylla, M. B. (2021). The climatic analysis of summer monsoon extreme precipitation events over West Africa in CMIP6 simulations. Earth Systems and Environment, 5(1), 25-41.

Klutse, N. A. B., Sylla, M. B., Diallo, I., Sarr, A., Dosio, A., Diedhiou, A., & Büchner, M. (2016). Daily characteristics of West African summer monsoon precipitation in CORDEX simulations. Theoretical and Applied Climatology, 123(1), 369-386.

Kobayashi, S., Ota, Y., Harada, Y., Ebita, A., Moriya, M., Onoda, H., & Takahashi, K. (2015). The JRA-55 reanalysis: General specifications and basic characteristics. *Journal of the Meteorological Society of Japan. Ser. II*, *93*(1), 5-48.

Koné, B., Diedhiou, A., Diawara, A., Anquetin, S., Bamba, A., & Kobea, A. T. (2022). Influence of initial soil moisture in a regional climate model study over West Africa–Part 2: Impact on the climate extremes. *Hydrology and Earth System Sciences*, *26*(3), 731-754.

Kraehenmann, S., Kothe, S., Panitz, H. J., & Ahrens, B. (2013). Evaluation of daily maximum and minimum 2-m temperatures as simulated with the Regional Climate Model COSMO-CLM over Africa. *Meteorol Z*, *22*(3), 297-316.

Kramer, M., Heinzeller, D., Hartmann, H., van den Berg, W., & Steeneveld, G. J. (2020). Assessment of MPAS variable resolution simulations in the grey-zone of convection against WRF model results and observations. Climate Dynamics, 55(1), 253-276.

Kraus, E. B. (1977). Subtropical Droughts and Cross-Equatorial Energy Transports.

Krishnamurti, T. N. (1971). Tropical east-west circulations during the northern summer. Journal of Atmospheric Sciences, 28(8), 1342-1347.

Krishnamurthy, V., & Ajayamohan, R. S. (2010). Composite structure of monsoon low-pressure systems and its relation to Indian rainfall. Journal of Climate, 23(16), 4285-4305.

Lafore, J. P., Flamant, C., Giraud, V., Guichard, F., Knippertz, P., Mahfouf, J. F., & Williams, E. R. (2010). Introduction to the AMMA Special Issue on'Advances in understanding atmospheric processes over West Africa through the AMMA field campaign'. Quarterly Journal of the Royal Meteorological Society, 136(SUPP 1), 2-7.

Laing, A. G., Carbone, R., Levizzani, V., & Tuttle, J. (2008). The propagation and diurnal cycles of deep convection in northern tropical Africa. Quarterly Journal of the Royal Meteorological Society: A journal of the atmospheric sciences, applied meteorology and physical oceanography, 134(630), 93-109.

Landu, K., Leung, L. R., Hagos, S., Vinoj, V., Rauscher, S. A., Ringler, T., & Taylor, M. (2014). The dependence of ITCZ structure on model resolution and dynamical core in aquaplanet simulations. Journal of climate, 27(6), 2375-2385.

Le Barbé, L., Lebel, T., & Tapsoba, D. (2002). Rainfall variability in West Africa during the years 1950–90. Journal of climate, 15(2), 187-202.

Lebel, T., Diedhiou, A., & Laurent, H. (2003). Seasonal cycle and interannual variability of the Sahelian rainfall at hydrological scales. Journal of Geophysical Research: Atmospheres, 108(D8)

Lebonnois, S., Hourdin, F., Eymet, V., Crespin, A., Fournier, R., & Forget, F. (2010). Superrotation of Venus' atmosphere analyzed with a full general circulation model. Journal of Geophysical Research: Planets, 115(E6).

Lélé, M. I., & Lamb, P. J. (2010). Variability of the intertropical front (ITF) and rainfall over the West African Sudan–Sahel zone. Journal of Climate, 23(14), 3984-4004.

L'hote, Yann, Gil Mahé, Bonaventure Somé, and Jean Pierre Triboulet. (2002). "Analysis of a Sahelian annual rainfall index from 1896 to 2000; the drought continues." Hydrological Sciences Journal 47, no. 4 : 563-572.

Lobell, D. B., Schlenker, W., & Costa-Roberts, J. (2011). Climate trends and global crop production since 1980. Science, 333(6042), 616-620.

Losada, T., Rodríguez-Fonseca, B., Janicot, S., Gervois, S., Chauvin, F., & Ruti, P. (2010). A multi-model approach to the Atlantic Equatorial mode: impact on the West African monsoon. Climate Dynamics, 35(1), 29-43.

Lui, Y. S., Tse, L. K. S., Tam, C. Y., Lau, K. H., & Chen, J. (2021). Performance of MPAS-A and WRF in predicting and simulating western North Pacific tropical cyclone tracks and intensities. Theoretical and Applied Climatology, 143(1), 505-520.

Maoyi, M. L., & Abiodun, B. J. (2021). How well does MPAS-atmosphere simulate the characteristics of the Botswana High? *Climate Dynamics*, *57*(7), 2109-2128.

Martini, M. N., Gustafson Jr, W. I., O'Brien, T. A., & Ma, P. L. (2015). Evaluation of tropical channel refinement using MPAS-A aquaplanet simulations. Journal of Advances in Modeling Earth Systems, 7(3), 1351-1367.

Matte, D., Laprise, R., Thériault, J. M., & Lucas-Picher, P. (2017). Spatial spin-up of fine scales in a regional climate model simulation driven by low-resolution boundary conditions. Climate Dynamics, 49(1), 563-574.

Mekonnen, A., Thorncroft, C. D., & Aiyyer, A. R. (2006). Analysis of convection and its association with African easterly waves. Journal of Climate, 19(20), 5405-5421.

Michaelis, A. C., Lackmann, G. M., & Robinson, W. A. (2019). Evaluation of a unique approach to high-resolution climate modeling using the Model for Prediction Across Scales–Atmosphere (MPAS-A) version 5.1. Geoscientific Model Development, 12(8), 3725-3743.

Miles, M. K., & Follard, C. K. (1974). Changes in the latitude of the climatic zones of the Northern Hemisphere. Nature, 252(5484), 616-616.

Mohr, K. I., & Thorncroft, C. D. (2006). Intense convective systems in West Africa and their relationship to the African easterly jet. Quarterly Journal of the Royal Meteorological Society: A journal of the atmospheric sciences, applied meteorology and physical oceanography, 132(614), 163-176.

Monin, A. S., & Obukhov, A. M. (1954). Basic laws of turbulent mixing in the surface layer of the atmosphere. Contrib. Geophys. Inst. Acad. Sci. USSR, 151(163), e187.

Monthly Weather Review, 105, 1009–1018. https://doi.org/10.1175/1520-

Munich, R. E. (2011). *NatCatSERVICE: Natural catastrophe know-how for risk management and research*.

Murakami, T., Godbole, R. V., & Kelkar, R. R. (1970). Numerical simulation of the monsoon along 80° E. In Proceedings of the Conference on the Summer Monsoon of Southeast Asia (pp. 39-51). Norfolk, Virginia: Navy Weather Research Facility.

New, M., Hewitson, B., Stephenson, D. B., Tsiga, A., Kruger, A., Manhique, A., & Lajoie, R. (2006). Evidence of trends in daily climate extremes over southern and west Africa. *Journal of Geophysical Research: Atmospheres*, *111*(D14).

Ngo-Duc, T., Tangang, F. T., Santisirisomboon, J., Cruz, F., Trinh-Tuan, L., Nguyen-Xuan, T., ... & Aldrian, E. (2017). Performance evaluation of RegCM4 in simulating extreme rainfall and temperature indices over the CORDEX-Southeast Asia region. *International Journal of Climatology*, *37*(3), 1634-1647.

Nicholson, S. E. (1981). Rainfall and atmospheric circulation during drought periods and wetter years in West Africa. Monthly Weather Review, 109(10), 2191-2208.

Nicholson, W. L., Munakata, N., Horneck, G., Melosh, H. J., & Setlow, P. (2000). Resistance of Bacillus endospores to extreme terrestrial and extraterrestrial environments. Microbiology and molecular biology reviews, 64(3), 548-572.

Nicholson, S. E. (2008). The intensity, location and structure of the tropical rainbelt over west Africa as factors in interannual variability. International Journal of Climatology: A Journal of the Royal Meteorological Society, 28(13), 1775-1785.

Nicholson, S. E. (2013). The West African Sahel: A review of recent studies on the rainfall regime and its interannual variability. *International Scholarly Research Notices*, *2013*.

Nicholson, S. E., & Grist, J. P. (2003). The seasonal evolution of the atmospheric circulation over West Africa and equatorial Africa. Journal of climate, 16(7), 1013-1030.

Nicholson, S. E., & Selato, J. C. (2000). The influence of La Nina on African rainfall. International Journal of Climatology: A Journal of the Royal Meteorological Society, 20(14), 1761-1776.

Nicholson, S. E., & Webster, P. J. (2007). A physical basis for the interannual variability of rainfall in the Sahel. Quarterly Journal of the Royal Meteorological Society: A journal of the atmospheric sciences, applied meteorology and physical oceanography, 133(629), 2065-2084.

Nicholson, W. K. (2012). Introduction to abstract algebra. John Wiley & Sons.

Nicholson, S. E., & Grist, J. P. (2001). A conceptual model for understanding rainfall variability in the West African Sahel on interannual and interdecadal timescales. International Journal of Climatology: A Journal of the Royal Meteorological Society, 21(14), 1733-1757.

Nikiema, P. M., Sylla, M. B., Ogunjobi, K., Kebe, I., Gibba, P., & Giorgi, F. (2017). Multimodel CMIP5 and CORDEX simulations of historical summer temperature and precipitation variabilities over West Africa. *International Journal of Climatology*, *37*(5), 2438-2450.

Odoulami, R. C., Abiodun, B. J., & Ajayi, A. E. (2019). Modelling the potential impacts of afforestation on extreme precipitation over West Africa. Climate Dynamics, 52(3), 2185-2198.

Oguntunde, P. G., Abiodun, B. J., & Lischeid, G. (2011). Rainfall trends in Nigeria, 1901–2000. Journal of Hydrology, 411(3-4), 207-218.

Oh, S. G., Park, J. H., Lee, S. H., & Suh, M. S. (2014). Assessment of the RegCM4 over East Asia and future precipitation change adapted to the RCP scenarios. *Journal of Geophysical Research: Atmospheres*, *119*(6), 2913-2927.

Omotosho, J. B., & Abiodun, B. J. (2007). A numerical study of moisture build-up and rainfall over West Africa. Meteorological Applications: A journal of forecasting, practical applications, training techniques and modelling, 14(3), 209-225.

Oueslati, B., Pohl, B., Moron, V., Rome, S., & Janicot, S. (2017). Characterization of heat waves in the Sahel and associated physical mechanisms. Journal of Climate, 30(9), 3095-3115.

Paeth, H., & Friederichs, P. (2004). Seasonality and time scales in the relationship between global SST and African rainfall. Climate Dynamics, 23(7), 815-837.

Paeth, Heiko, and Andreas Hense.(2004). "SST versus climate change signals in West African rainfall: 20th-century variations and future projections." Climatic change 65, no: 179-208.

Pal, J. S., Giorgi, F., Bi, X., Elguindi, N., Solmon, F., Gao, X., ... & Steiner, A. L. (2007). Regional climate modeling for the developing world: the ICTP RegCM3 and RegCNET. Bulletin of the American Meteorological Society, 88(9), 1395-1410.

Panitz, H. J., Dosio, A., Büchner, M., Lüthi, D., & Keuler, K. (2014). COSMO-CLM (CCLM) climate simulations over CORDEX-Africa domain: analysis of the ERA-

Interim driven simulations at 0.44 and 0.22 resolution. *Climate dynamics*, *42*(11), 3015-3038.

Park, S., Bretherton, C. S., & Rasch, P. J. (2014). Integrating cloud processes in the Community Atmosphere Model, version 5. Journal of Climate, 27(18), 6821-6856.

Pattanaik, D. R., & Satyan, V. (2000). Fluctuations of Tropical Easterly Jet during contrasting monsoons over India: A GCM study. Meteorology and Atmospheric Physics, 75(1), 51-60.

Perkins, D. M., Bailey, R. A., Dossena, M., Gamfeldt, L., Reiss, J., Trimmer, M., & Woodward, G. (2015). Higher biodiversity is required to sustain multiple ecosystem processes across temperature regimes. Global change biology, 21(1), 396-406

Perkins, G. D., Handley, A. J., Koster, R. W., Castrén, M., Smyth, M. A., Olasveengen, T., ... & Greif, R. (2015). European Resuscitation Council Guidelines for Resuscitation 2015: Section 2. Adult basic life support and automated external defibrillation. Resuscitation, 95, 81-99.

Piersig, W. (1944). Los disturbios ciclónicos del Atlántico subtropical del Nor-este: Adaptado de las partes II y III de "Variaciones de presión y viento, un tratado sobre el tiempo de la región de los vientos alisios del Atlántico Nor-este". Bulletin of the American Meteorological Society, 25(1), 17-17.

Pilon, R., Zhang, C., & Dudhia, J. (2016). Roles of deep and shallow convection and microphysics in the MJO simulated by the model for prediction across scales. Journal of Geophysical Research: Atmospheres, 121(18), 10-575.

Poan, E. D., Gachon, P., Dueymes, G., Diaconescu, E., Laprise, R., & Seidou Sanda, I. (2016). West African monsoon intraseasonal activity and its daily precipitation indices in regional climate models: diagnostics and challenges. *Climate Dynamics*, *47*(9), 3113-3140.

Rao, B. S., Rao, D. B., & Rao, V. B. (2004). Decreasing trend in the strength of Tropical Easterly Jet during the Asian summer monsoon season and the number of tropical cyclonic systems over Bay of Bengal. Geophysical Research Letters, 31(14).

Redelsperger, J. L., Thorncroft, C. D., Diedhiou, A., Lebel, T., Parker, D. J., & Polcher, J. (2006). African Monsoon Multidisciplinary Analysis: An international research project and field campaign. Bulletin of the American Meteorological Society, 87(12), 1739-1746.

Reed, R. J., Norquist, D. C., & Recker, E. E. (1977). The structure and properties of African wave disturbances as observed during phase III of GATE. Monthly Weather Review, 105(3), 317-333

Ricciardulli, L., & Sardeshmukh, P. D. (2002). Local time-and space scales of organized tropical deep convection. Journal of climate, 15(19), 2775-2790.

Ringard, J., Dieppois, B., Rome, S., Diedhiou, A., Pellarin, T., Konaré, A., ... & Descroix, L. (2016). The intensification of thermal extremes in west Africa. Global and Planetary Change, 139, 66-77.

Ringler, T. D., Jacobsen, D., Gunzburger, M., Ju, L., Duda, M., & Skamarock, W. (2011). Exploring a multiresolution modeling approach within the shallow-water equations.

Monthly Weather Review, 139(11), 3348–3368. https://doi.org/10.1175/MWR-D-10-05049.1

Rowell, D. P., Folland, C. K., Maskell, K., & Ward, M. N. (1995). Variability of summer rainfall over tropical North Africa (1906–92): Observations and modelling. Quarterly Journal of the Royal Meteorological Society, 121(523), 669-704.

Russo, E., Kirchner, I., Pfahl, S., Schaap, M., & Cubasch, U. (2019). Sensitivity studies with the regional climate model COSMO-CLM 5.0 over the CORDEX Central Asia Domain. *Geoscientific Model Development*, *12*(12), 5229-5249.

Russo, S., Dosio, A., Graversen, R. G., Sillmann, J., Carrao, H., Dunbar, M. B., ... & Vogt, J. V. (2014). Magnitude of extreme heat waves in present climate and their projection in a warming world. *Journal of Geophysical Research: Atmospheres*, *119*(22), 12-500.

Russo, S., Marchese, A. F., Sillmann, J., & Immé, G. (2016). When will unusual heat waves become normal in a warming Africa? *Environmental Research Letters*, *11*(5), 054016.

Saha, S., Moorthi, S., Pan, H. L., Wu, X., Wang, J., Nadiga, S., Tripp, P., Kistler, R., Woollen, J., Behringer, D., Liu, H., Stokes, D., Grumbine, R., Gayno, G., Wang, J., Hou, Y. T., Chuang, H. Y., Juang, H. M. H., Sela, J., … Goldberg, M. (2010). The NCEP climate forecast system reanalysis. Bulletin of the American Meteorological Society, 91(8), 1015–1057. https://doi.org/10.1175/2010BAMS3001.1

Saha, S., Moorthi, S., Wu, X., Wang, J., Nadiga, S., Tripp, P., Behringer, D., Hou, Y. T., Chuang, H. Y., Iredell, M., Ek, M., Meng, J., Yang, R., Mendez, M. P., Van Den

Dool, H., Zhang, Q., Wang, W., Chen, M., & Becker, E. (2014). The NCEP climate forecast system version 2. Journal of Climate, 27(6), 2185–2208. https://doi.org/10.1175/JCLI-D-12-00823.1

Sarah E. Perkins, A review on the scientific understanding of heatwaves—Their measurement, driving mechanisms, and changes at the global scale, Atmospheric Research, Volumes 164–165,2015, Pages 242-267, ISSN 0169-8095, https://doi.org/10.1016/j.atmosres.2015.05.014.

Schmidt, F., 1977: Variable fine mesh in spectral global model. Beitr. Phys. Atmos., 50, 211−217.

Schneider, Udo; Becker, Andreas; Finger, Peter; Meyer-Christoffer, Anja; Ziese, Markus (2018): GPCC Full Data Monthly Product Version 2018 at 0.25°: Monthly Land-Surface Precipitation from Rain-Gauges built on GTS-based and Historical Data. DOI: 10.5676/DWD_GPCC/FD_M_V2018_025 .

Semazzi, F. H., & Sun, L. (1997). The role of orography in determining the Sahelian climate. International Journal of Climatology: A Journal of the Royal Meteorological Society, 17(6), 581-59

Shinoda, M., & Kawamura, R. (1994). Tropical rainbelt, circulation, and sea surface temperatures associated with the Sahelian rainfall trend. Journal of the Meteorological Society of Japan. Ser. II, 72(3), 341-357.

Sillmann, J., Kharin, V. V., Zhang, X., Zwiers, F. W., & Bronaugh, D. (2013). Climate extremes indices in the CMIP5 multimodel ensemble: Part 1. Model evaluation in the present climate. *Journal of Geophysical Research: Atmospheres*, *118*(4), 1716-1733.

Simpson, R. H., Frank, N., Shideler, D., & Johnson, H. M. (1969). Atlantic tropical disturbances of 1968. Monthly Weather Review, 97(3), 240-255.

Singh, D., Ghosh, S., Roxy, M. K., & McDermid, S. (2019). Indian summer monsoon: Extreme events, historical changes, and role of anthropogenic forcings. Wiley Interdisciplinary Reviews: Climate Change, 10(2), e571.

Sivakumar, M. V., Collins, C., Jay, A., & Hansen, J. (2014). Regional priorities for strengthening climate services for farmers in Africa and South Asia. CCAFS Working Paper.

Skamarock, W. C., Klemp, J. B., Duda, M. G., Fowler, L. D., Park, S. H., & Ringler, T. D. (2012). A multiscale nonhydrostatic atmospheric model using centroidal Voronoi tesselations and C-grid staggering. Monthly Weather Review, 140(9), 3090–3105. https://doi.org/10.1175/MWR-D-11-00215.1

Skamarock, W. C., Klemp, J. B., Duda, M. G., Fowler, L. D., Park, S. H., & Ringler, T. D. (2012). A multiscale nonhydrostatic atmospheric model using centroidal Voronoi tesselations and C-grid staggering. Monthly Weather Review, 140(9), 3090-3105.

Smiatek, G., & Kunstmann, H. (in review.). Potential impact of the pan-African Great Green Wall on Sahelian summer precipitation: A global modeling approach with MPAS. 1–21.

Smith, I., Moise, A., Katzfey, J., Nguyen, K., & Colman, R. (2013). Regional-scale rainfall projections: Simulations for the New Guinea region using the CCAM model. Journal of Geophysical Research: Atmospheres, 118(3), 1271-1280.

Speth, P., Christoph, M., & Diekkrüger, B. (Eds.). (2010). Impacts of global change on the hydrological cycle in West and Northwest Africa. Springer Science & Business Media.

Staniforth, A., and H. Mitchell (1978), A variable resolution finite element technique for regional forecasting with primitive equations, Mon. Weather Rev., 106, 439– 447.

Sultan, B., & Gaetani, M. (2016). Agriculture in West Africa in the twenty-first century: Climate change and impacts scenarios, and potential for adaptation. Frontiers in Plant Science, 7(AUG2016), 1–20. https://doi.org/10.3389/fpls.2016.01262

Sultan, B., & Janicot, S. (2000). Abrupt shift of the ITCZ over West Africa and intra-seasonal variability. Geophysical Research Letters, 27(20), 3353-3356.

Sultan, B., & Janicot, S. (2003). The West African monsoon dynamics. Part II: The "pre-onset" and "onset" of the summer monsoon. Journal of climate, 16(21), 3407-3427.

Sultan, B., Baron, C., Dingkuhn, M., Sarr, B., & Janicot, S. (2005). Agricultural impacts of large-scale variability of the West African monsoon. Agricultural and forest meteorology, 128(1-2), 93-110.

Sultan, B., Roudier, P., Quirion, P., Alhassane, A., Muller, B., Dingkuhn, M., ... & Baron, C. (2013). Assessing climate change impacts on sorghum and millet yields in the Sudanian and Sahelian savannas of West Africa. *Environmental Research Letters*, *8*(1), 014040.

Sultan, Benjamin, Serge Janicot, and Arona Diedhiou. (2003) "The West African monsoon dynamics. Part I: Documentation of intraseasonal variability." *Journal of Climate* 16, no. 21: 3389-3406.

Sylla, M. B. (2015). Projected Changes in the Annual Cycle of High-Intensity Precipitation Events over West Africa for the Late Twenty-First Century *. 28(16), 6475–6488. https://doi.org/10.1175/JCLI-D-14-00854.1

Sylla, M. B., Coppola, E., Mariotti, L., Giorgi, F., Ruti, P. M., Dell'Aquila, A., & Bi, X. (2010). Multiyear simulation of the African climate using a regional climate model (RegCM3) with the high-resolution ERA-interim reanalysis. Climate Dynamics, 35(1), 231-247.

Sylla, M. B., Gaye, A. T., & Jenkins, G. S. (2012). On the fine-scale topography regulating changes in atmospheric hydrological cycle and extreme rainfall over West Africa in a regional climate model projection. International Journal of Geophysics, 2012.

Sylla, M. B., Gaye, A. T., Pal, J. S., Jenkins, G. S., & Bi, X. Q. (2009). High-resolution simulations of West African climate using regional climate model (RegCM3) with different lateral boundary conditions. Theoretical and Applied Climatology, 98(3), 293-314.

Sylla, M. B., Giorgi, F., Coppola, E., & Mariotti, L. (2013). Uncertainties in daily rainfall over Africa: assessment of gridded observation products and evaluation of a regional climate model simulation. International Journal of Climatology, 33(7), 1805-1817.

Sylla, Mouhamadou Bamba, Giorgi, F., Pal, J. S., Gibba, P., Kebe, I., & Nikiema, M. (2015). Projected changes in the annual cycle of high-intensity precipitation events over West

Africa for the late twenty-first century. Journal of Climate, 28(16), 6475–6488. https://doi.org/10.1175/JCLI-D-14-00854.1

Tall, A., Mason, S. J., Van Aalst, M., Suarez, P., Ait-Chellouche, Y., Diallo, A. A., & Braman, L. (2012). Using seasonal climate forecasts to guide disaster management: the Red Cross experience during the 2008 West Africa floods. International Journal of Geophysics, 2012.

Tamoffo, A. T., Dosio, A., Amekudzi, L. K., & Weber, T. (2022). Process-oriented evaluation of the West African Monsoon system in CORDEX-CORE regional climate models. Climate Dynamics, 1-24.

Thanh, N.-D., Fredolin, T. T., Jerasorn, S., Faye, C., Long, T.-T., Thanh, N.-X., Tan, P.-V., Liew, J., Gemma, N., Patama, S., Dodo, G., and Edvin, A.(2017).Performance evaluation of RegCM4 in simulating extreme rainfall and temperature indices over the CORDEX-Southeast Asia region, Int. J. Climatol., 37, 1634–1647, https://doi.org/10.1002/joc.4803,

Thorncroft, C. D., & Blackburn, M. (1999). Maintenance of the African easterly jet. Quarterly Journal of the Royal Meteorological Society, 125(555), 763-786.

Thuburn, J., Ringler, T. D., Skamarock, W. C., & Klemp, J. B. (2009). Numerical representation of geostrophic modes on arbitrarily structured C-grids. Journal of Computational Physics, 228(22), 8321–8335. https://doi.org/10.1016/j.jcp.2009.08.006

Tiedtke, M. I. C. H. A. E. L. (1989). A comprehensive mass flux scheme for cumulus parameterization in large-scale models. Monthly weather review, 117(8), 1779-1800.

Tomas, R. A., & Webster, P. J. (1997). The role of inertial instability in determining the location and strength of near-equatorial convection. Quarterly Journal of the Royal Meteorological Society, 123(542), 1445-1482.

Turco, M., Palazzi, E., Hardenberg, J. Von, & Provenzale, A. (2015). Observed climate change hot-spots. https://doi.org/10.1002/2015GL063891

USAID. (2014). Enhancing rainfed agriculture. https://www.usaid.gov/what-wedo/.../promoting.../enhancing-rainfed

van Loenhout, J.A.F., Delbiso, T.D., Kiriliouk, A. *et al.* Heat and emergency room admissions in the Netherlands. *BMC Public Health* **18**, 108 (2018). https://doi.org/10.1186/s12889-017-5021-1

Vautard, R., Gobiet, A., Jacob, D., Belda, M., Colette, A., Déqué, M., ... & Yiou, P. (2013). The simulation of European heat waves from an ensemble of regional climate models within the EURO-CORDEX project. *Climate Dynamics*, *41*(9), 2555-2575.

Viltard, A. D., De Felice, P., & Oubuih, J. (1997). Comparison of the African and the 6–9 day wave-like disturbance patterns over West-Africa and the tropical Atlantic during summer 1985. Meteorology and Atmospheric Physics, 62(1), 91-99.

Vizy, E. K., & Cook, K. H. (2002). Development and application of a mesoscale climate model for the tropics: Influence of sea surface temperature anomalies on the West African monsoon. Journal of Geophysical Research: Atmospheres, 107(D3), ACL-2.

Vizy, E. K., & Cook, K. H. (2012). Mid-twenty-first-century changes in extreme events over northern and tropical Africa. *Journal of Climate*, *25*(17), 5748-5767.

Wang, G., & Eltahir, E. A. (2000). Ecosystem dynamics and the Sahel drought. Geophysical research letters, 27(6), 795-798.

Ward, M. N. (1998). Diagnosis and short-lead time prediction of summer rainfall in tropical North Africa at interannual and multidecadal timescales. Journal of climate, 11(12), 3167-3191.

Warnatzsch, E. A., & Reay, D. S. (2019). Temperature and precipitation change in Malawi: Evaluation of CORDEX-Africa climate simulations for climate change impact assessments and adaptation planning. *Science of the Total Environment*, *654*, 378-392.

Wu, M. L. C., Reale, O., Schubert, S. D., Suarez, M. J., Koster, R. D., & Pegion, P. J. (2009). African easterly jet: Structure and maintenance. Journal of Climate, 22(17), 4459-4480.

Xie, P.-P., Chen, M., & Shi, W. (2010). CPC unified gauge-based analysis of global daily precipitation 24th Conf. on Hydrology. American Meteor Society. Retrieved from https://ams.confex.com/ams/90annual/techprogram/paper_163676.htm

Xue, Y., De Sales, F., Lau, W. M., Boone, A., Feng, J., Dirmeyer, P., ... & Wu, M. L. C. (2010). Intercomparison and analyses of the climatology of the West African Monsoon in the West African Monsoon Modeling and Evaluation project (WAMME) first model intercomparison experiment. Climate Dynamics, 35(1), 3-27

Xue, Y., De Sales, F., Vasic, R., Mechoso, C. R., Arakawa, A., & Prince, S. (2010). Global and seasonal assessment of interactions between climate and vegetation biophysical processes: A GCM study with different land–vegetation representations. Journal of Climate, 23(6), 1411-1433.

Yamada, T. J., Kanae, S., Oki, T., & Hirabayashi, Y. (2012). The onset of the West African monsoon simulated in a high-resolution atmospheric general circulation model with reanalyzed soil moisture fields. Atmospheric Science Letters, 13(2), 103–107. https://doi.org/10.1002/asl.36

Zhang, C., Wang, Y., & Hamilton, K. (2011). Improved representation of boundary layer clouds over the southeast Pacific in ARW-WRF using a modified Tiedtke cumulus parameterization scheme. Monthly Weather Review, 139(11), 3489-3513.

Zhang, Q., Berntell, E., Li, Q., & Ljungqvist, F. C. (2021). Understanding the variability of the rainfall dipole in West Africa using the EC-Earth last millennium simulation. *Climate Dynamics*, *57*(1), 93-107.

APPENDIX

PUBLICATIONS SUBMITTED FROM THE THESIS

A.1 Paper1 submitted to springer

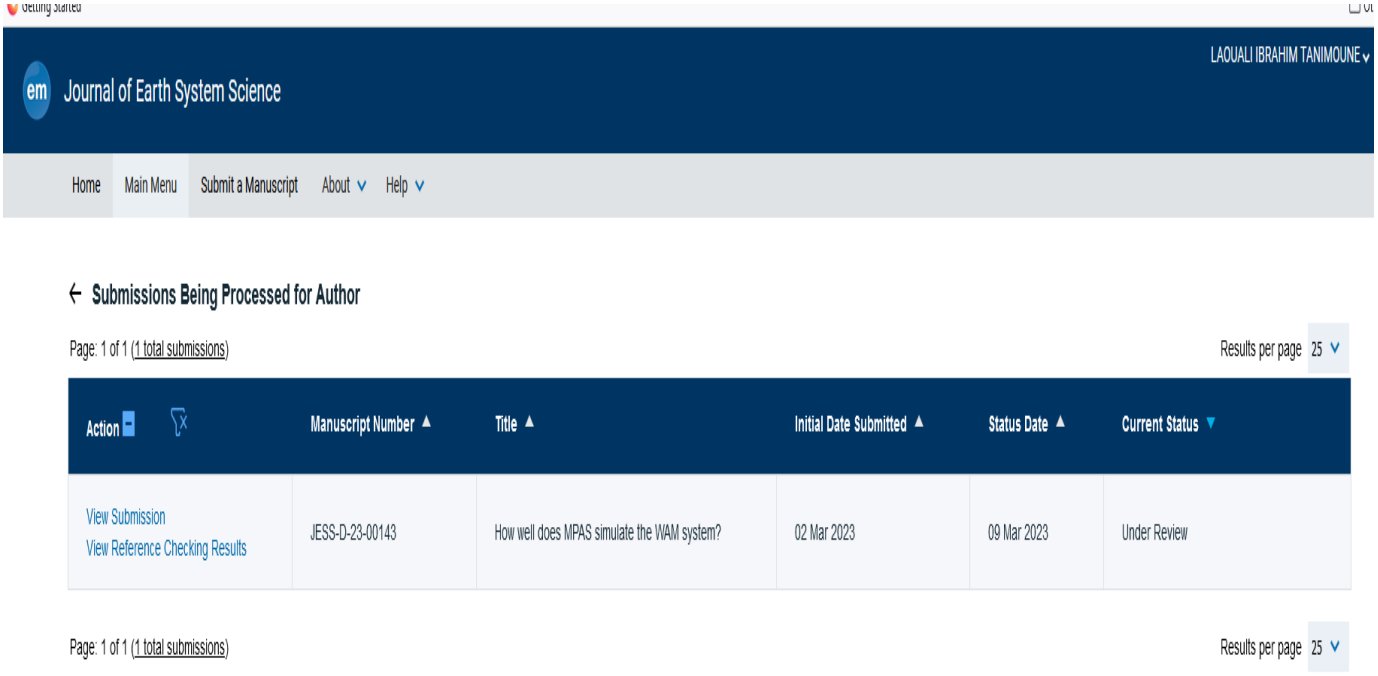

A.2 Paper 2 submitted to AGU

AGU PUBLICATIONS

Journal Home | GEMS Desktop | Author Instructions | Reviewer Instructions | Change Journal | Contact | AGU.org | Join AGU

JOURNAL OF GEOPHYSICAL RESEARCH
Atmospheres
AN AGU JOURNAL

JGR

Detailed Status Information

Collapse Manuscript Details

Manuscript #	2023JD039055
Current Revision #	0
Submission Date	2023-04-12 05:37:42
Current Stage	Under Review **Days in Folder: 4**
Title	Simulation of temperature extremes over West Africa and the Eastern Sahel with MPAS
Manuscript Type	Research Article
Special Collection	N/A
Authors	1 Laouali Tanimoune (Federal University of Technology of Akure, Nigeria) 2 Gerhard Smiatek (Karlsruhe Institute of Technology) (corr-auth) 3 Harald Kunstmann (Karlsruhe Institute of Technology (KIT)) 4 Babatunde Abiodun (University of Cape Town)
Abstract	*A large ensemble of 51 simulations with the Model for Prediction Across Scales (MPAS) has been applied to assess its ability to reproduce extreme temperatures and heat waves in the area of West Africa and the Eastern Sahel. With its global approach the model avoids transition errors influencing the performance of limited area climate models. The MPAS simulations were driven with sea surface temperature (SST) and sea ice extent as the only boundary condition.* *The results reveal moderate cold biases in the range from -0.6° to -0.9° C for the daily mean temperature and -1.4° to -2.0° C for the area mean of the daily maximum temperature. The bias in the number of tropical nights ranges from +3 to -10 days. An underestimation by up to 50% is also present regarding the number of summer days. The heat wave duration index is underestimated regionally by 10% to 60%. Compared to the reanalyses, the biases revealed by the MPAS simulations are generally smaller than with measured observational reference. The results from long term runs and from short term runs with selected SST years are similar.* *Shortcomings in the reproduction of the temperature and precipitation indices found in the present investigation indicate that the global MPAS approach does provide a fidelity similar to that of the regional climate models.*
Plain Language Summary	Large number of simulations with the global weather and climate model MPAS has been applied to investigate extreme temperatures and related heat waves. The considered area is West Africa and the Eastern Sahel. In the simulations sea surface temperature and sea ice extent were the only boundary condition. The results reveal moderate underestimation in the range from -0.6{degree sign} to -0.9{degree sign} C for the daily mean temperature.